Chapter-4

RESULTS AND DISCUSSION

The main objective of this research was to identify the effect of gas metal arc welding process parameters that affect the mechanical properties and microstructure of welded joint of IS 2062 and AISI 304 steel weldments. The results of experimental work describe in Chapter 3 are presented, and discussed here. The results pertain to the butt welded joints at different welding conditions. The entire test specimens were prepared from IS 2062-2006 structural steel weldments and AISI 304 steel weldments. The voltage was varied from 25V to 28 V, wire feed speed varied from 7.62 m/min to 11.43 m/min, and gas flow rate from 10l/m to 25 l/m for IS 2062 steel weldments and voltage varied from 20V to 23V, wire feed speed from 6.35 m/min to 10.16 m/min, and gas flow rate from 10 l/m to 25l/m for AISI 304 steel respectively. The welded joints were prepared under different welding conditions by varying voltage, gas flow rate, wire feed speed, and plate thickness and have different values of yield strength, ultimate tensile strength, toughness, microhardness (VHN), and percentage elongation. The microstructures of the weldments have also been found to vary with the variation in the welding parameters.

The results so obtained during experimentation are being discussed under the following headings:

4.1 Effect of voltage, wire feed speed, and shielding gas flow rate on yield strength

Effect of wire feed speed on yield strength from 25V to 28V at 10 to 25 l/m, and 3.22 to 4.47 kJ/mm heat input respectively of IS 2062 structural steel weldments.

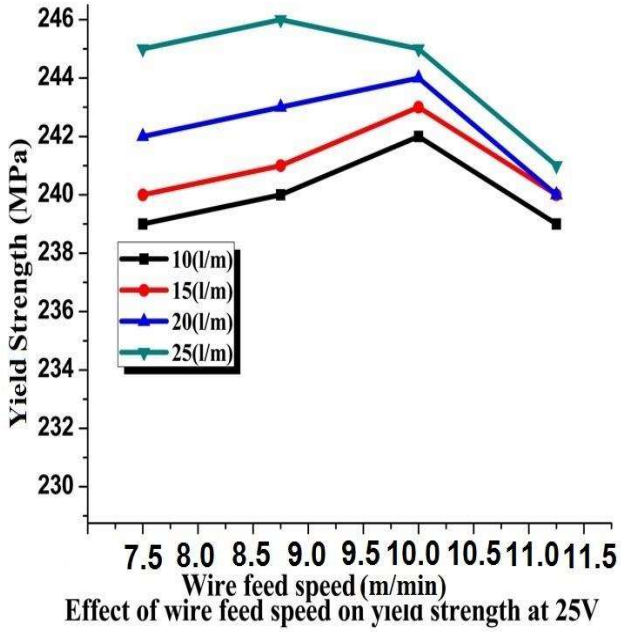

Figure 4.1 Effect of wire feed speed on the yield strength of IS 2062 steel at 25V with different shielding gas flow rate at 3.22 kJ/mm heat input

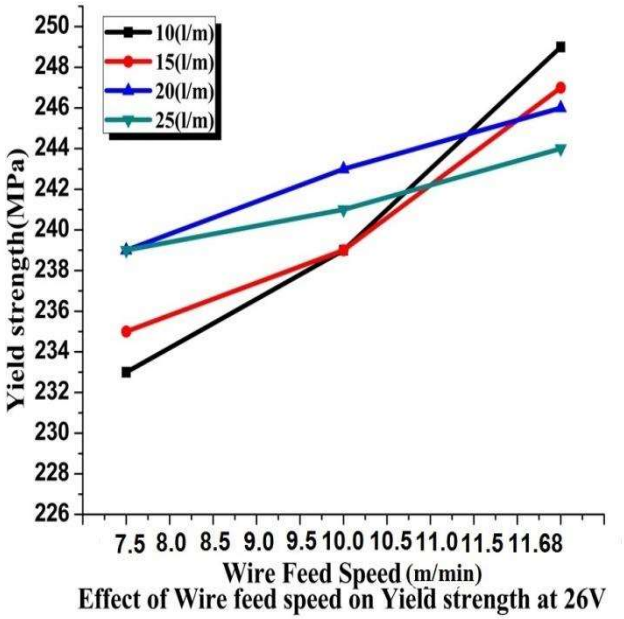

Figure 4.2 Effect of wire feed speed on the yield strength of IS 2062 steel at 26V with different shielding gas flow rate at 3.58 kJ/mm heat input

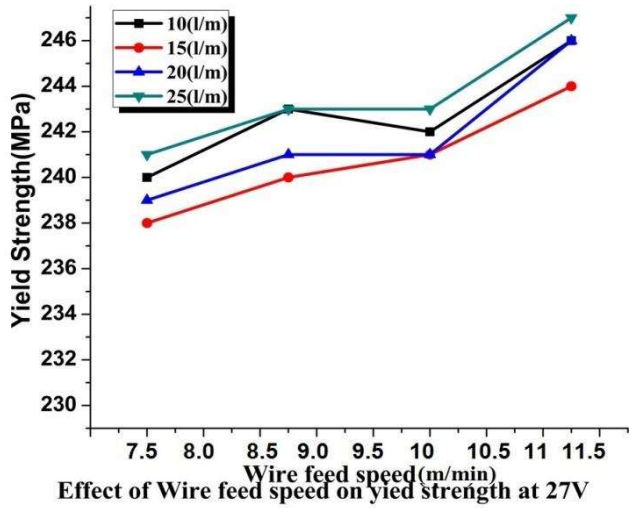

Figure 4.3 Effect of wire feed speed on the yield strength of IS 2062 steel at 27V with different shielding gas flow rate at 3.88 kJ/mm heat input

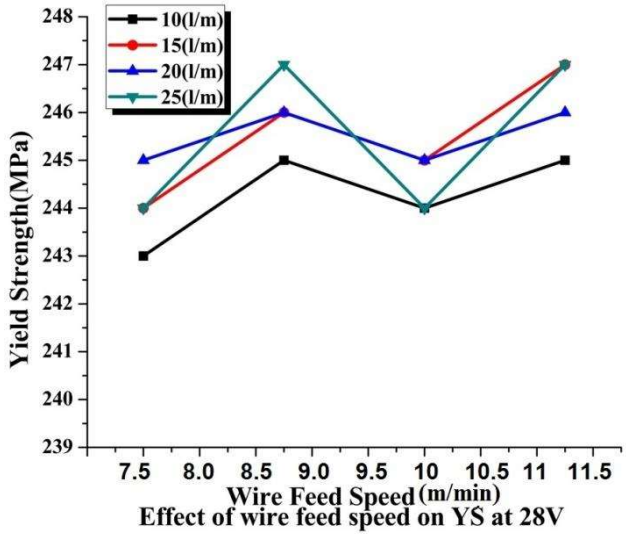

Figure 4.4 Effect of wire feed speed on the yield strength of IS 2062 steel at 28V with different shielding gas flow rate at 4.47 kJ/mm heat input

Figure 4.1 to 4.4 shows the effect of wire feed speed on the yield strength of IS 2062 steel weldment test pieces. The voltage varies from 25 to 28V, and shielding gas flow rate varies from 10 to 25l/m at different heat input. Figure 4.1 is plotted for IS 2062 steel weldment at 25V, and at 10 to 25 l/m shielding gas flow rate at 3.22 kJ/mm heat input. From figure 4.1 it is clear that yield strength of weldment first increases and then decreases. Figure 4.2 to figure 4.4 is plotted for IS

2062 steel weldment at 26V, 27V, and 28V at 10 to 25 l/m shielding gas flow rate and at 3.58,3.88, and 4.47 kj/mm heat input respectively**.** Figure 4.2 to figure 4.4 reveal that on increasing the heat input, yield strength of IS 2062 weldment increases and trends of figure 4.2 to figure 4.4 having approximant same. Yield strength and tensile strength of IS 2062 steel weldment is mostly affected by a higher order of welding current and number of welding passes [91].

Amit P. Shinde et al [92] evaluates the tensile strength of IS 2062 steel weldment, welded by metal inert gas welding (GMAW) process and they optimized the process parameters by application of response surface methodology, and they developed a model, experiments were planned using central composite rotatable design (CCRD), and they claimed that yield strength and ultimate tensile strength are significantly affected by higher order of welding current, and shielding gas flow rate. Results of optimization study depict that welding current of 170 amperes, shielding gas flow rate of 12 liter/min, and the arc voltage of 24V (volts) results in maximum values of tensile strength and yield strength of welded joint

4.2 Effect of voltage, wire feed speed, and shielding gas flow rate on the ultimate tensile strength

Effect of Wire feed speed on ultimate tensile strength from 25 V to 28V at 10 to 25l/m respectively

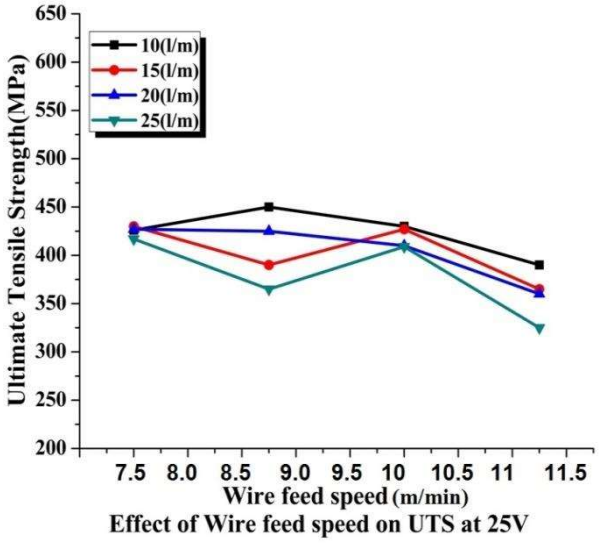

Figure 4.5 Effect of wire feed speed on the ultimate tensile strength of IS 2062 steel at 25V with different shielding gas flow rate at 3.22 kJ/mm heat input

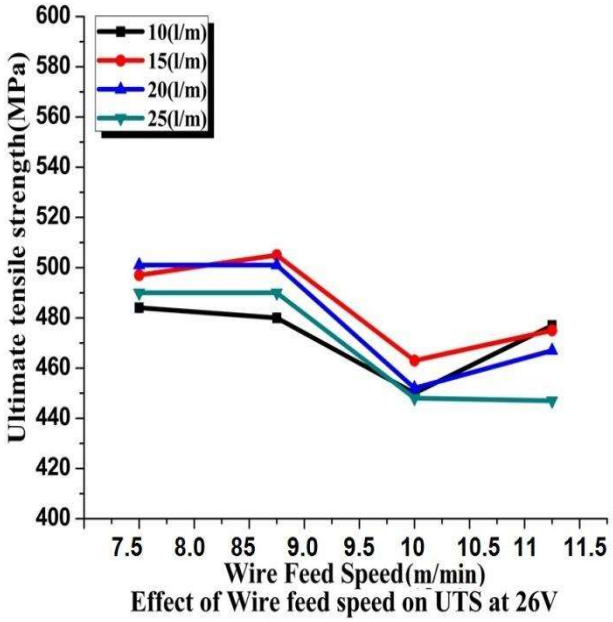

Figure 4.6 Effect of wire feed speed on the ultimate tensile strength of IS 2062 steel at 26V with different shielding gas flow rate at 3.58 kJ/mm heat input

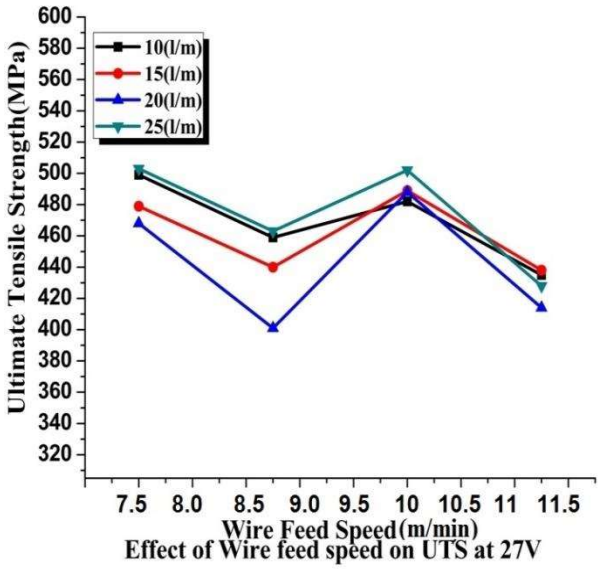

Figure 4.7 Effect of wire feed speed on the ultimate tensile strength of IS 2062 steel at 27V with different shielding gas flow rate at 3.88 kJ/mm heat input

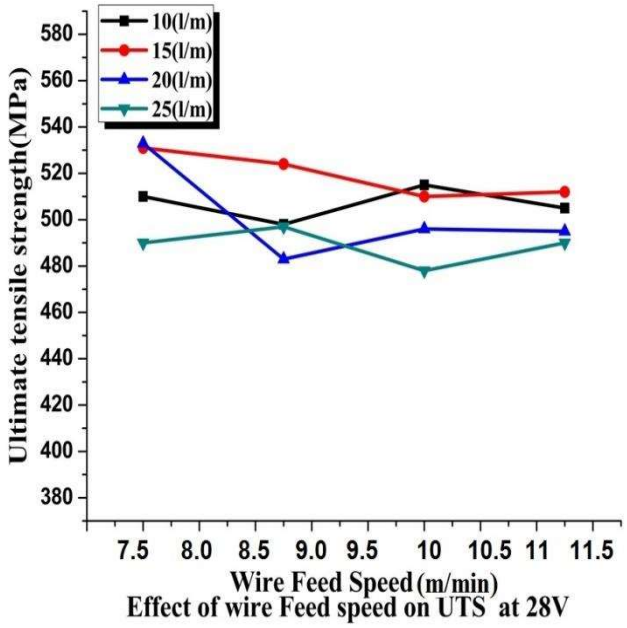

Figure 4.8 Effect of wire feed speed on the ultimate tensile strength of IS 2062 steel at 28V with different shielding gas flow rate at 4.47 kJ/mm heat input

Figure 4.5 to 4.8 depict the effect of wire feed speed on the ultimate tensile strength of IS 2062 steel weldment test pieces and the voltage varies from 25 to 28V, and shielding gas flow rate varies from 10 to 25l/m at different heat input. Figure 4.5 is plotted for IS 2062 steel weldment at 25V, and at 10 to 25 l/m shielding gas flow rate at 3.22 kJ/mm heat input. On examination of figure 4.5, it is clear that ultimate tensile strength of weldment is going to decrease. Figure 4.6 shows that at 3.58 kJ/mm heat input ultimate tensile strength of IS 2062 weldment decreases and then increases. At heat input 3.88 kJ/mm ultimate tensile strength of weldment increases and then decreases, figure 4.7 at 4.47 kJ/mm heat inputs, some decreasing trend is there in ultimate tensile strength. In figure 4.8 all ultimate points try to coincide at same point. From the literature review, it is clear that ultimate tensile strength and yield strength of a weldment is a function of heat input and greatly influence by the heat input [93].

R.Sudarshan and M.Devaiah (2018) [94] studied the effect of GMA welding process parameters during the welding of IS 2062 steel, they applied a software-based technique to develop a model and in their experimental results, they mentioned that mechanical properties are the functions of heat input, on increasing the heat input mechanical properties of weldment decreases.

Talabi, S.I et al (2014) [18] studied the effect of welding variables on mechanical properties of low carbon steel weldment by SMA welding process and they reported that Increase in the arc voltage, and welding current results in increases in hardness values, and decreases yield strength, tensile strength, and impact toughness and it was observed that on increasing heat input there is reduction in mechanical properties.

M. A. Bodude and I. Momohjimoh (2015) [95] concluded that tensile strength, hardness, and Impact toughness of weldment are functions of the microstructure; hence these are structural sensitive and joint strength decreases as increases in heat input.

Hong Liang Li et al (2018) [96] mentioned in their result that on increase in the heat input, the ultimate tensile strength (UTS), and toughness of welded join increased due to solid solution strengthening of alloying elements, and heat input has a limited role in reducing the hardness of CGHAZ, although the cooling rate slowed down.

4.3 Effect of voltage, wire feed speed, and shielding gas flow rate on toughness

Effect of wire feed speed at toughness from 25V-28V at 10-25 l/m

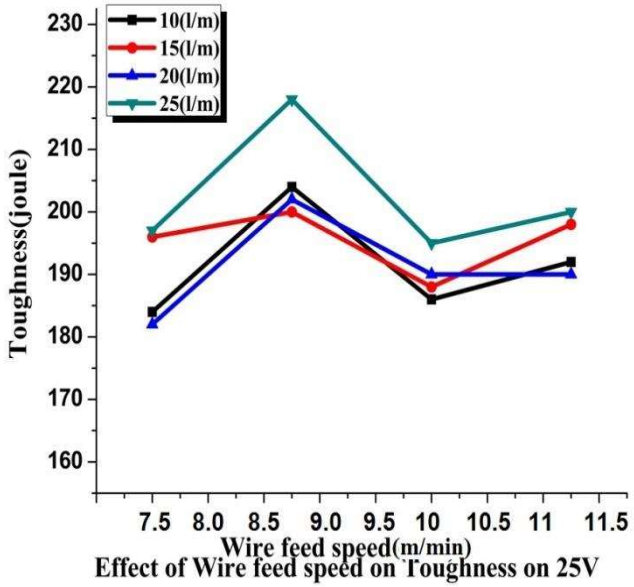

Figure 4.9 Effect of wire feed speed on toughness of IS 2062 steel at 25V with different shielding gas flow rate at 3.22 kJ/mm heat input

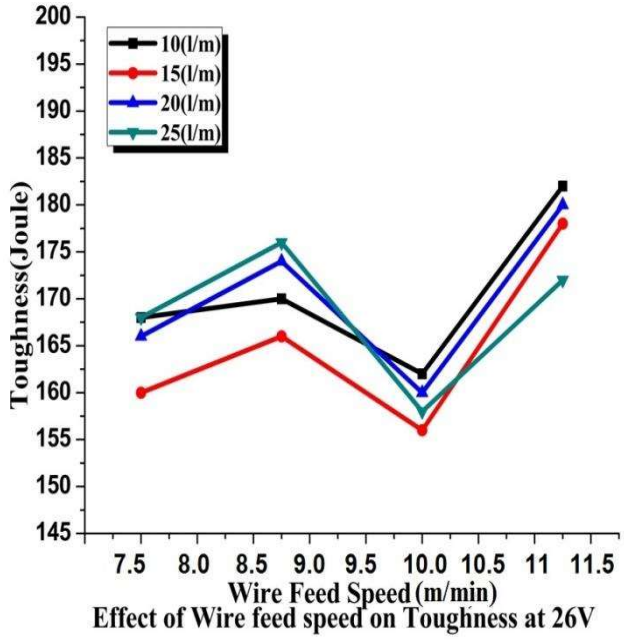

Figure 4.10 Effect of wire feed speed on toughness of IS 2062 steel at 26V with different shielding gas flow rate at 3.58 kJ/mm heat input

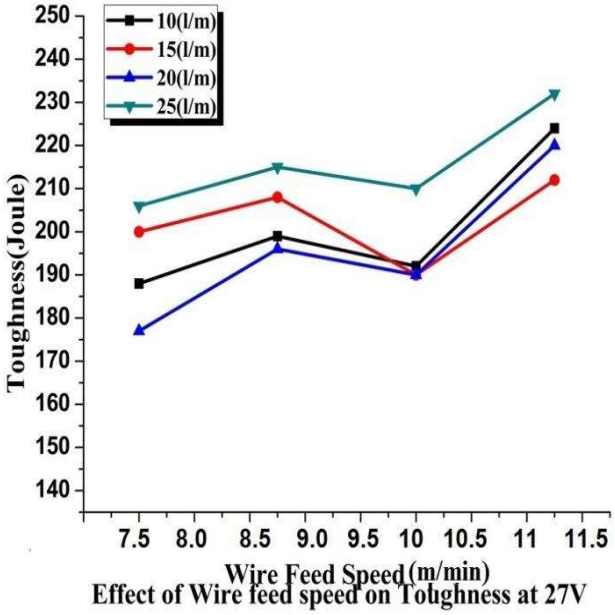

Figure 4.11 Effect of wire feed speed on toughness of IS 2062 steel at 27V with different shielding gas flow rate at 3.88 kJ/mm heat input

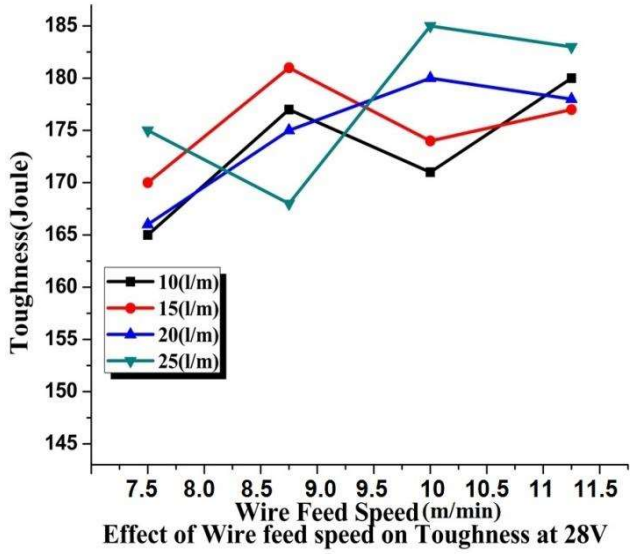

Figure 4.12 Effect of wire feed speed on toughness of IS 2062 steel at 28V with different shielding gas flow rate at 4.47 kJ/mm heat input

Figure 4.9 to 4.12 shows the effect of wire feed speed on Toughness of IS 2062 steel weldment test pieces and the voltage varies from 25 to 28V, and shielding gas flow rate varies from 10 to 25l/m at different heat input. Figure 4.9 is drowned for IS 2062 steel weldment at 25V, and at 10 to 25 l/m shielding gas flow rate at 3.22 kJ/mm heat input. From figure 4.9 it is clear that of weldment of IS 2062 steel is going to increases. Figure 4.10 to 4.12 at heat input 3.58 kJ/mm, 3.88Kj/mm, and 4.47 kJ/mm respectively shows the increasing trends in toughness of weldments. Figures reveal that on increasing the heat input toughness of weldment of IS 2062 steel increases.

Minghao SHI et al (2014) [97] welded low carbon steel and considered the heat input to determine the effect of heat input on toughness, and coarse gain in HAZ region and they observed from their results that best toughness (more than 100 j) was achieved at 1000 kJ/cm heat input with CGHAZ in this experimental work. Impact toughness of CGHAZ with 400 kJ/cm (230 j) was the maximum, as austenite grain size of CGHAZ with 400 kJ/cm favors the formation of AF inside the grain.

Wang Juan et al (2003) [98] determined the effect of heat inputs on the toughness of super high strength steel (HQ130) and they stated that Impact energy in the HAZ of HQ130 steel decreases when the weld heat input (E) changed from 9×2 kJ/cm to 26×4 kJ/cm. In order to ensure

toughness, the weld heat input should be strictly less than or equal to 20 kJ/cm. They also mentioned in their results that carbide from HAZ can be removed, by controlling the heat input and microstructure can be assured.

Abd El Fattah Mustafa Khurshid, Mohamed Ahmed Ghanem (2013) [99] calculated the effect of heat input on the toughness and strength of LNG storage tank welded joint and they observed from their results that at low heat input toughness, and strength of welded joint improves. They also observed that on moderate cooling in HAZ region producing the fine grain structure.

N. Ramasamy and R. Kathiravan (2017) [100] determined the effect of welding heat input on toughness, and microstructure of High Strength Low carbon steel weldments and they found that toughness of HAZ region was not monotonously enhanced with the increase of heat input. They also claimed that on increasing the heat input restrained the development of martensite, and promoted the conversion of martensite to bainite. When the heat input was 0.67 kJ/mm, the microstructure in HAZ was found fine lower bainite with some part of acicular ferrite, and upper bainite was formed in HAZ when heat input was 0.77 kJ/mm.

4.4 Effect of wire feed speed, and shielding gas flow rate on microhardness (VHN)

Effect of wire feed speed on Vickers hardness from 25-28V at 10-25 l/m

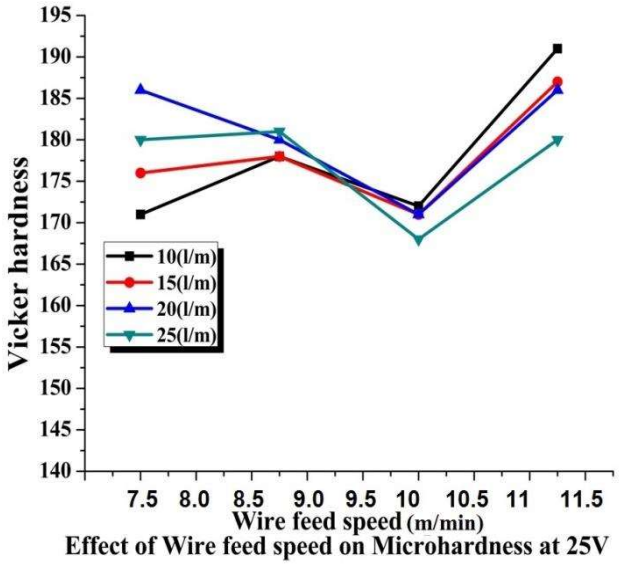

Figure 4.13 Effect of wire feed speed on microhardness (VHN) of IS 2062 steel at 25V with different shielding gas flow rate at 3.22 kJ/mm heat input

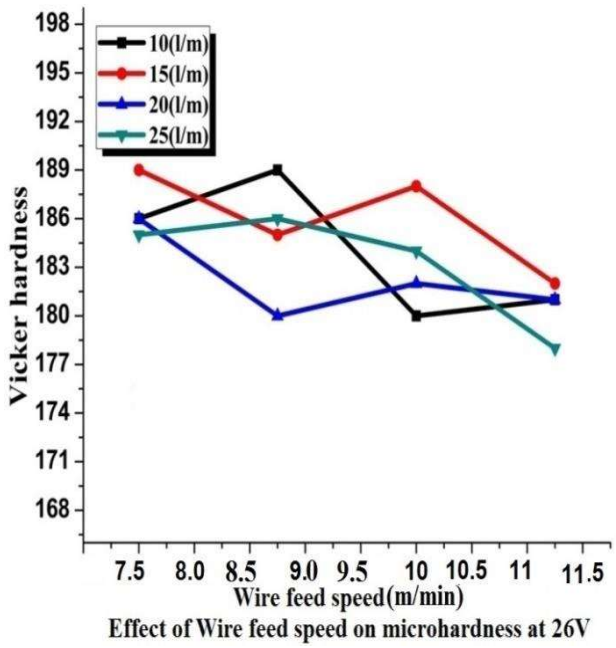

Figure 4.14 Effect of wire feed speed on microhardness (VHN) of IS 2062 steel at 26V with different shielding gas flow rate at 3.58 kJ/mm heat input

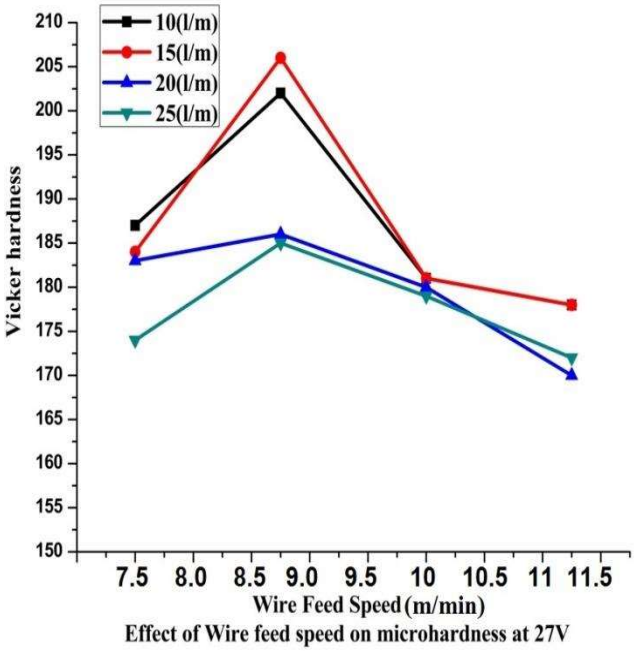

Figure 4.15 Effect of wire feed speed on microhardness (VHN) of IS 2062 steel at 27V with different shielding gas flow rate at 3.88 kJ/mm heat input

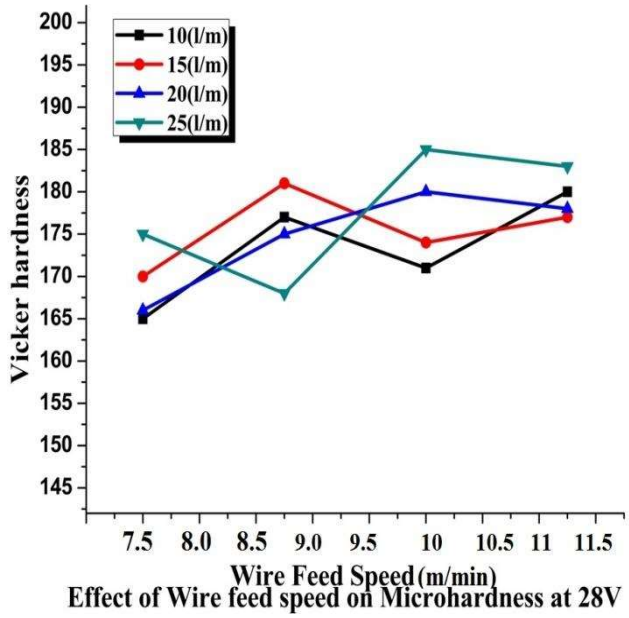

Figure 4.16 Effect of wire feed speed on microhardness (VHN) of IS 2062 steel at 28V with different shielding gas flow rate at 4.47 kJ/mm heat input

Figure 4.13 to 4.16 shows the effect of wire feed speed on microhardness (VHN) of IS 2062 steel weldment test pieces, and the voltage varies from 25 to 28V, and shielding gas flow rate varies from 10 to 25l/m at different heat input. Figure 4.13 is plotted for IS 2062 steel weldment at 25V, and at 10 to 25 l/m shielding gas flow rate at 3.22 kJ/mm heat input. Figure 4.13 reveals that weldment of IS 2062 steel first decreases and then increases. Figure 4.14 to 4.15 at heat input 3.58 kJ/mm, 3.88kj/mm goes to decreasing, while at 4.47 kJ/mm heat input increases. Heat input is primary factors which affect the hardness of weldment [101]. Grains formed at faster cooling rate are greatly finers as compare to slow cooling rate, and low heat input and higher cooling rate results in fine grain size in HAZ region and causes the higher hardness[102].

Wan Shaiful Hasrizam Wan Muda et al (2015) [33] calculated the effect of heat input on mechanical properties, and microstructure of ABS A grade steel. For experimental purpose they considered the three heat input I,e low heat 0.99 kJ/mm, medium heat 1.22 kJ/mm and high heat 2.25 kJ/mm and they concluded that higher the heat input, the lower the hardness value at CGHAZ. Retention of heat in the CGHAZ zone contributes to lower the hardness value. Higher the grain size, the lower value of the hardness and toughness. They also mentioned in their results that higher the input, the coarse the microstructure.

Anna Unt and Antti Salminen (2015) [103] investigated the effect of welding parameters, and the heat input on weld bead profile of structural steel and they told that the hardness, measured from the fusion lines of the weld, was rather the same throughout the test piece thickness.

Ehsan Gharibshahiyan et al (2011) [31] they observed that on elevation of heat input reduced the hardness in the HAZ, for instance, increasing the heat input from 5 to 8 kJ/cm decreased the hardness value from 160 to 148 HBN, which reveal that on increasing the heat input decreases the hardness (VHN). They also added that high heat input led to grain coarsening which was more pronounced in the HAZ, as well as reducing the toughness value of weldment.

4.5 Effect of voltage, wire feed speed, and shielding gas flow rate on % age elongation

Effect of wire feed speed on % age elongation from 25-28V at 10-25 l/m

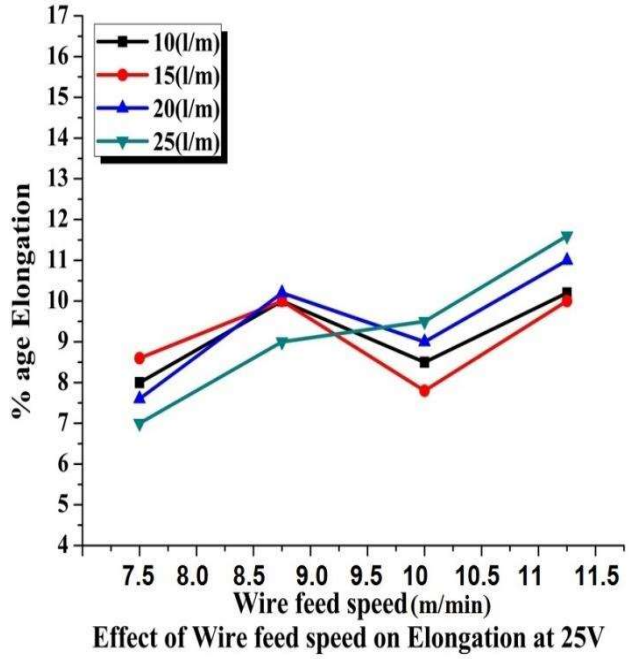

Figure 4.17 Effect of wire feed speed on % age elongation of IS 2062 steel at 25V with different shielding gas flow rate at 3.22 kJ/mm heat input

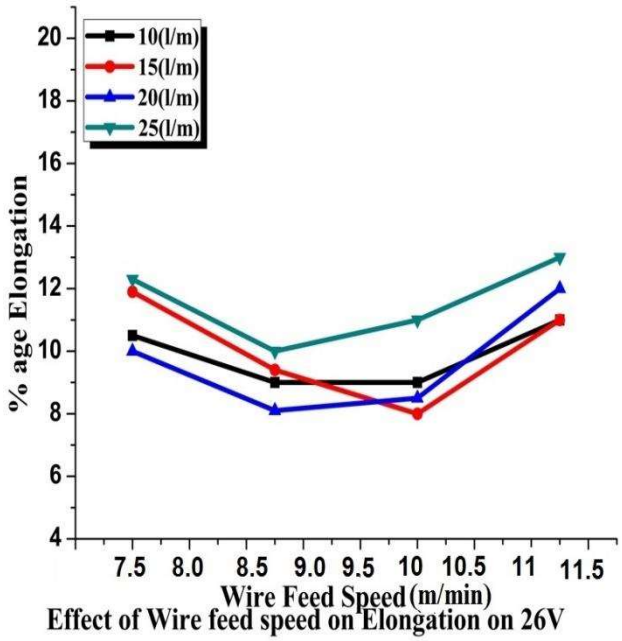

Figure 4.18 Effect of wire feed speed on % age elongation of IS 2062 steel at 26V with different shielding gas flow rate at 3.58 kJ/mm heat input

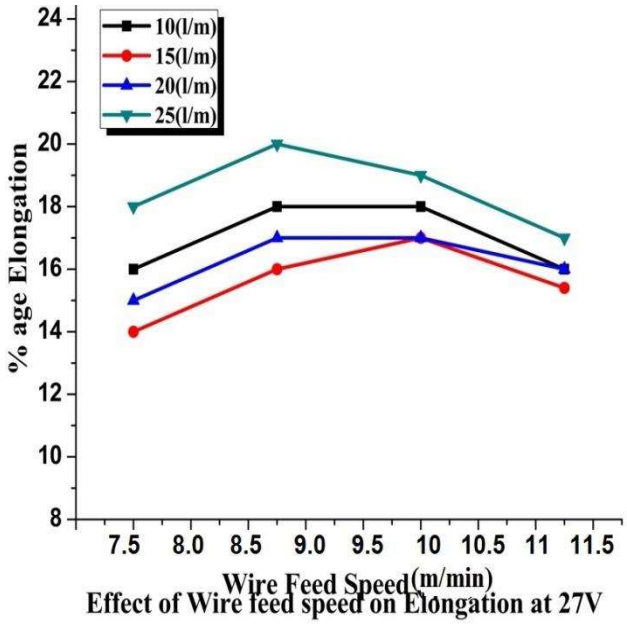

Figure 4.19 Effect of wire feed speed on % age elongation of IS 2062 steel at 27V with different shielding gas flow rate at 3.88 kJ/mm heat input

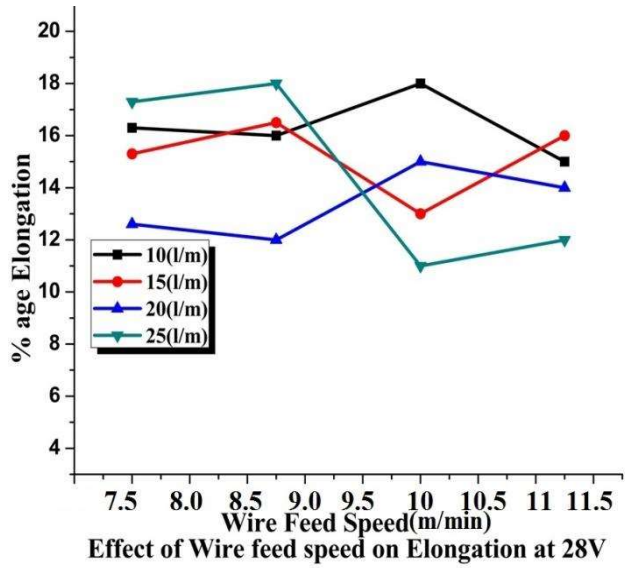

Figure 4.20 Effect of wire feed speed on % age elongation of IS 2062 steel at 28V with different shielding gas flow rate at 4.47 kJ/mm heat input

Figure 4.17 to 4.20 represents the effect of wire feed speed on % age elongation of IS 2062 steel weldment test pieces, and the voltage varies from 25 to 28V, and shielding gas flow rate varies from 10 to 25 l/m at different heat input. Figure 4.17 is drowned for IS 2062 steel weldment at 25V, and at 10 to 25 l/m shielding gas flow rate at 3.22 kJ/mm heat input. Figure 4.17 reveals that elongation of IS 2062 steel weldment first decreases and then increases. Figure 4.18 also having the increasing trends in heat input 3.58 kJ/mm, while figure 4.19 and 4.20 having the decreasing trends of elongation at 3.88 kJ/mm and 4.47 kJ/mm heat input respectively. Hardness and tensile strength of a weldment have an inverse correlation with the quantity of acicular ferrite in lath martensite in the microstructure. The toughness of weldment increases principally with increasing the amount of acicular ferrite in the weldment.

The results of table A-1 to A-8 listed in appendix-A were plotted in figure 4.1 to 4.20. To evaluate the effect of GMA welding process parameters I,e heat input on mechanical properties, and microstructure, the test specimen exposed to mechanical and metallurgical examinations. The differences in mechanical properties were correlated with microstructural variations associated with the different welding conditions. Figure 4.23 to 4.37 depicts the microstructure photograph of IS 2062 steel weldments under different welding conditions, while figure 4.59 to 4.67 shows the microstructure photograph of AISI 304 steel weldments. From the literature review, it is very

clear those mechanical properties of weldments to much effect by the microstructure of weldments.

4.6 Microstructure photograph of base metals

It is well known that the mechanical properties of a weldment are influenced by the microstructure. Therefore during this experimental work, investigation of the microstructure of IS 2062 steel and AISI 304 steel weldment have been correlated with mechanical properties of IS 2062 and AISI 304 steel weldment. Figure 4.15 and 4.16 represent the microstructure of IS 2062 and AISI 304 steel base metals, respectively.

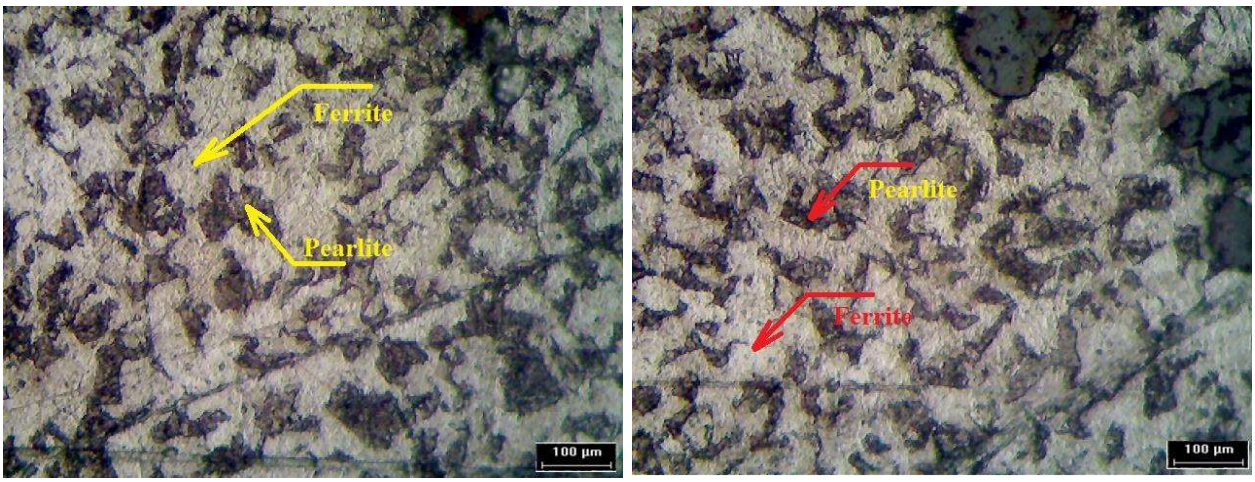

(a) (b)

Figure 4.21 Optical micrograph as –received IS 2062 steel.

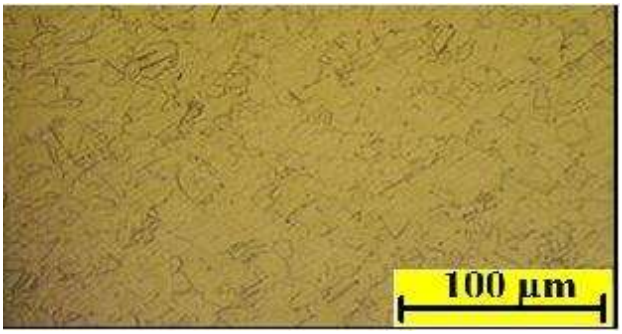

Figure 4.22 Optical micrograph as –received AISI 304 steel

4.7 Microstructure photograph of IS 2062 steel weldments

Figure 4.23 to 4.55 represents the microstructure photographs of IS 2062 steel weldments prepared under different welding conditions and figure 4.23 to 4.37 represents the microstructure photographs of AISI 304 steel weldments prepared under different welding conditions.

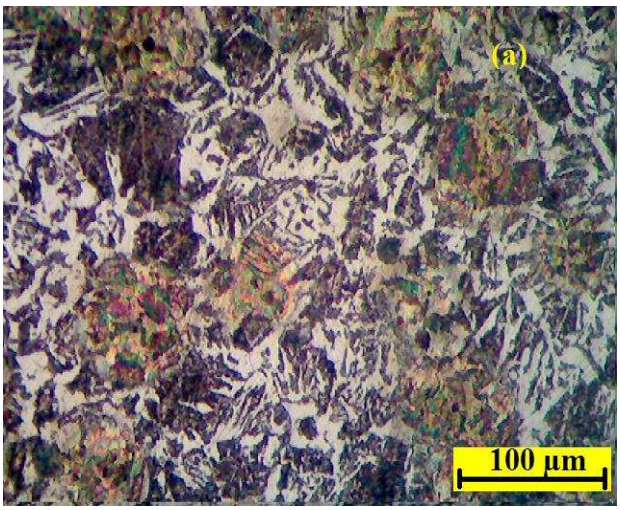

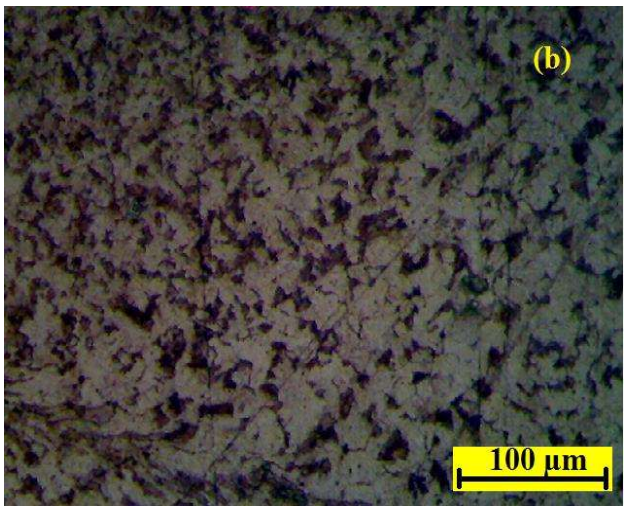

The microstructure having ferrite and pearlite

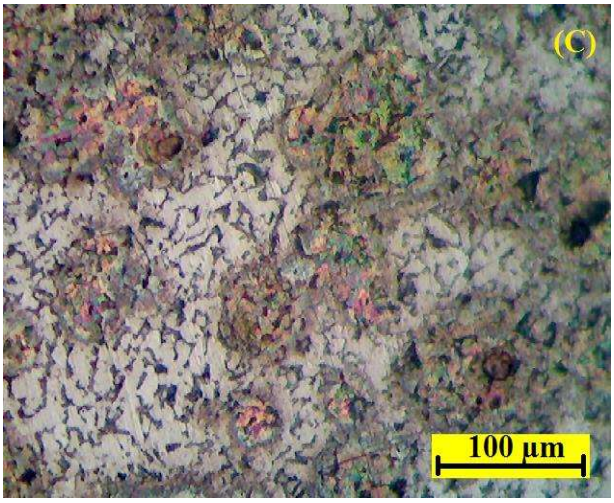

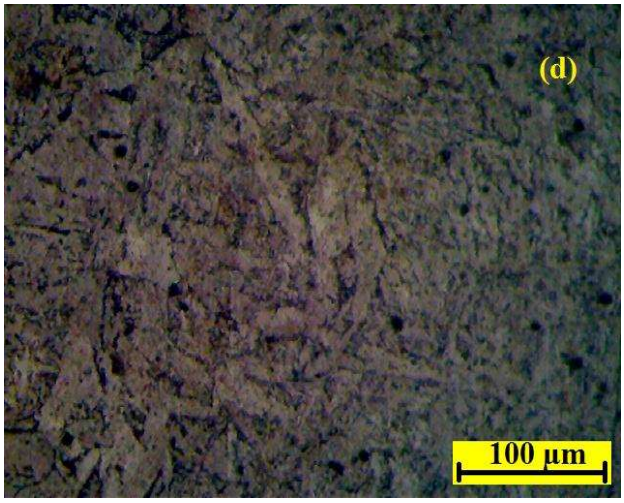

Grain size 46.1µm Grain size 39.8 µm

The microstructure having ferrite plus pearlite.

Figure 4.23(a-d) microstructure photograph of heat affected zone (HAZ) of IS 2062 steel weldment at 10-25 l/m shielding gas flow rate, at 7.62 m/min produced at 3.22 kJ/mm heat input

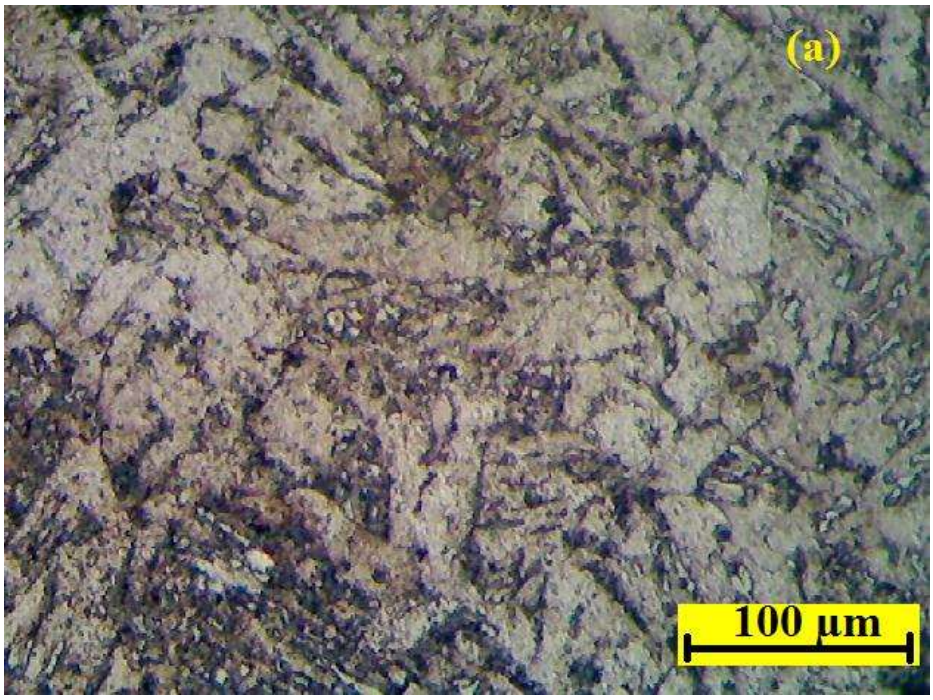

Grain size 39.4 µm

The microstructure of coarse grain heat affected zone (CGHAZ) with ferrite and pearlite

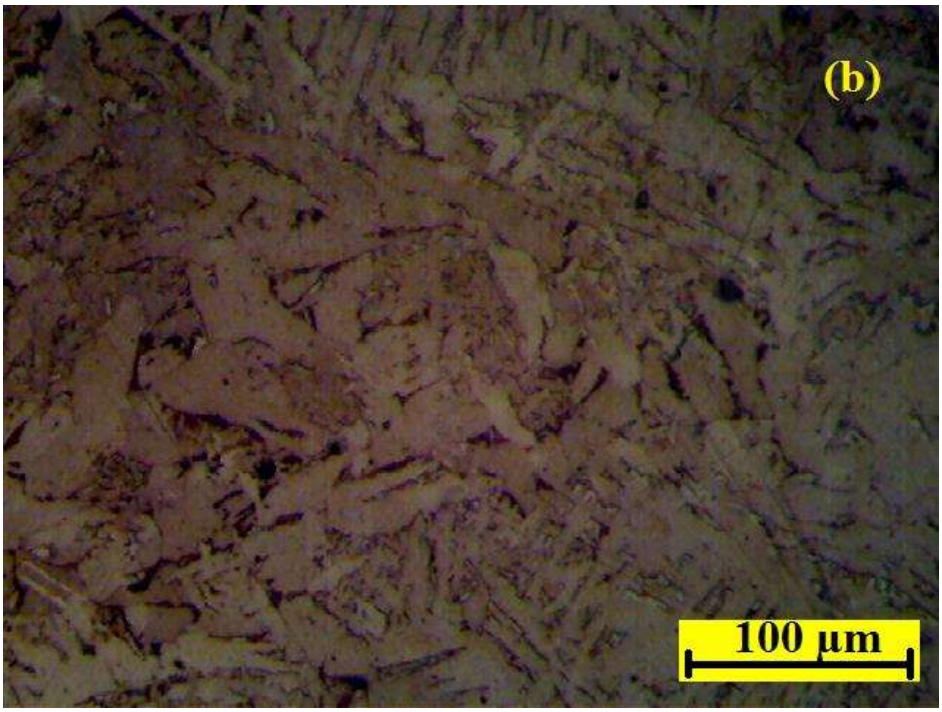

Grain size 34.4µm

The microstructure of coarse grain heat affected zone (CGHAZ) with bainite

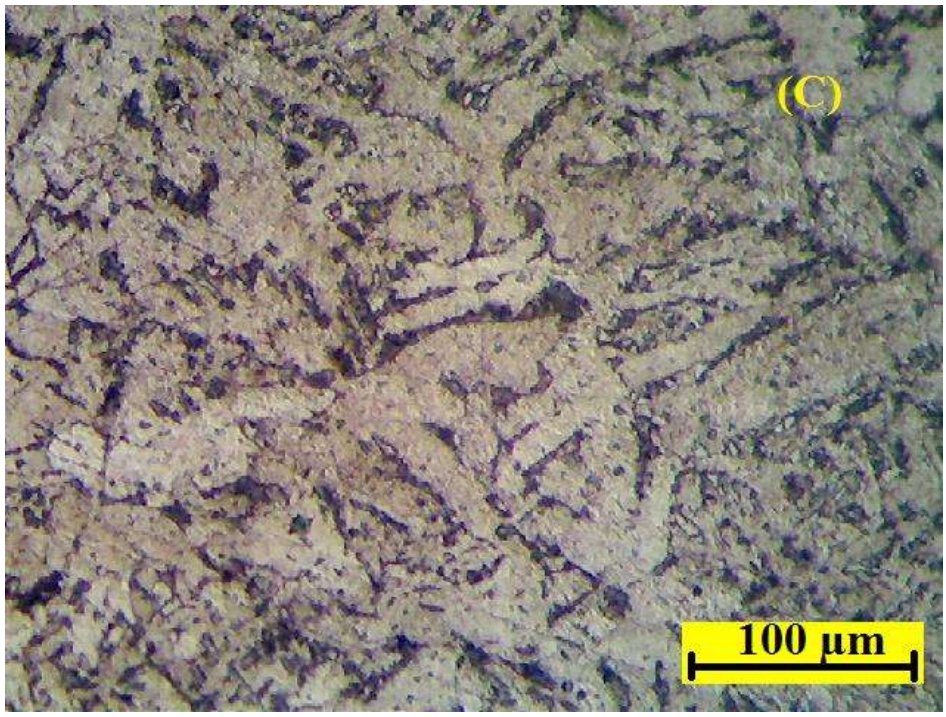

Grain size 41.7µm

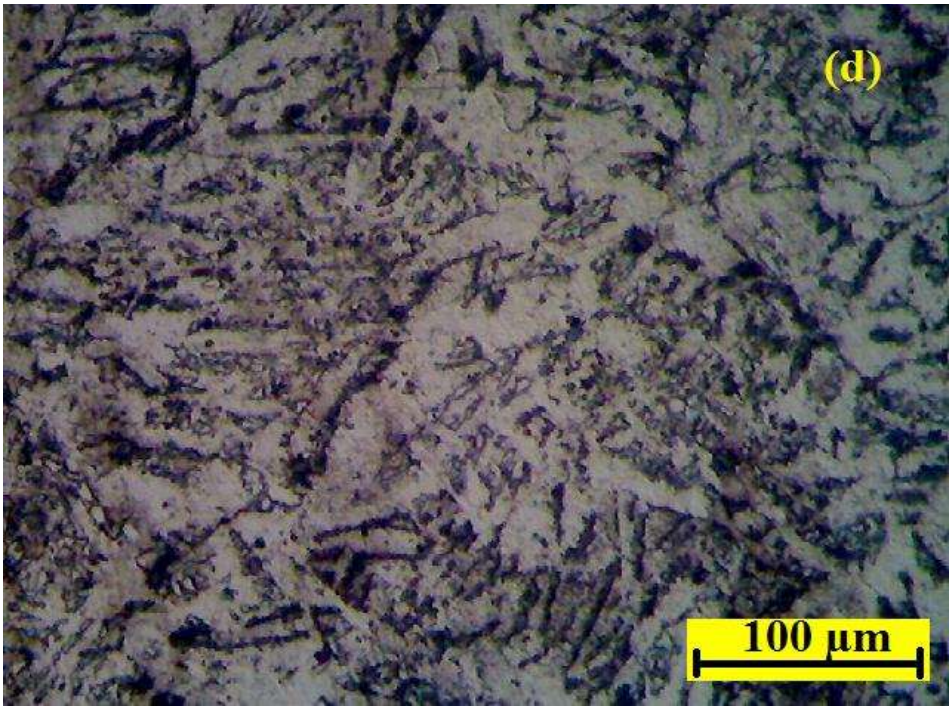

Grain size 29.6µm

Figure 4.24(a-d) microstructure photograph of heat affected zone (HAZ) of IS 2062 steel weldment at 10-25 l/m shielding gas flow rate, at 8.89 m/min produced at 3.22 kJ/mm heat input

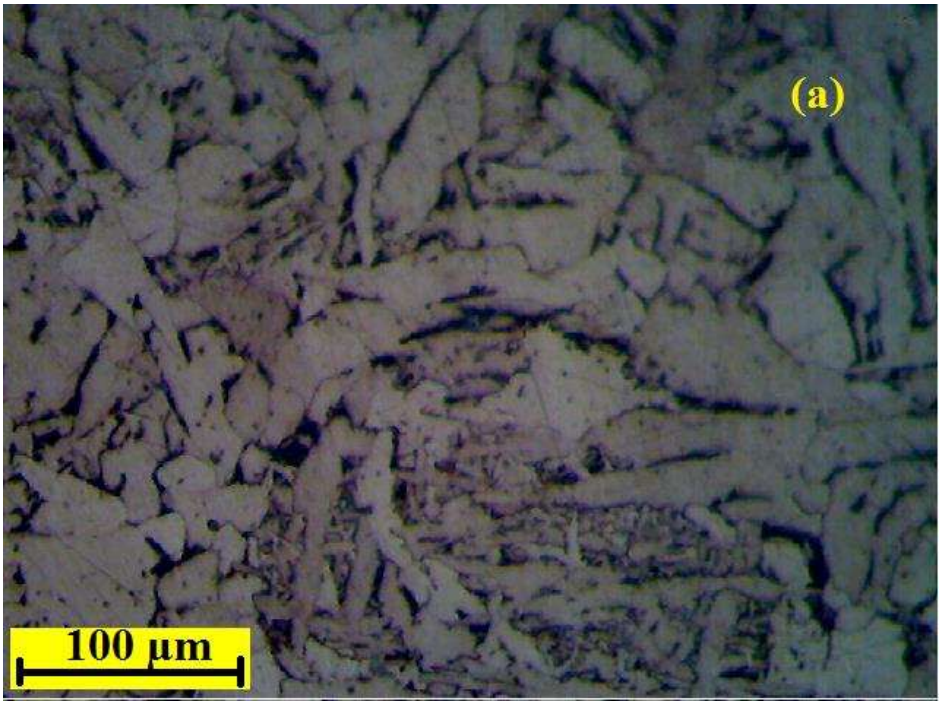

Grain size 35.4µm

The microstructure of coarse grain heat affected zone (CGHAZ) with bainite.

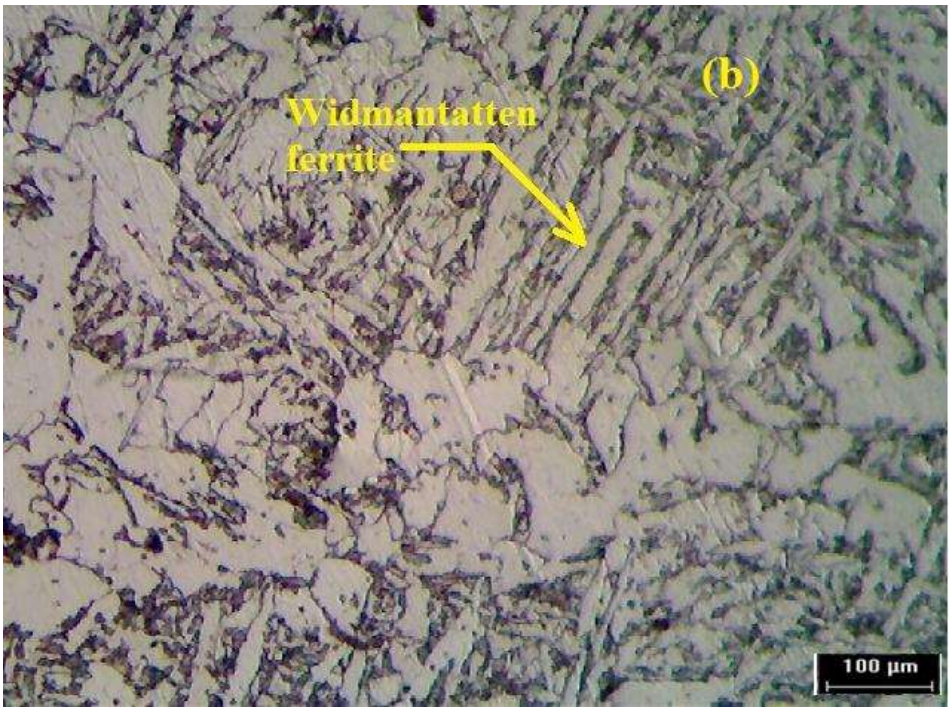

Grain size 33.1µm

The microstructure of coarse grain heat affected zone (CGHAZ) steel weldment with widsmantatten ferrite.

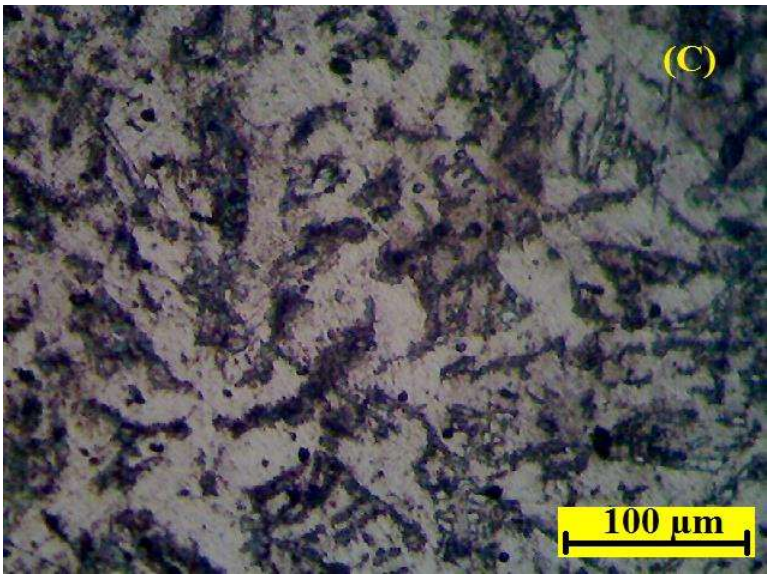

Grain size 28.4µm

The microstructure of coarse grain heat affected zone (CGHAZ) steel weldment with ferrite and pearlite

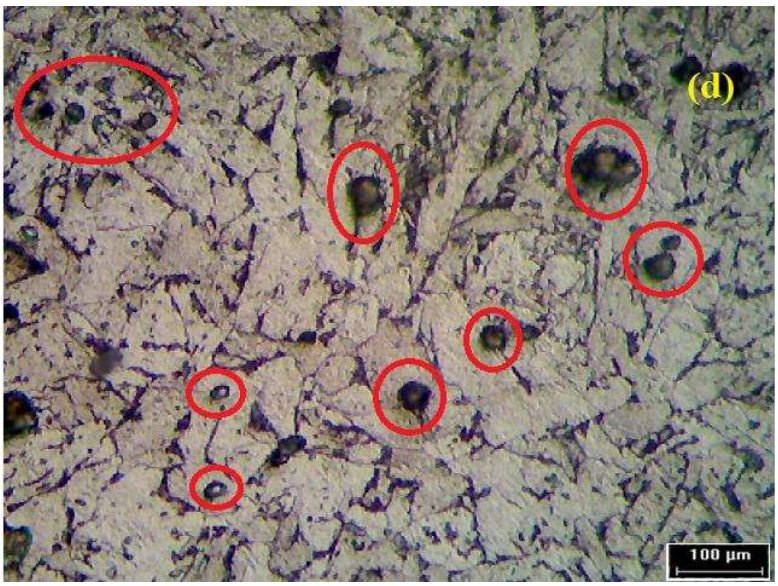

Grain size 38.4µm

The microstructure of coarse grain heat affected zone (CGHAZ) having inclusion. A large number of the inclusions exhibit surface cavities or voids, which are thought to be the result of gas evolution (e.g., hydrogen) or solidification contraction.

Figure 4.25(a-d) microstructure photograph of heat affected zone (HAZ) of IS 2062 steel weldment at 10-25 l/m shielding gas flow rate, at 10.16 m/min produced at 3.22 kJ/mm heat input

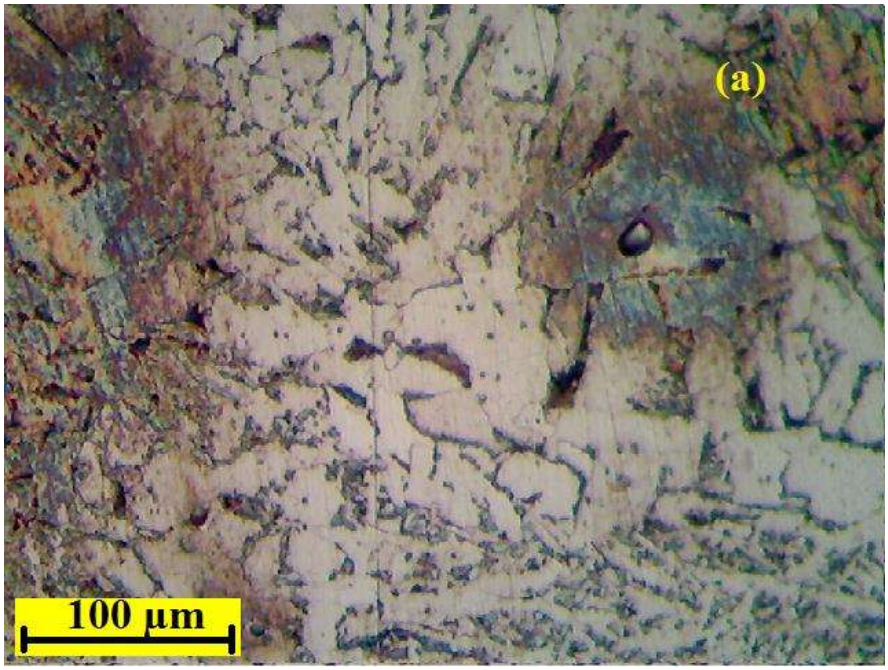

Grain size 39.9 µm

Microstructure of coarse grain heat affected zone (CGHAZ) steel weldment with a little amount of widsmantatten ferrite

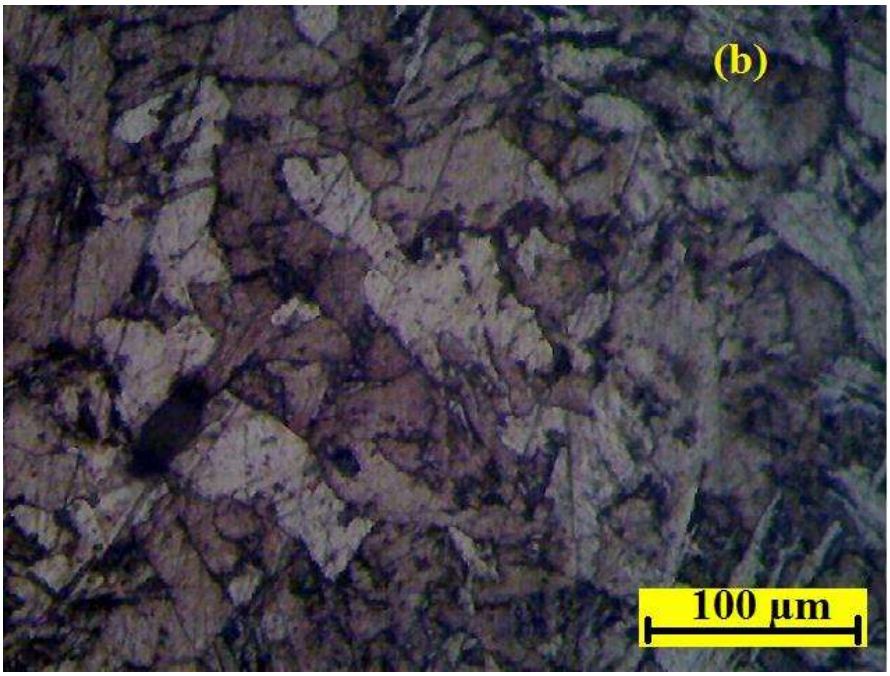

Grain size 35.4µm

The microstructure of coarse grain heat affected zone (CGHAZ) steel weldment with polygonal ferrite and pearlite

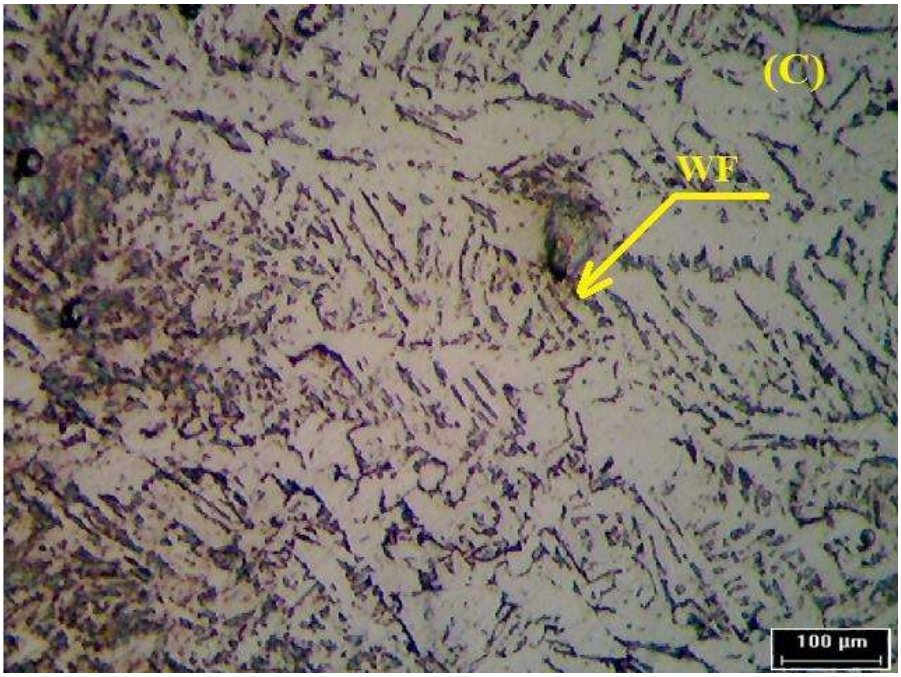

Grain size 40.2µm

The microstructure of heat affected zone (HAZ) of IS 2062 steel weldment having widmanstatten ferrite

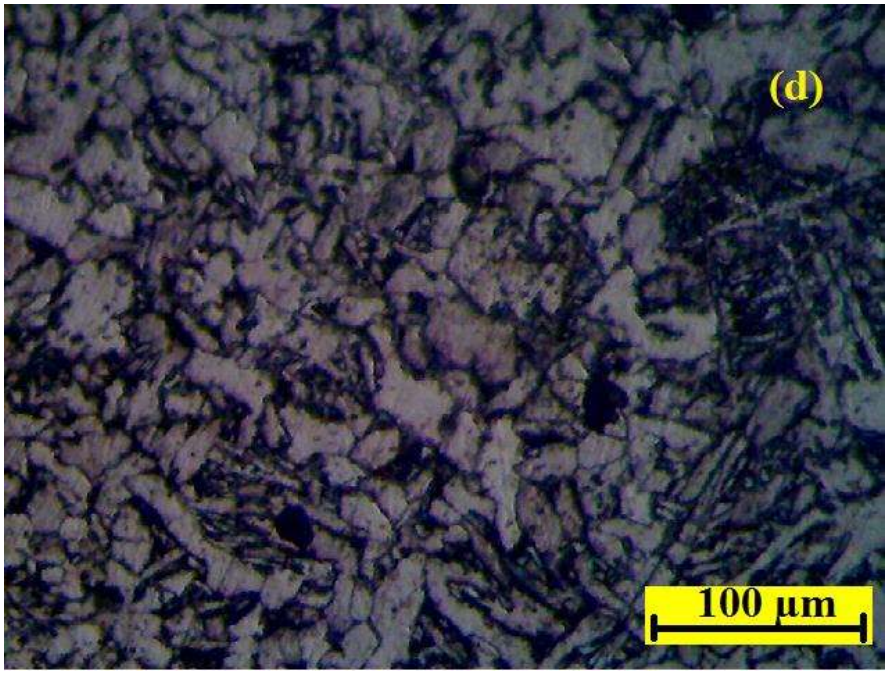

Grain size 38.4µm

Figure 4.26(a-d) microstructure photograph of heat affected zone (HAZ) of IS 2062 steel weldment at 10-25 l/m shielding gas flow rate, at 11.43 m/min produced at 3.22 kJ/mm heat input

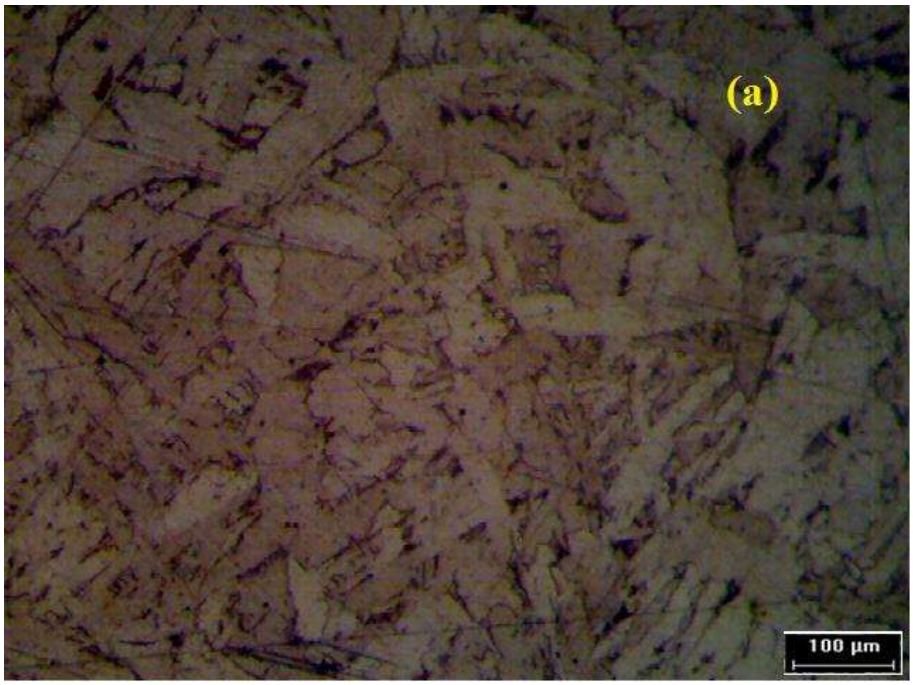

Grain size 40.2µm

The microstructure of coarse grain heat affected zone (CGHAZ) of IS 2062 steel weldment

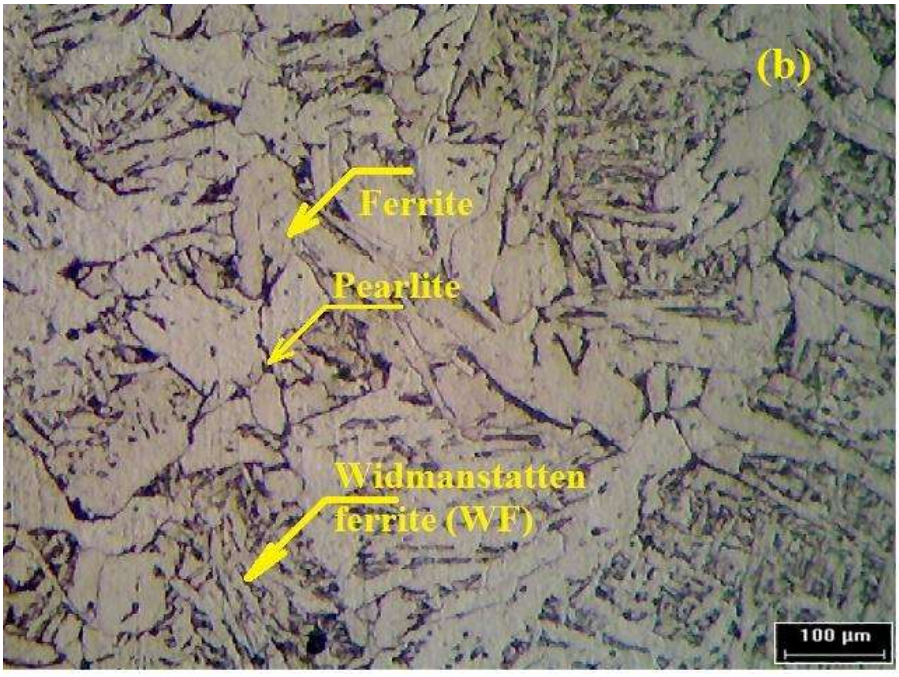

Grain size 42.3µm

The microstructure of heat affected zone (HAZ) of IS 2062 steel weldment with ferrite (White), pearlite (Black), widmanstatten ferrite, and bainite.

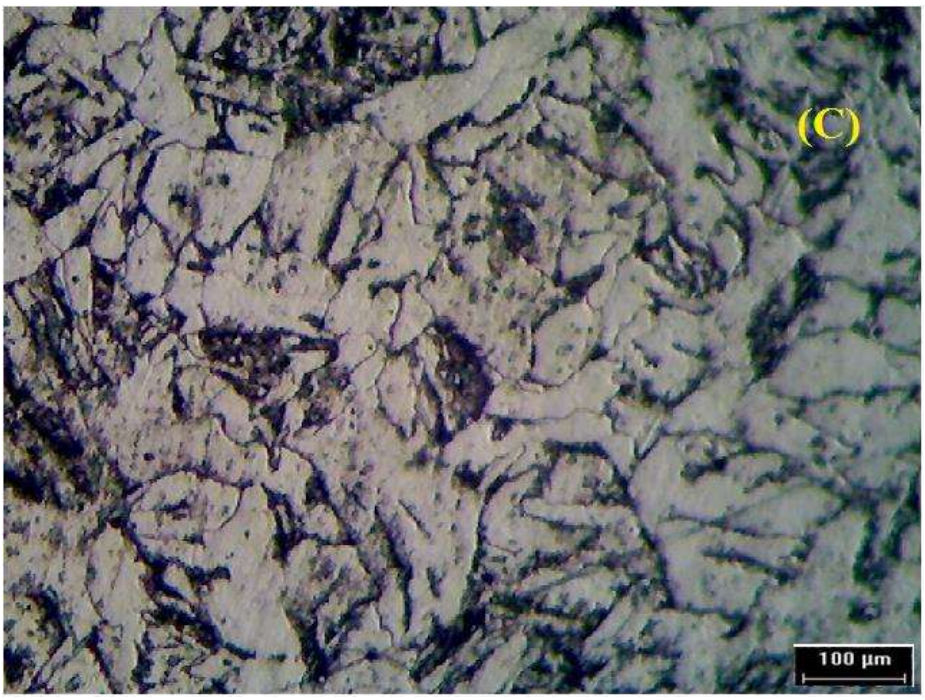

Grain size 40.2µm

The microstructure of coarse grain heat affected zone (CGHAZ) of IS 2062 steel weldment with ferrite, pearlite, and widmanstatten ferrite

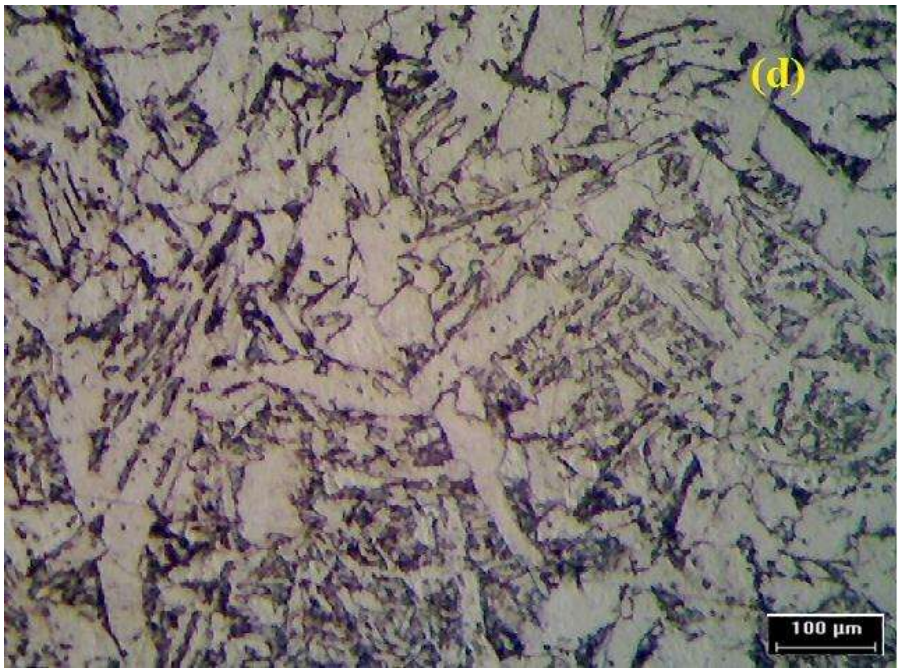

Grain size 39.8µm

Figure 4.27(a-d) microstructure photograph of heat affected zone (HAZ) of IS 2062 steel weldment at 10-25 l/m shielding gas flow rate, at 7.62 m/min produced at 3.58 kJ/mm heat input

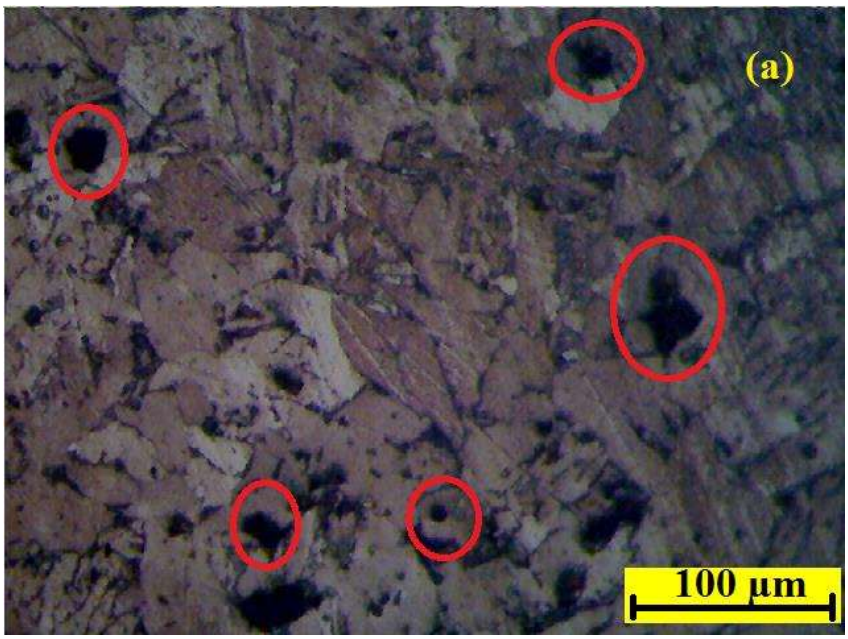

Grain size 30.4µm

The microstructure of heat affected zone (HAZ) of IS 2062 steel weldment with porosity. A large number of the inclusions exhibit surface cavities or voids, which are thought to be the result of gas evolution (e.g., hydrogen) or solidification contraction.

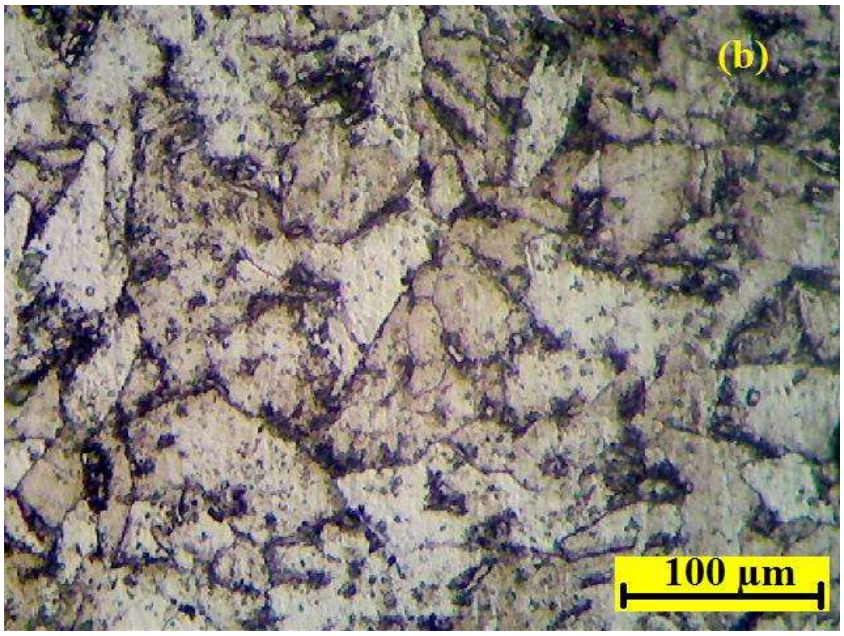

Grain size 42.1µm

The microstructure of coarse grain of IS 2062 steel weldment (WM) with polygonal ferrite and little amount of pearlite.

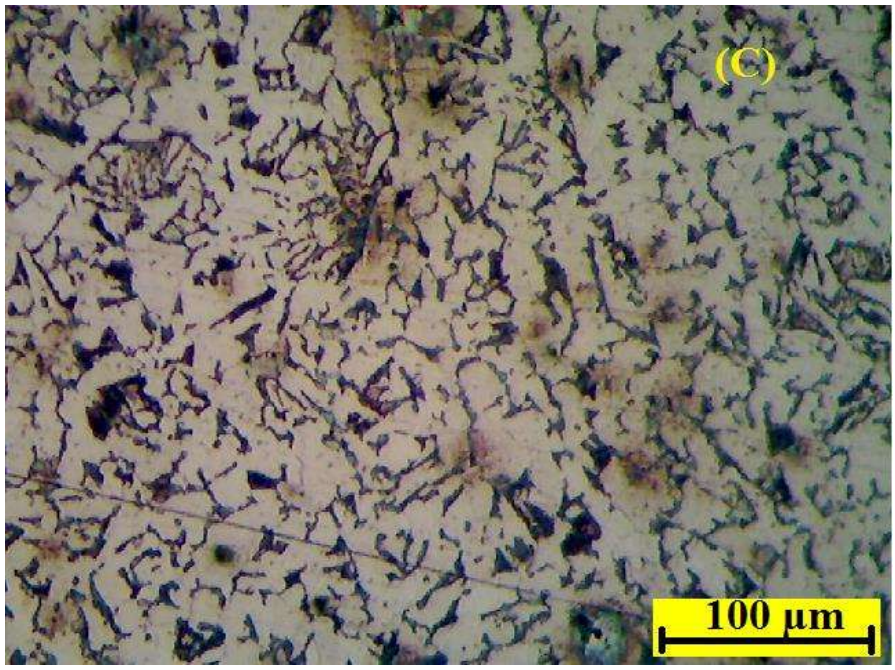

Grain size 26.5µm

The microstructure of fine grain (FGHAZ) of IS 2062 steel weldment with ferrite (White) and pearlite (Black)

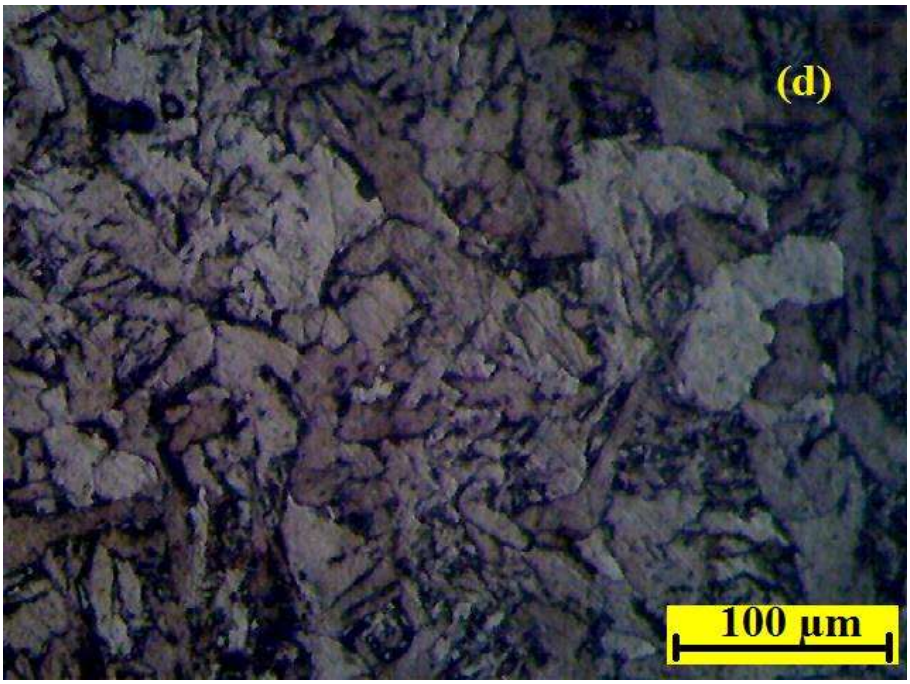

Grain size 31.2µm

Figure 4.28(a-d) microstructure photograph of heat affected zone (HAZ) of IS 2062 steel weldment at 10-25 l/m shielding gas flow rate, at 8.89 m/min produced at 3.58 kJ/mm heat input

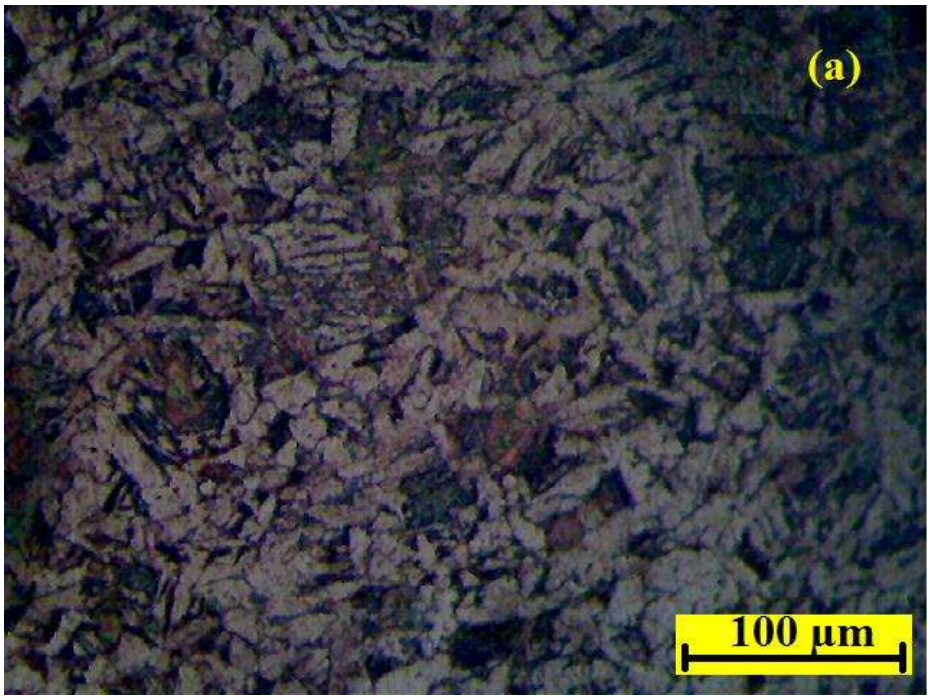

Grain size 26.7µm

The microstructure of fine grain (FG) of IS 2062 steel weldment with ferrite (White) and pearlite (Black)

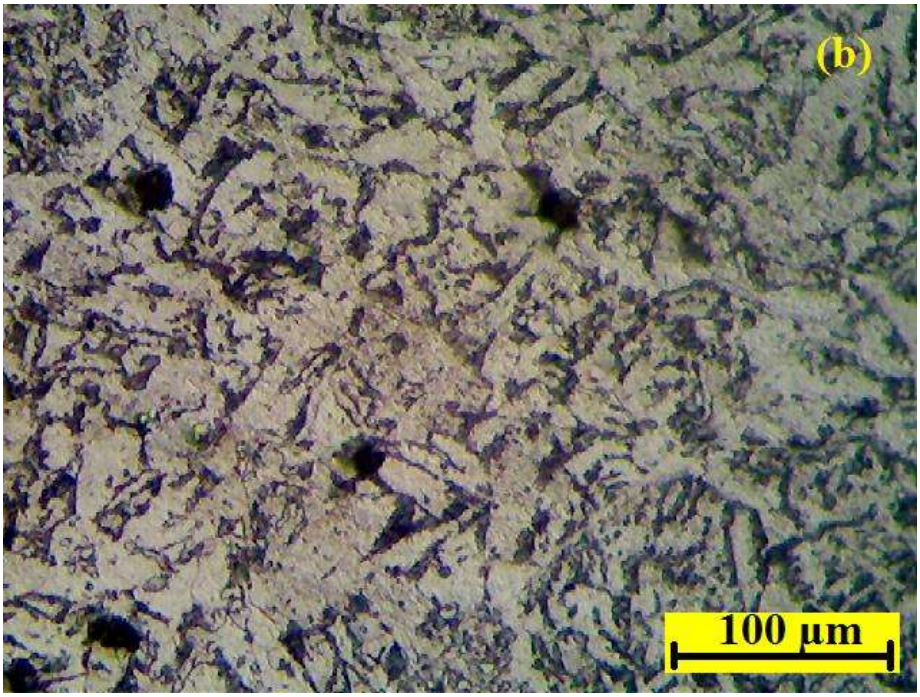

Grain size 28.9µm

The microstructure of fine grain (FG) of IS 2062 steel weldment with little widmanstatten ferrite

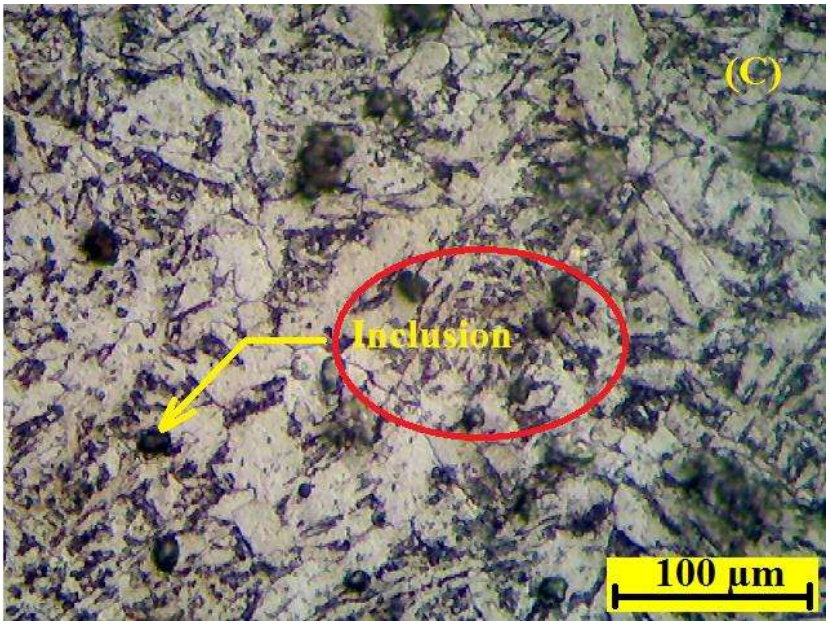

Grain size 32.7µm

The microstructure of fine grain (FGHAZ) of IS 2062 steel weldment with ferrite, pearlite, little bainite, and the inclusions appear to be completely randomly disturbed through the microsturcutre.Small size of inclusion found in weldment due to slow speed of wire feed.

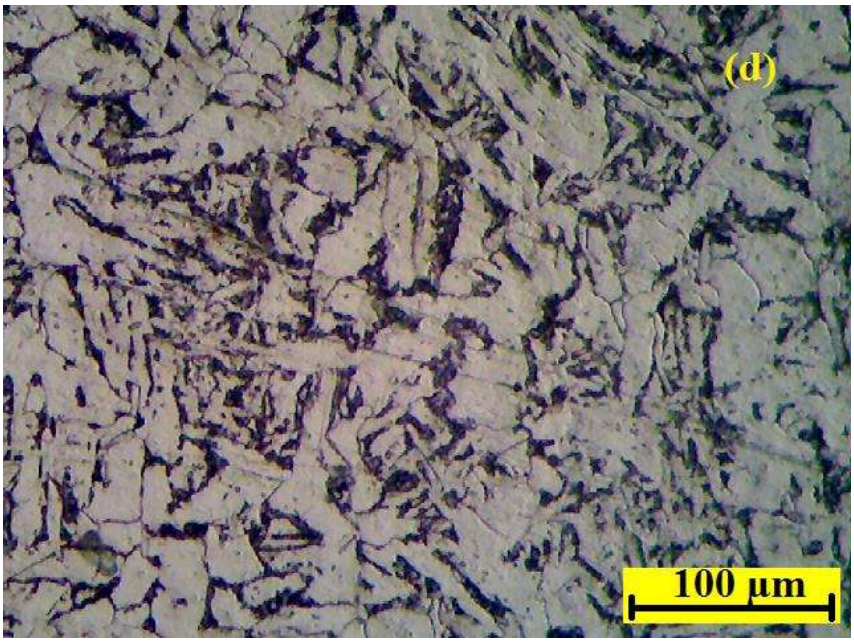

Grain size 40.1µm

Figure 4.29(a-d) microstructure photograph of heat affected zone (HAZ) of IS 2062 steel weldment at 10-25 l/m shielding gas flow rate, at 10.16 m/min produced at 3.58 kJ/mm heat input

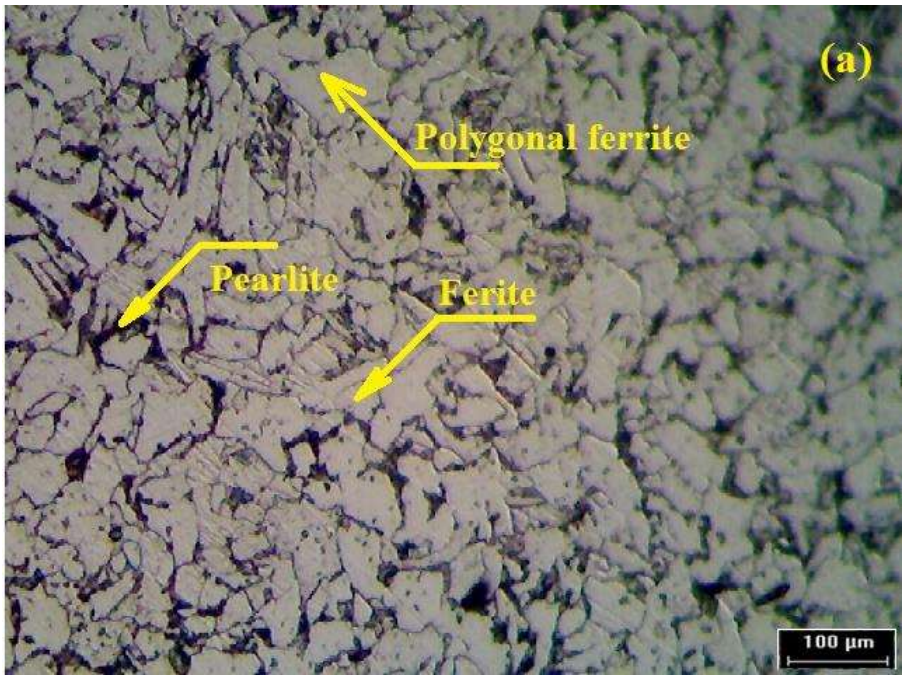

Grain size 24.3µm

The microstructure of fine grain heat affected zone (FGHAZ) steel weldment with polygonal ferrite, ferrite, and little pearlite.

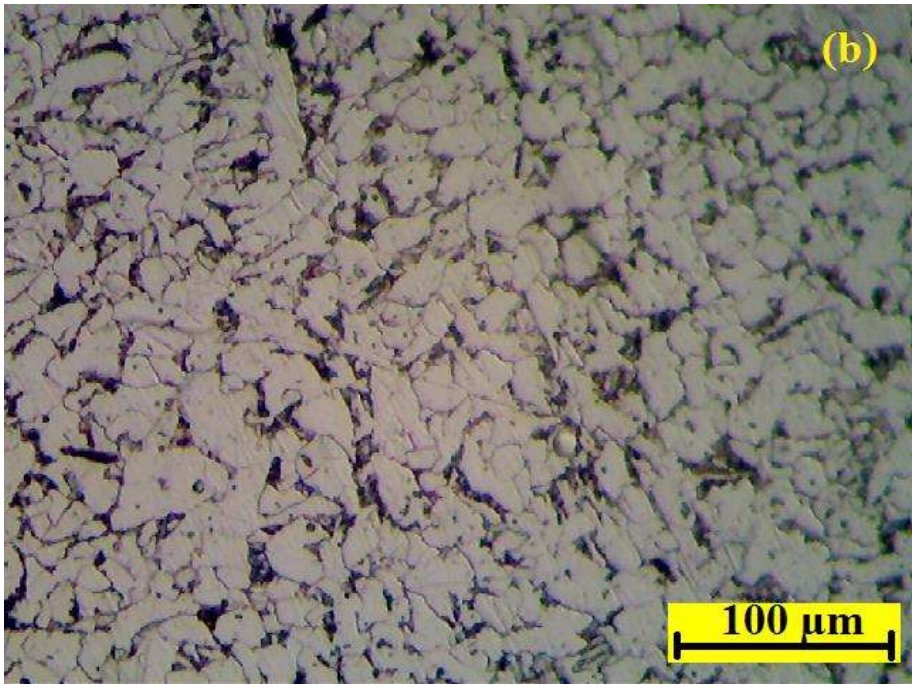

Grain size 21.4µm

The microstructure of fine grain heat affected zone (FGHAZ) steel weldment with ferrite and little amount of pearlite.

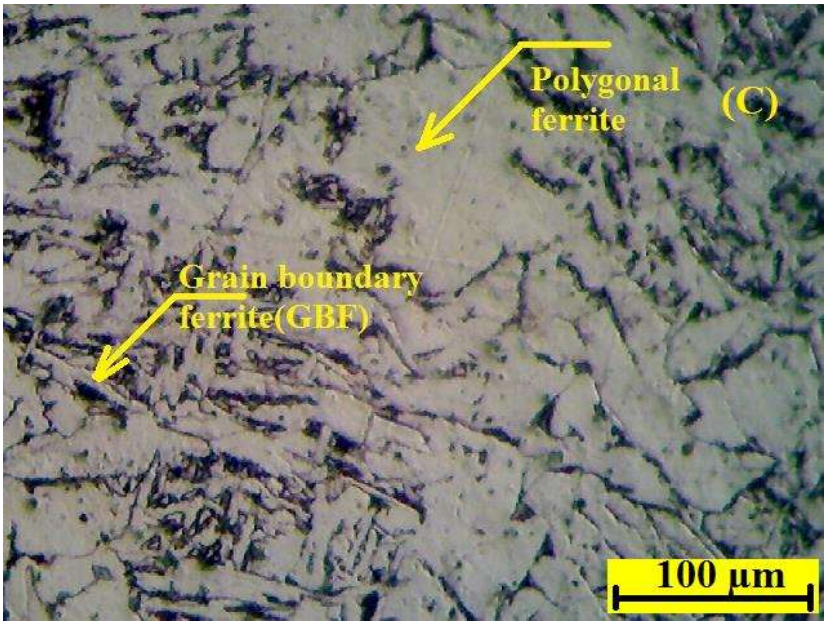

Grain size 46.2µm

The microstructure of CGHAZ of IS 2062 steel weldment with polygonal ferrite, and grain boundary ferrite

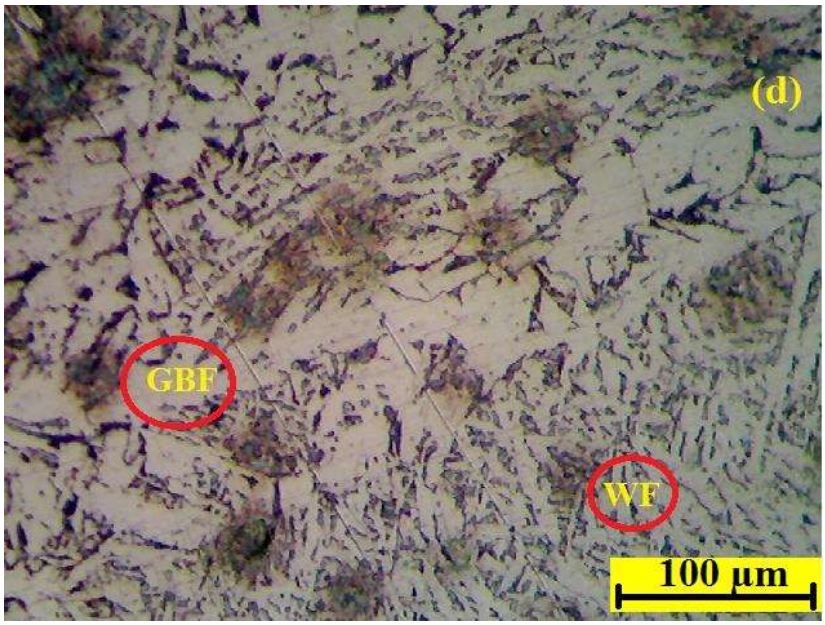

Grain size 28.3µm

The microstructure of CGHAZ of IS 2062 steel weldment with grain boundary ferrite and widmanstatten ferrite

Figure 4.30(a-d) microstructure photograph of heat affected zone (HAZ) of IS 2062 steel weldment at 10-25 l/m shielding gas flow rate, at 11.43 m/min produced at 3.58 kJ/mm heat input

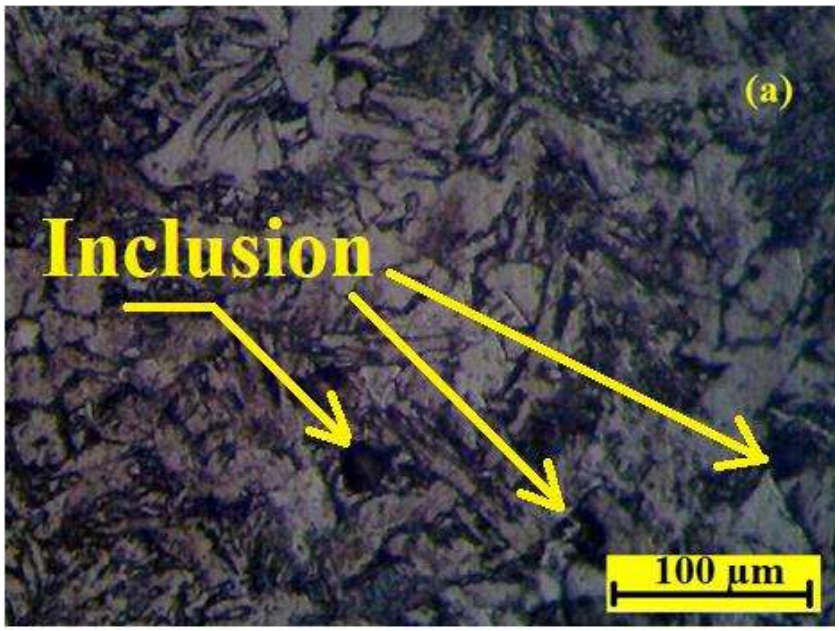

Grain size 32.4µm

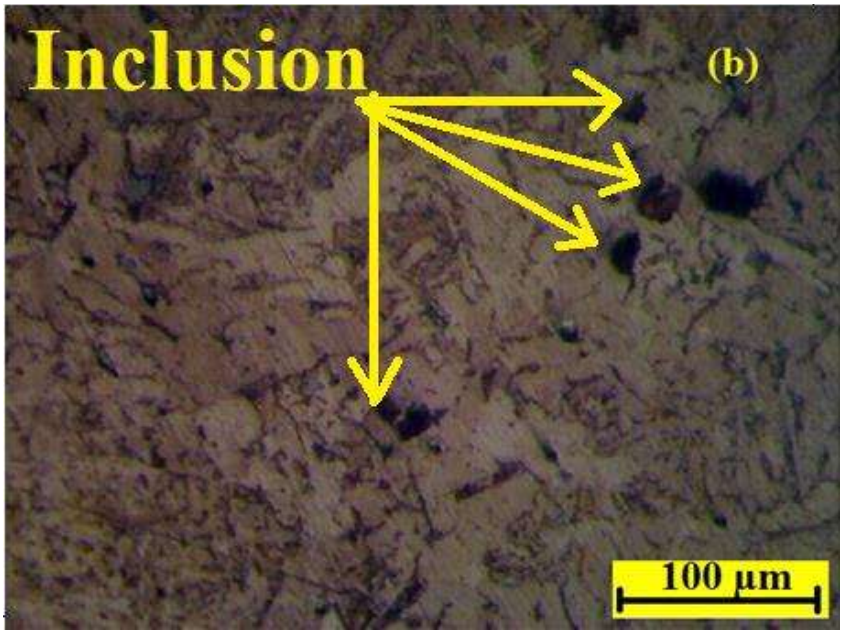

Grain size 39.1µm

In fig (a) and (b) there are inclusion are presents in the microstructure. Inclusions are in larger in size and randomly distributed. The large size of inclusion are formed due to large amount of O_2 presence of weld and Oxide inclusions considered to be the basic reasons for higher toughness as it promotes accicular ferrite. Large size of inclusion in weldment occurs due to high wire feed speed.

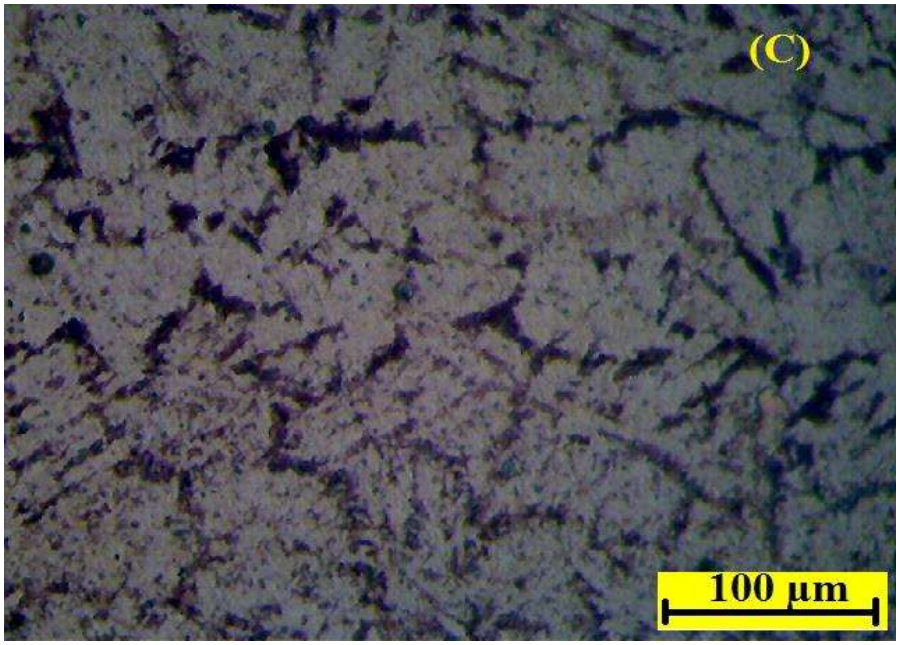

Grain size 44.6µm

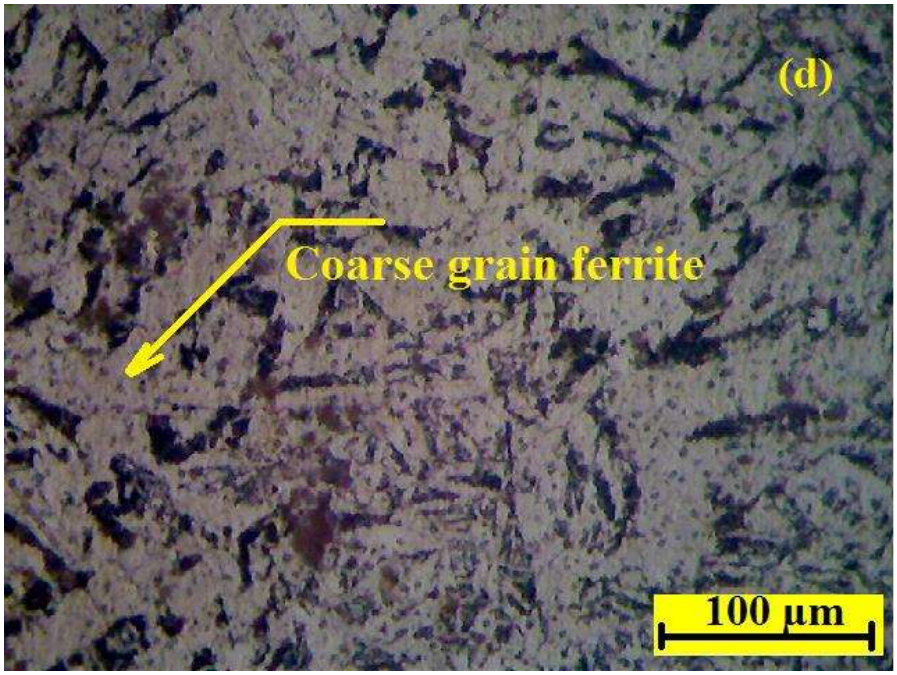

Grain size 45.6µm

Figure 4.31(a-d) microstructure photograph of heat affected zone (HAZ) of IS 2062 steel weldment at 10-25 l/m shielding gas flow rate, at 7.62 m/min produced at 3.88 kJ/mm heat input

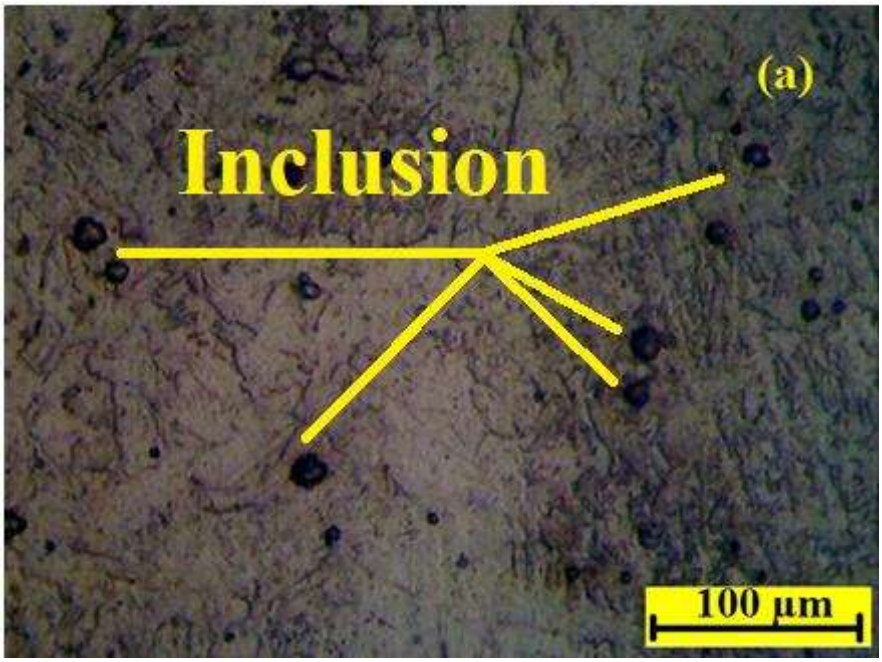

Grain size 36.1µm

In figure (a) a large amount of inclusions are observed. Some inclusions are in larger in size while some inclusions are smaller in size and all inclusions are randomly distributed.

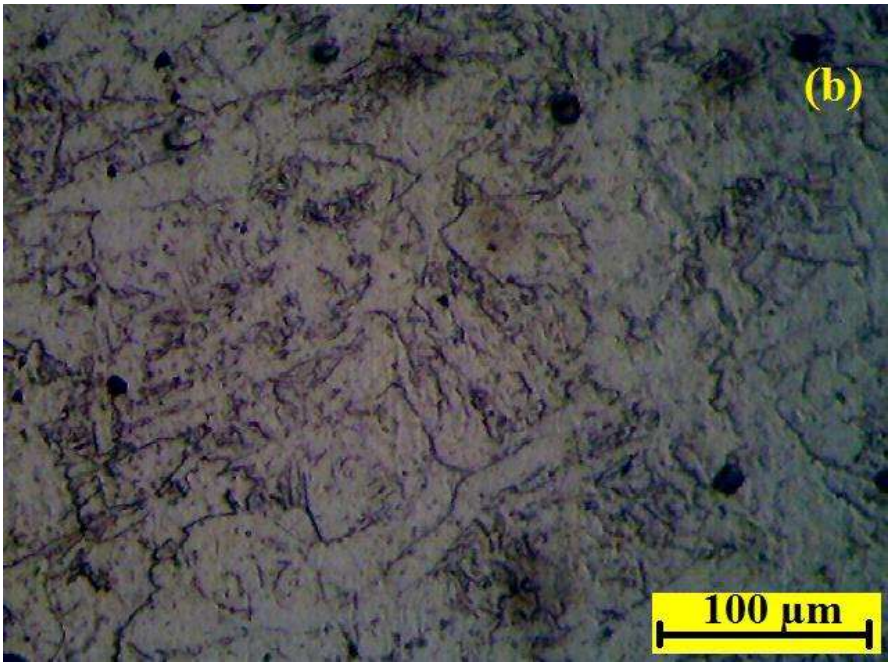

Grain size 38.7µm

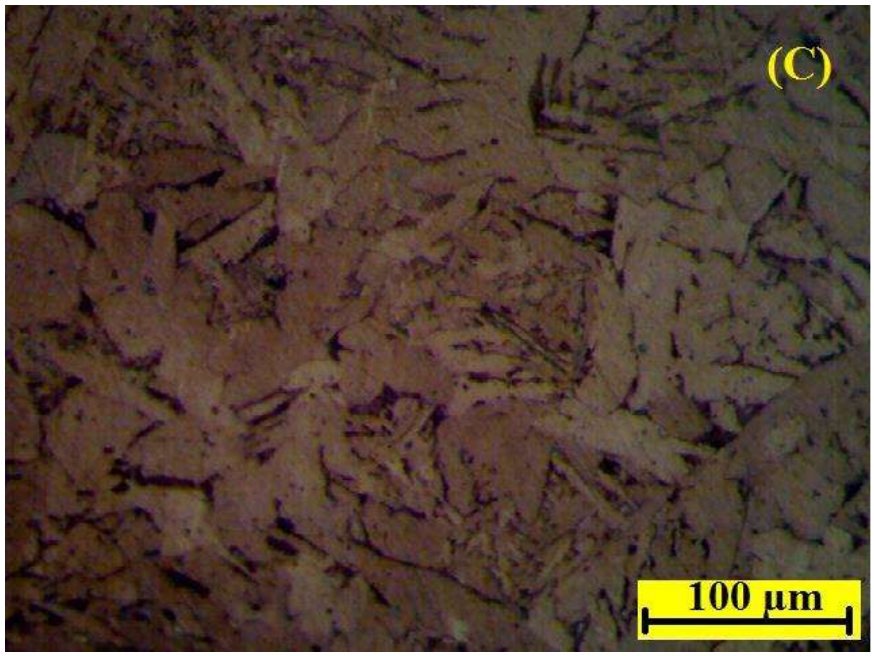

Grain size 45.8µm

The microstructure of CGHAZ of IS 2062 steel weldment with ferrite and widmanstatten ferrite

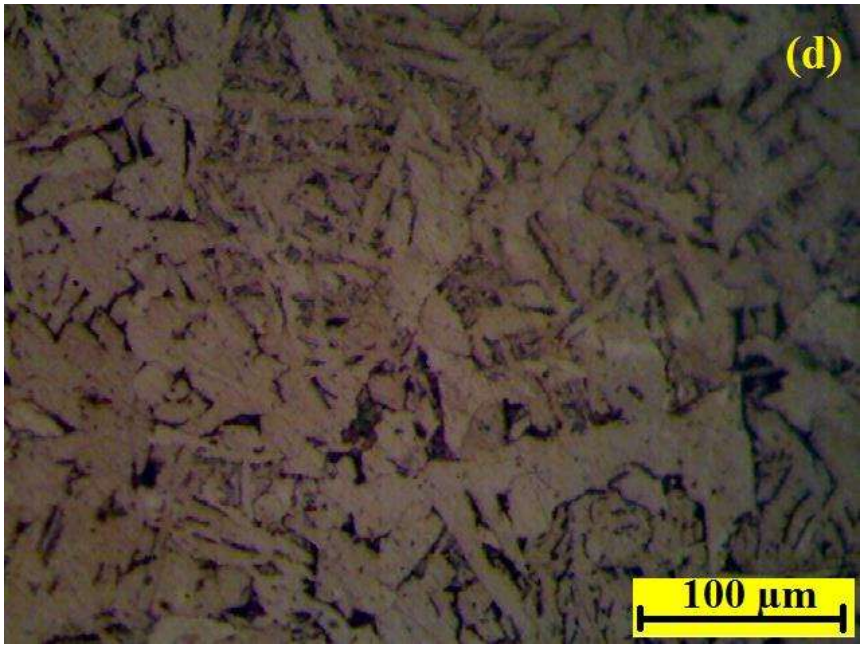

Grain size 42.2µm

Coarse grain ferrite with widmanstatten ferrite and bainite

Figure 4.32(a-d) microstructure photograph of heat affected zone (HAZ) of IS 2062 steel weldment at 10-25 l/m shielding gas flow rate, at 8.89 m/min produced at 3.88 kJ/mm heat input

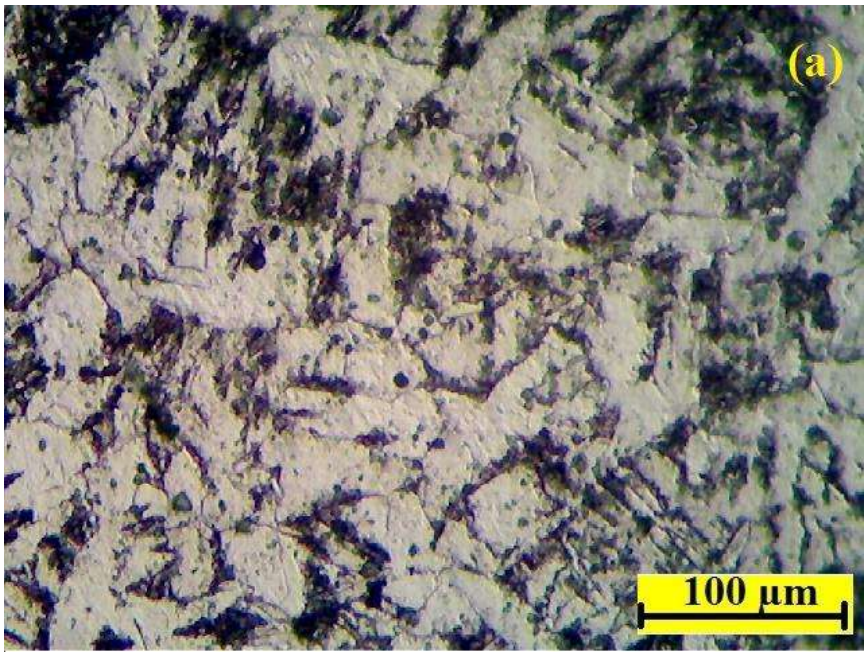

Grain size 43.2µm

Coarse grain ferrite with a little amount of pearlite

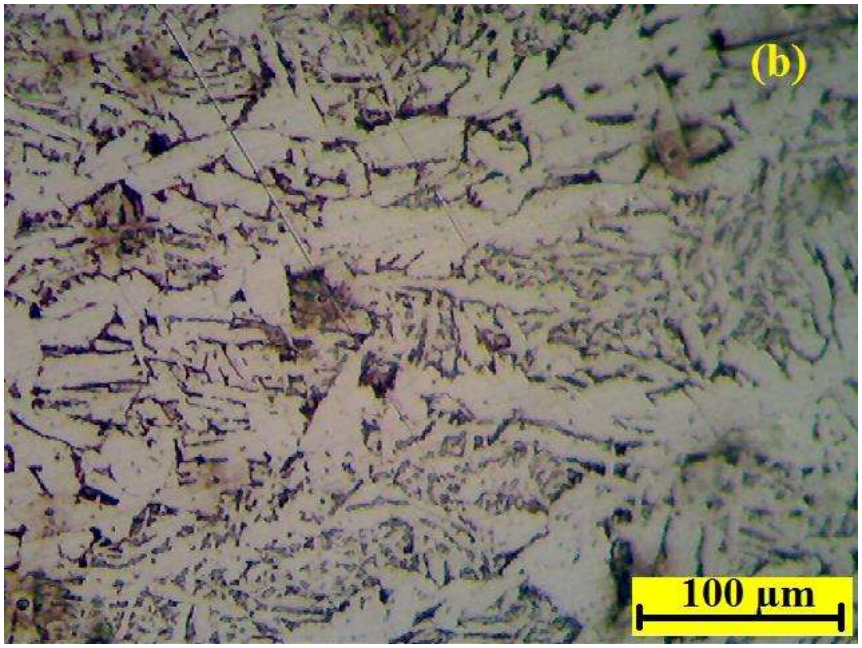

Grain size 36.1µm

Coarse grain ferrite with grain boundary ferrite, and widmanstatten ferrite. Acicular ferrite usually nucleates on inclusions present in the columnar austenite grains, which stimulates other acicular ferrite plate to nucleate automatically.

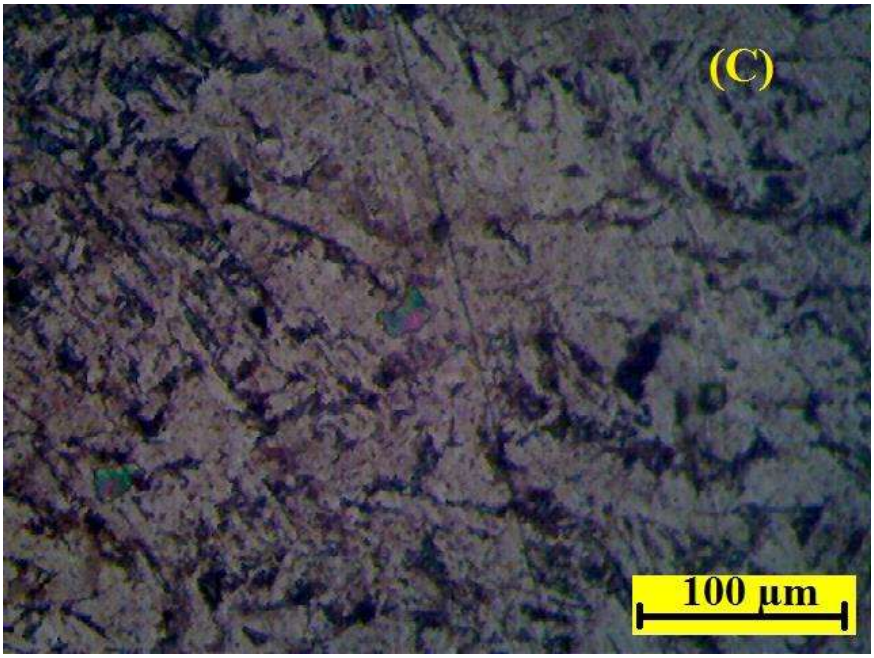

Grain size 45.3µm

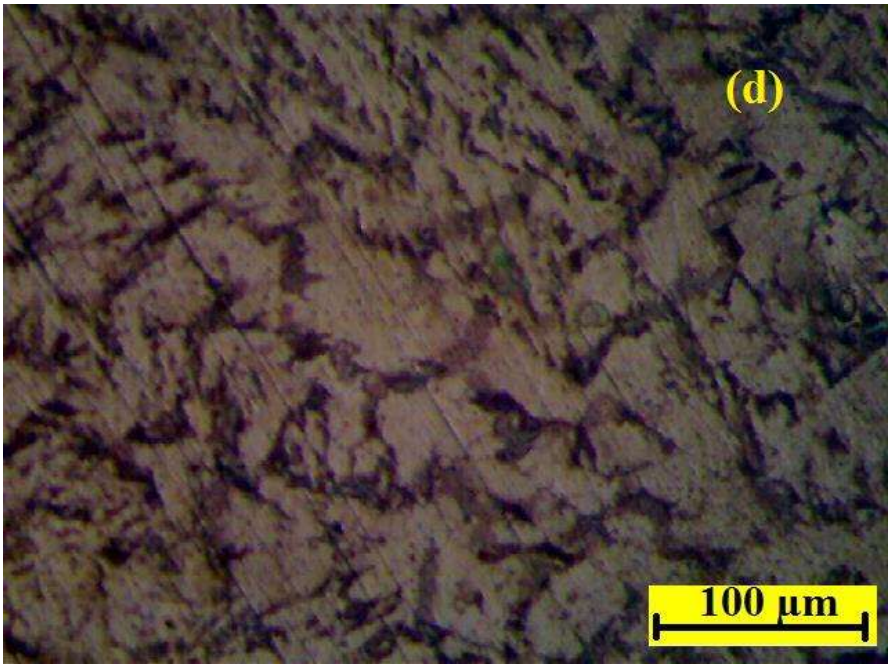

Grain size 46.2µm

Figure 4.33(a-d) microstructure photograph of heat affected zone (HAZ) of IS 2062 steel weldment at 10-25 l/m shielding gas flow rate, at 10.16 m/min produced at 3.88 kJ/mm heat input

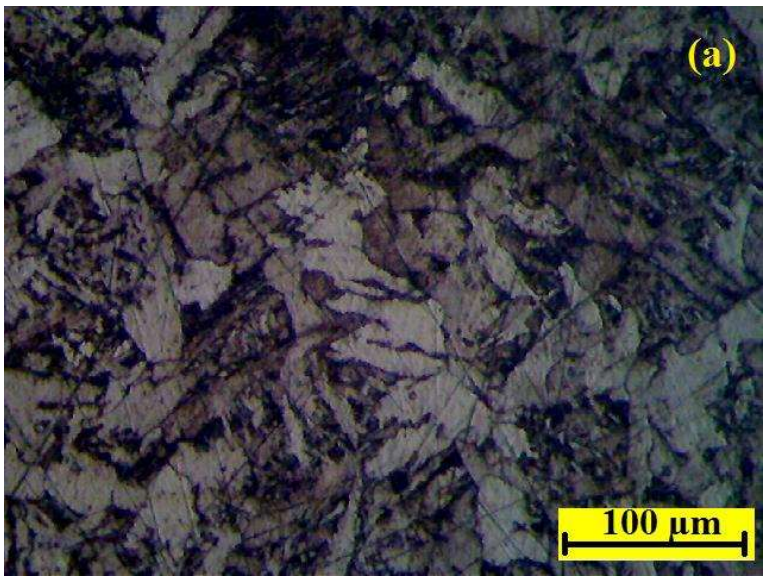

Grain size 35.7µm

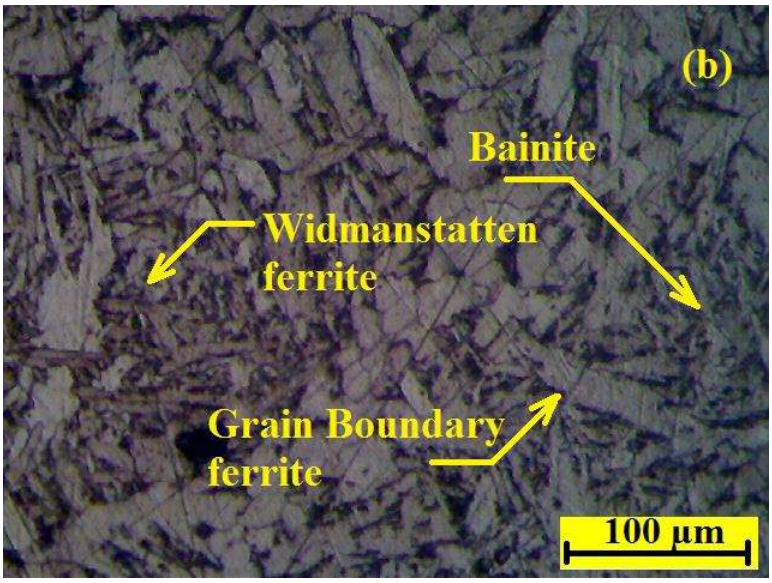

Grain size 32.9µm

The microstructure of CGHAZ of IS 2062 steel weldment with grain boundary ferrite, widmanstatten ferrite, and bainite. Microstructure of CGHAZ with high heat input thermal cycle consisted of high volume fraction of Acicular Ferrite (AF) inside grain and grain boundary ferrite (GBF) at prior austenite grain boundaries. Grain size of CGHAZ increases with heat input increasing due to long holding time at peak temperature.

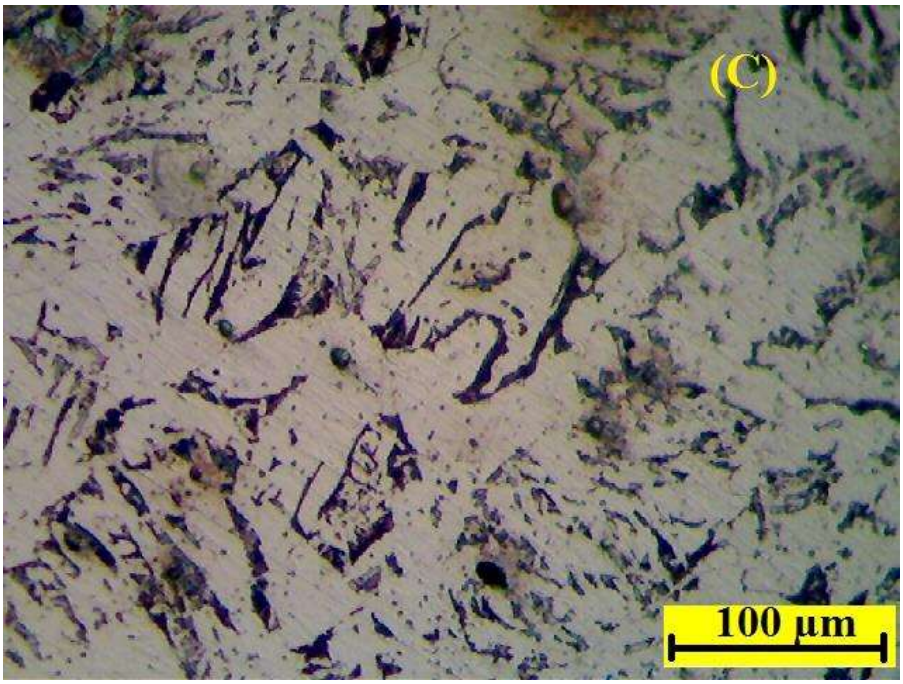

Grain size 39.6µm

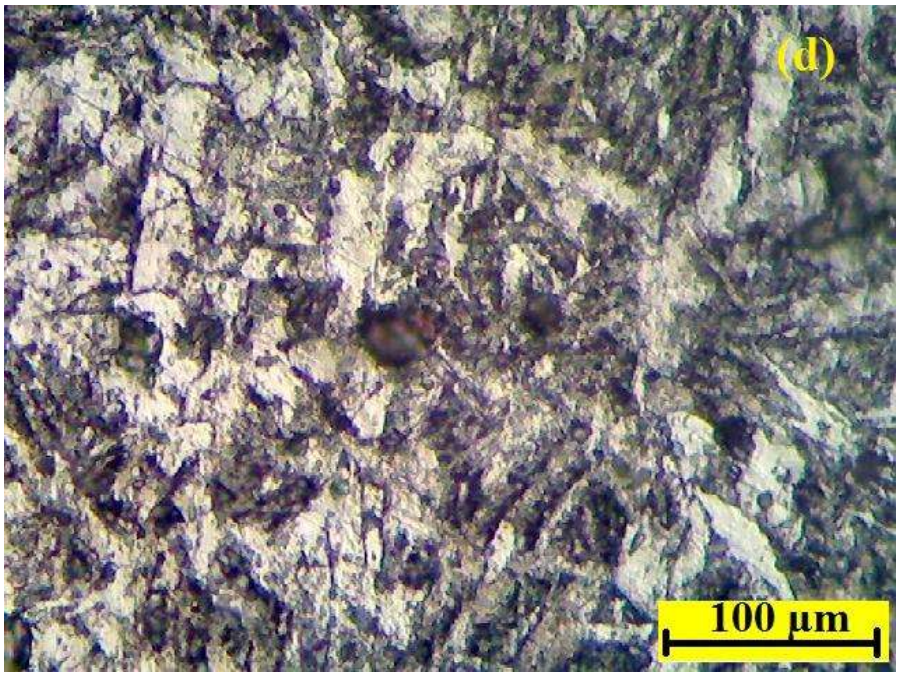

Grain size 26.7µm

The microstructure of CGHAZ of IS 2062 steel weldment with ferrite and pearlite

Figure 4.34(a-d) microstructure photograph of heat affected zone (HAZ) of IS 2062 steel weldment at 10-25 l/m shielding gas flow rate, at 11.43 m/min produced at 3.88 kJ/mm heat input

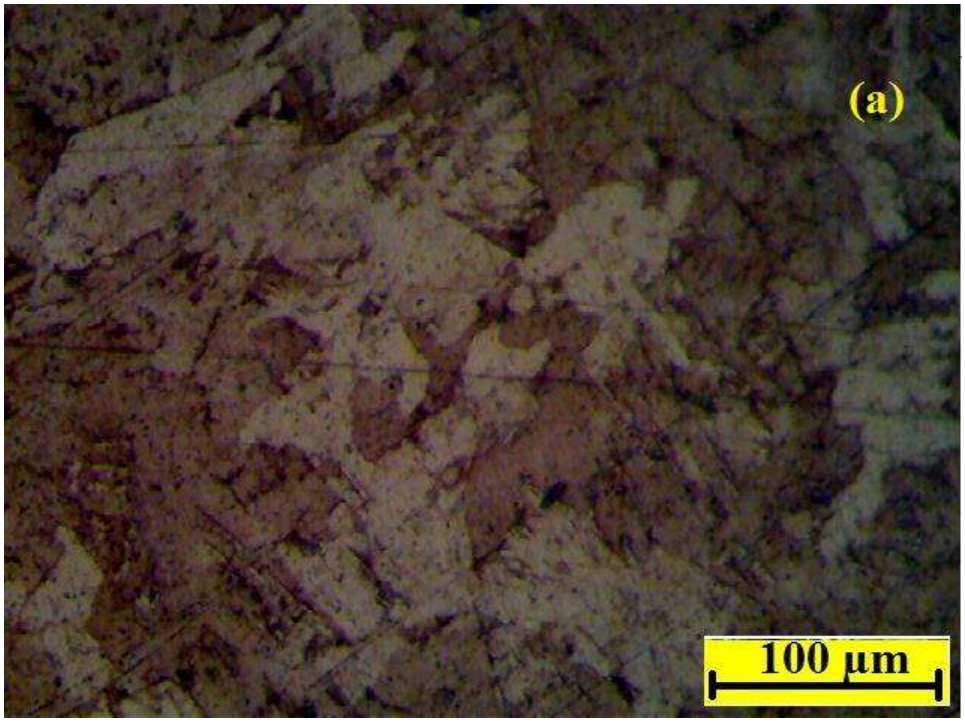

Grain size 42.5µm

Coarse grain heat affected zone (CGHAZ)

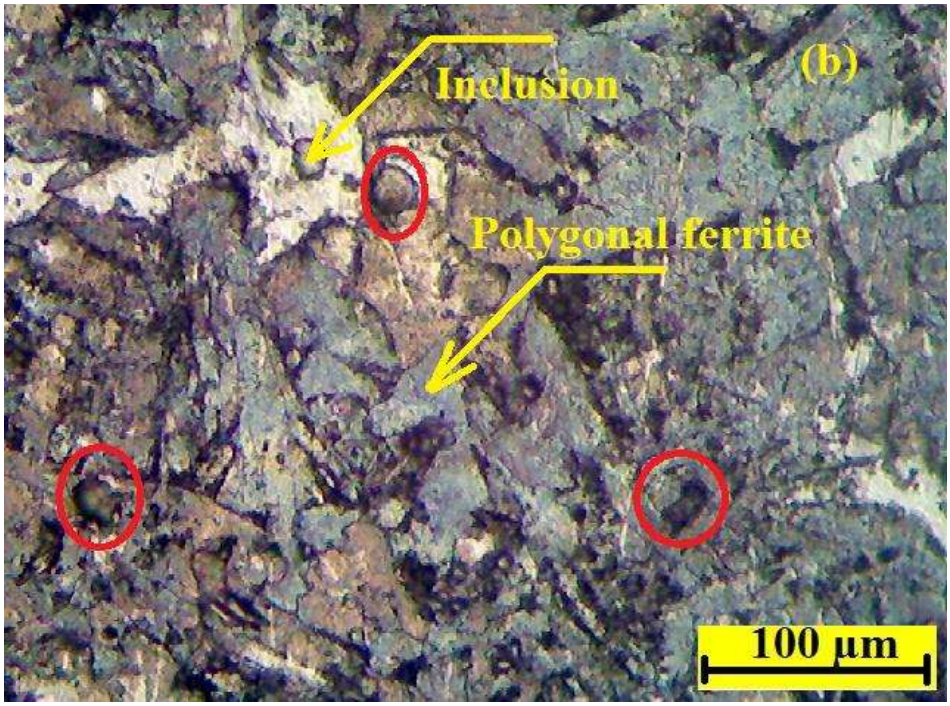

Grain size 46.2µm

It is important to know that this inclusion in the weldment observed due to the shielding gas composition of 75%Ar +25 CO_2.

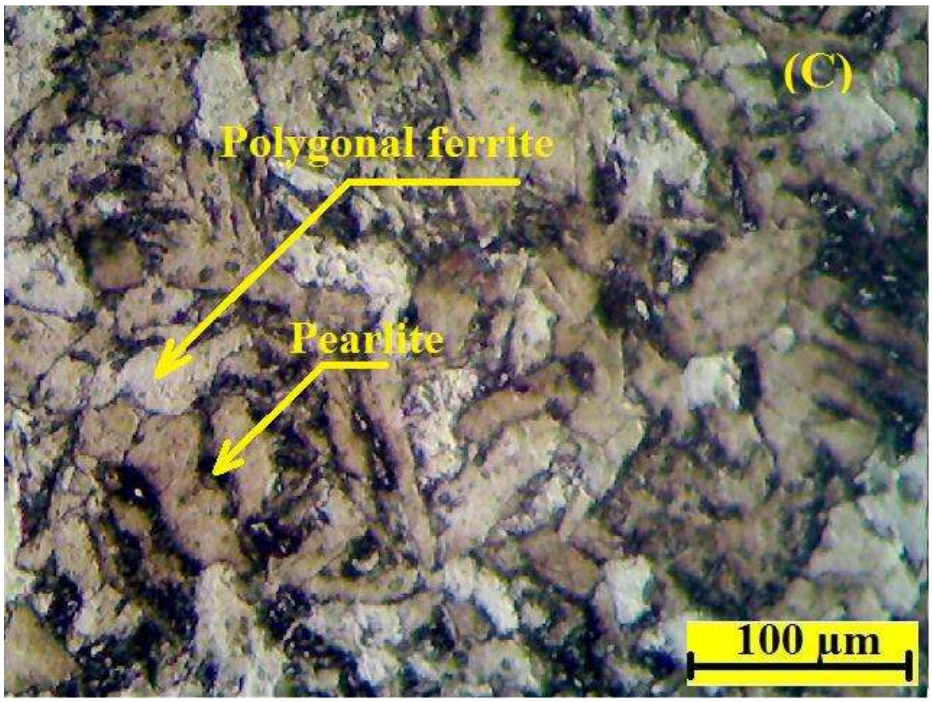

Grain size 38.8µm

Coarse grain heat affected zone (CGHAZ) with polygonal ferrite and pearlite

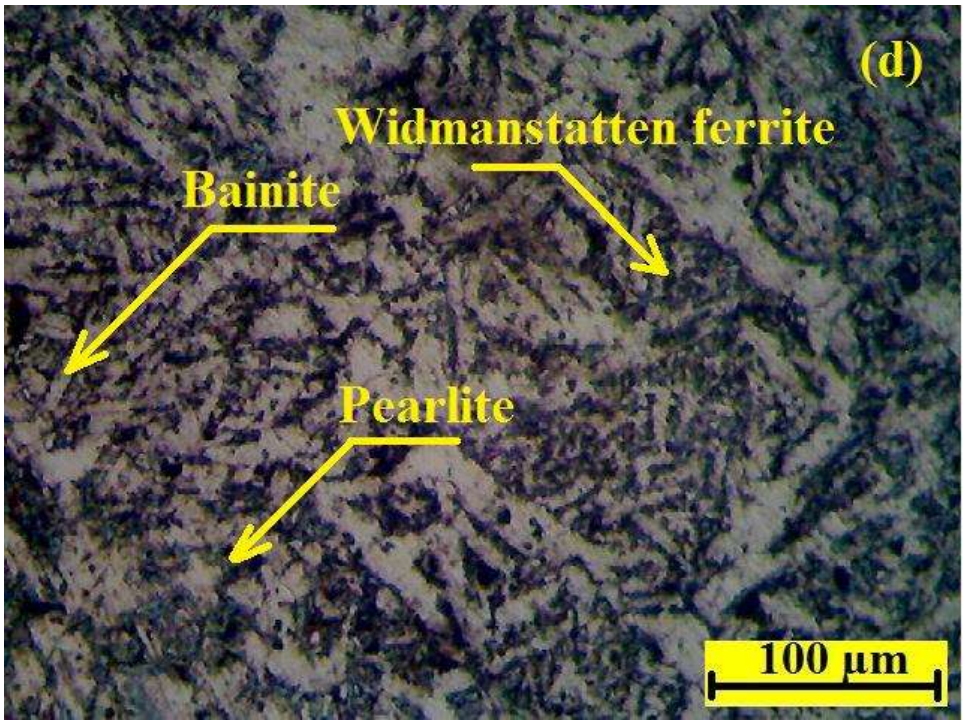

Grain size 34.6µm

Figure 4.35(a-d) microstructure photograph of heat affected zone (HAZ) of IS 2062 steel weldment at 10-25 l/m shielding gas flow rate, at 7.62 m/min produced at 4.47 kJ/mm heat input

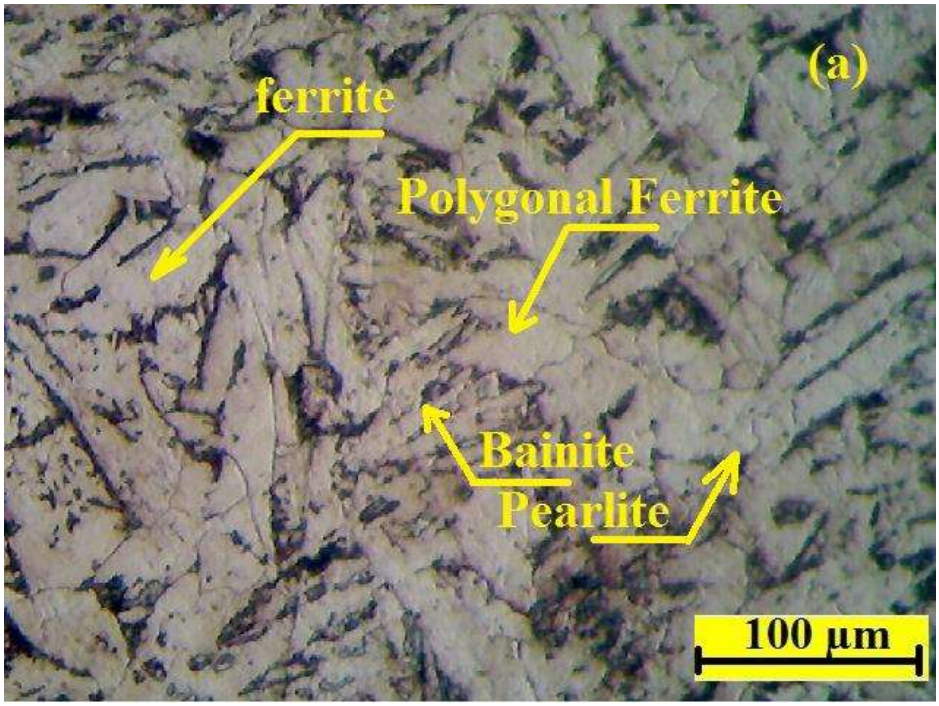

Grain size 43.6µm

Coarse grain ferrite with polygonal ferrite, bainite, and pearlite

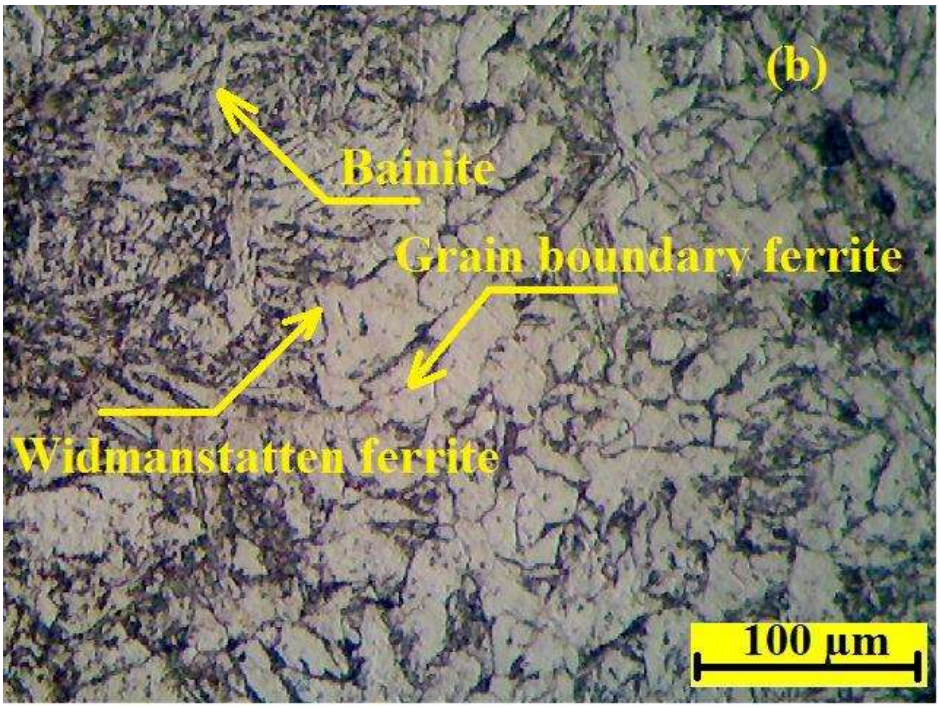

Grain size 27.7µm

Fine grain ferrite with grain boundary ferrite, bainite, and widmanstatten ferrite

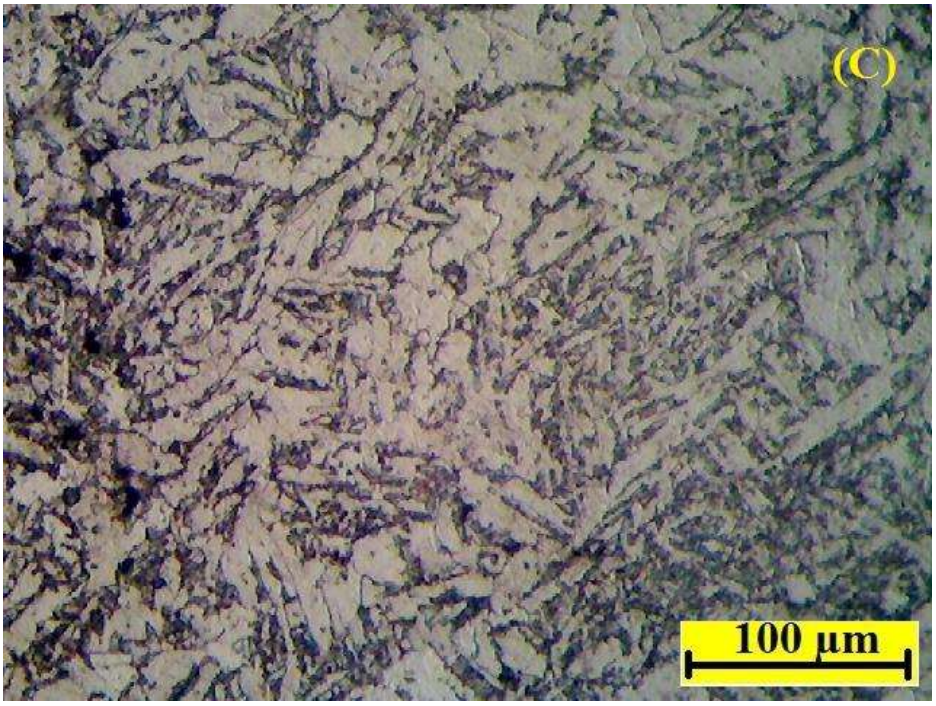

Grain size 28.1µm

Grain boundary ferrite with bainite and widmastatten ferrite

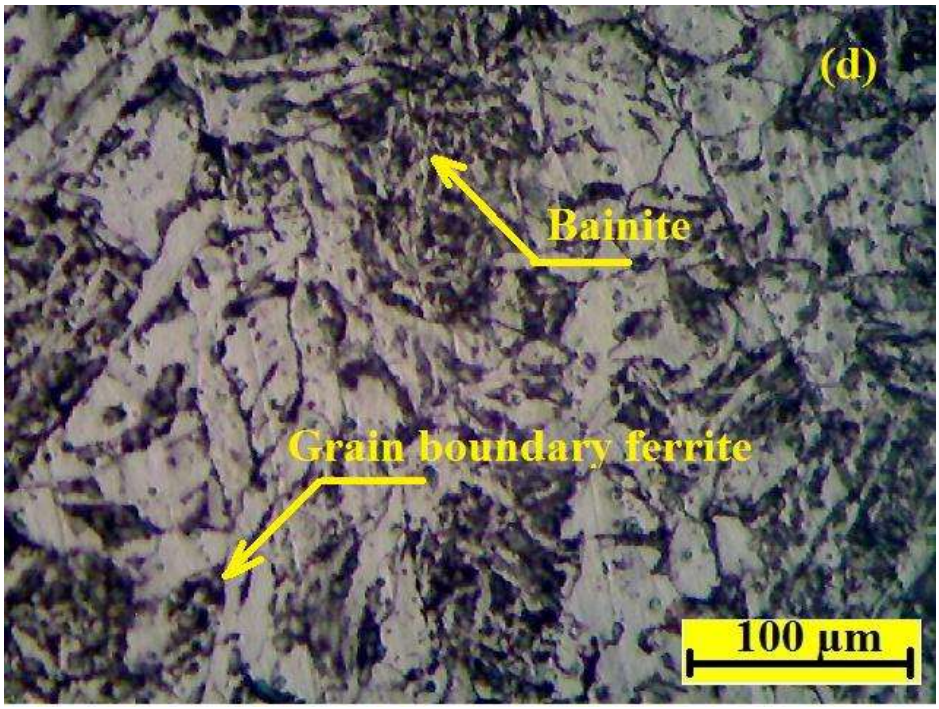

Grain size 34.7µm

Figure 4.36(a-d) microstructure photograph of heat affected zone (HAZ) of IS 2062 steel weldment at 10-25 l/m shielding gas flow rate, at 8.89 m/min produced at 4.47 kJ/mm heat input

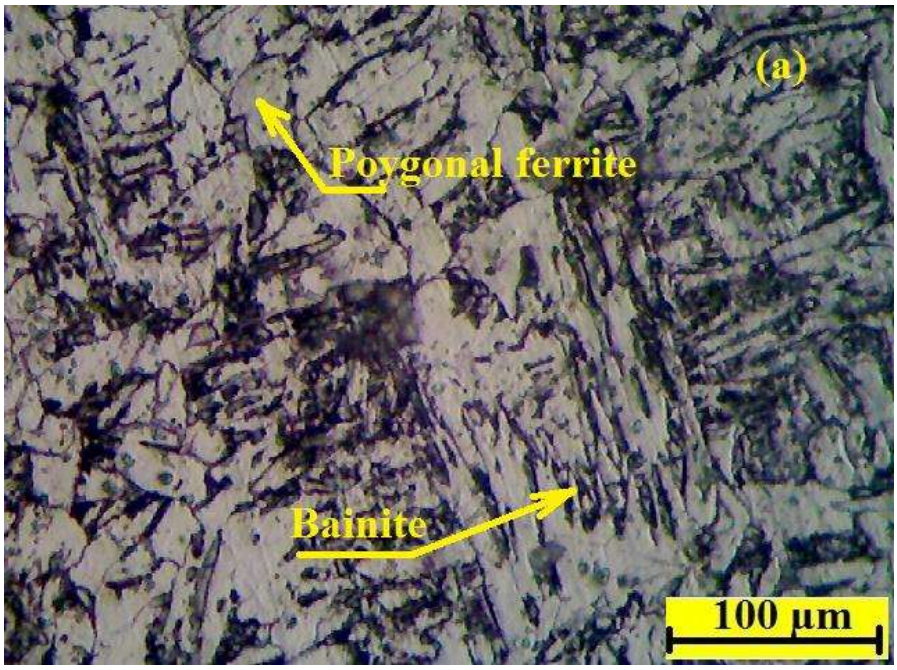

Grain size 32.7µm

Bainite, polygonal ferrite with widmanstatten ferrite

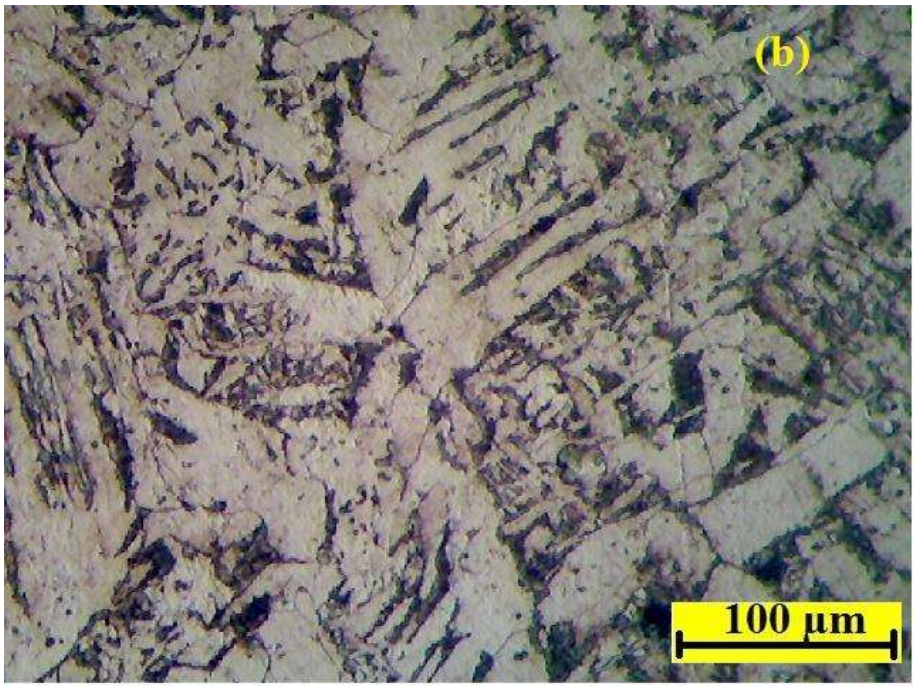

Grain size 42.3µm

The microstructure of coarse grain ferrite (CGHAZ) of IS 2062 steel weldment with grain boundary ferrite, widmanstatten ferrite, and bainite

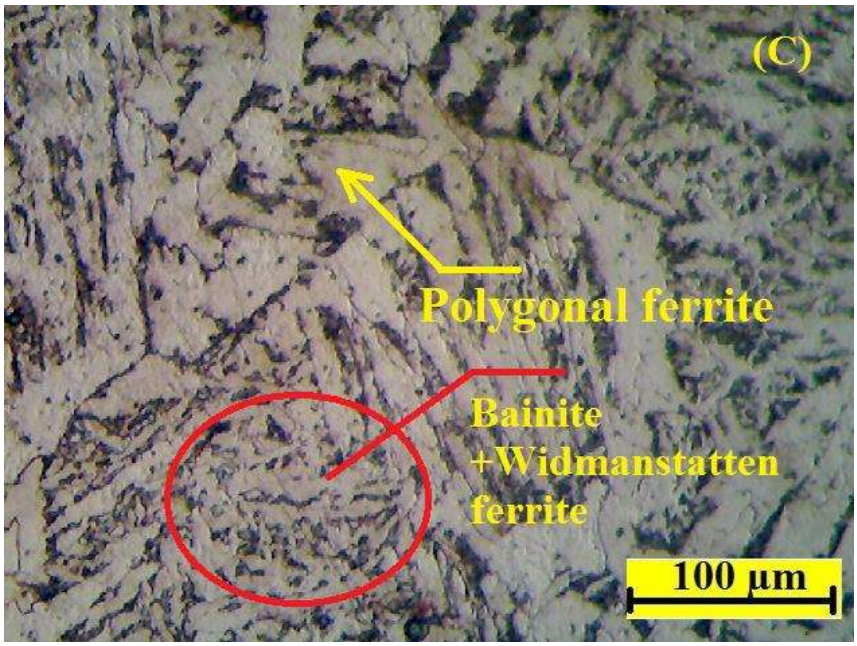

Grain size 39.1µm

The microstructure of CGHAZ of IS 2062 steel weldment with grain boundary ferrite, widmanstatten ferrite, bainite, and ferrite

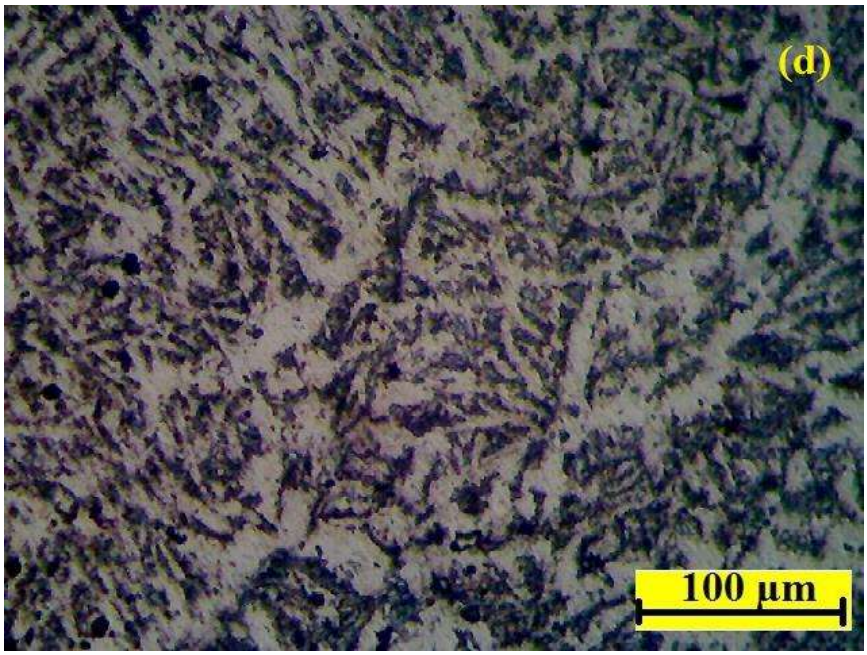

Grain size 22.9µm

widsmantatten ferrite and bainite is formed in low carbon and low alloy steel.

Figure 4.37(a-d) microstructure photograph of heat affected zone (HAZ) of IS 2062 steel weldment at 10-25 l/m shielding gas flow rate, at 10.16 m/min produced at 4.47 kJ/mm heat input.

4.8 Effect of voltage, wire feed speed, and shielding gas flow rate on yield strength

Effect of different Wire feed speed on yield strength from 20 V to 23V at 10 to 25l/m respectively for AISI 304 weldments

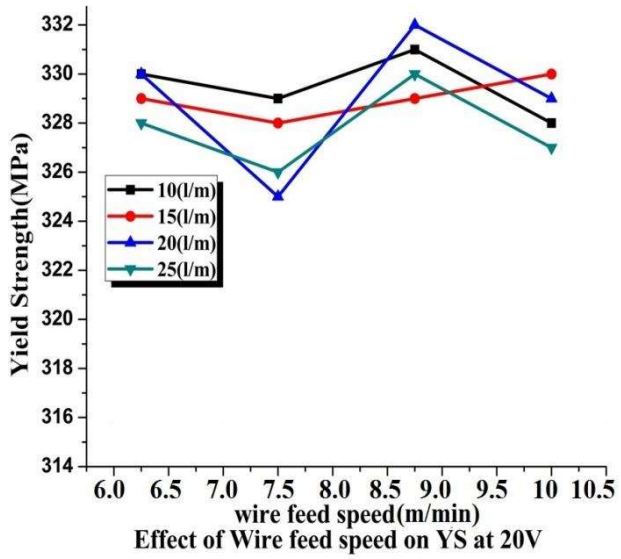

Figure 4.38 Effect of wire feed speed on the yield strength of AISI 304 steel at 20V at a different shielding gas flow rate at 1.89 kJ/mm heat input

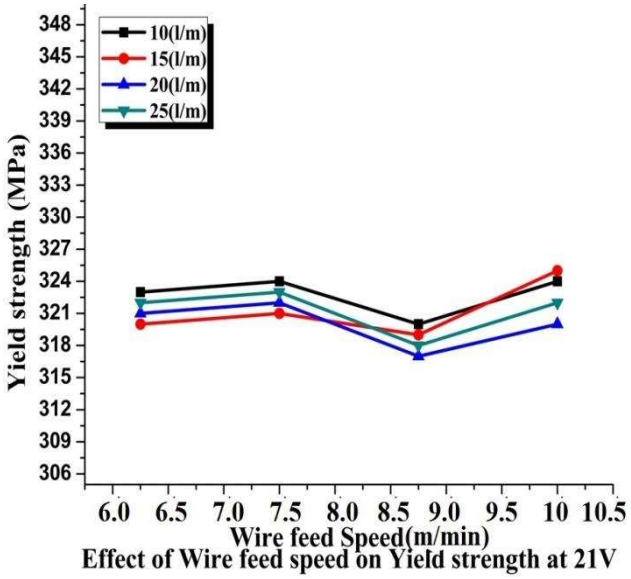

Figure 4.39 Effect of wire feed speed on the yield strength of AISI 304 steel at 21V at a different shielding gas flow rate at 2.17 kJ/mm heat input

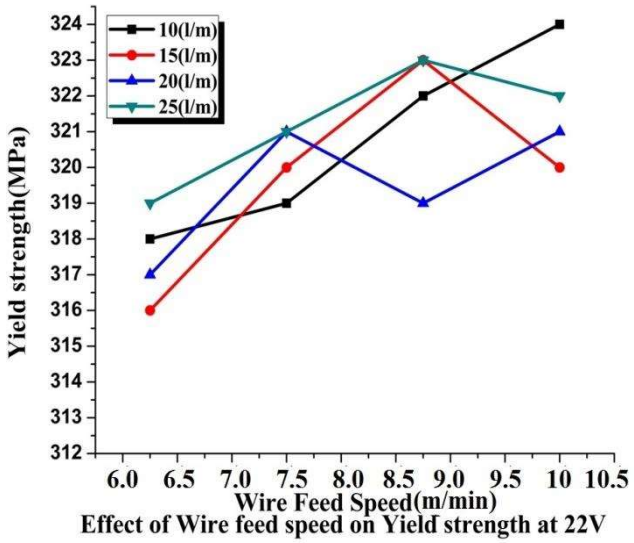

Figure 4.40 Effect of wire feed speed on the yield strength of AISI 304 steel at 22V at a different shielding gas flow rate at 2.78 kJ/mm heat input

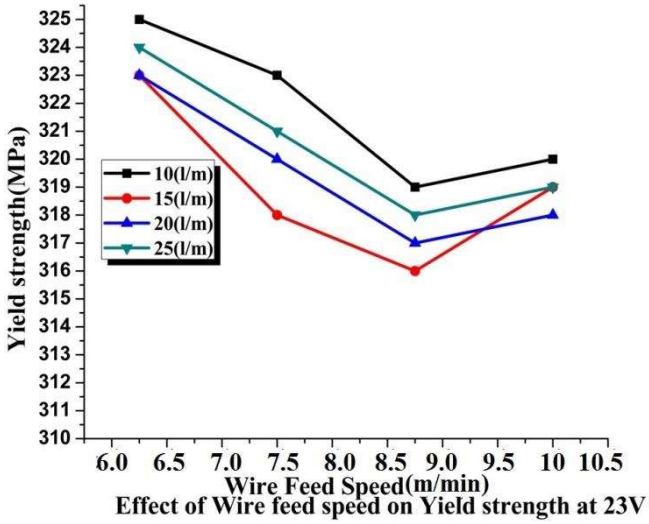

Figure 4.41 Effect of wire feed speed on the yield strength of AISI 304 steel at 23V at a different shielding gas flow rate at 3.01kj/mm heat input

Figure 4.38 to 4.41 shows the Effect of wire feed speed on the yield strength of AISI 304 steel weldment test pieces. The voltage was varied from 20 to 23V and shielding gas flow rate varies from 10 to 25l/m at different heat input. As thermal conductivity of stainless steel is lower hence less voltage is required for welding of AISI 304 steel. Figure 4.38 is plotted for AISI 304 steel

weldment at 20V, and at 10 to 25 l/m shielding gas flow rate at 1.89 kJ/mm heat input. From figure 4.38 it is clear that yield strength of weldment first increases and then decreases. Figure 4.39 to figure 4.41 is plotted for AISI 304 steel weldment at 21V, 22V and 23V at 10 to 25 l/m shielding gas flow rate and at 2.17, 2.78 and 3.01 kJ/mm heat input respectively**.** Figure 4.39 to figure 4.40 reveal that on increasing the heat input, yield strength of AISI 304 weldments increases.

4.9 Effect of voltage, wire feed speed, and shielding gas flow rate on ultimate tensile strength

Effect of wire feed speed at on ultimate tensile strength from 20 V to 23V at 10 to 25 l/m respectively for AISI 304 weldment.

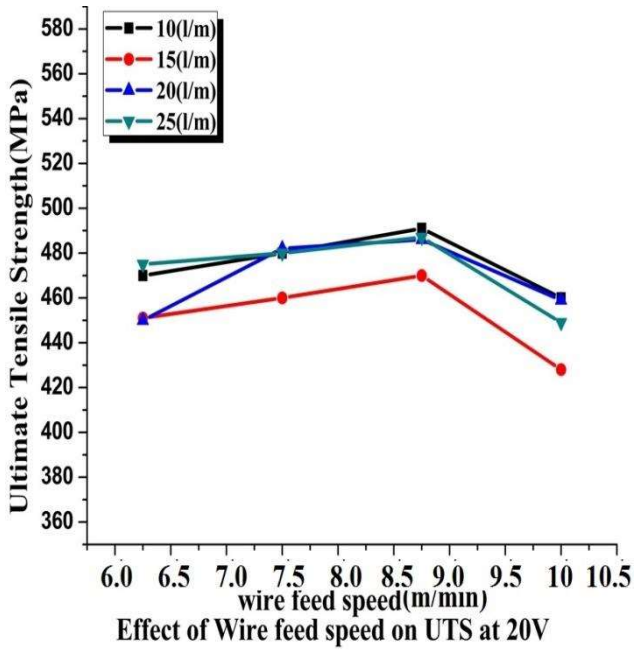

Figure 4.42 Effect of wire feed speed on the ultimate tensile strength of AISI 304 steel at 20V at a different shielding gas flow rate at 1.89 kJ/mm heat input

Fusion zone (FZ) ultimate tensile strength increases with increasing the welding speed and thereafter decreases [104].

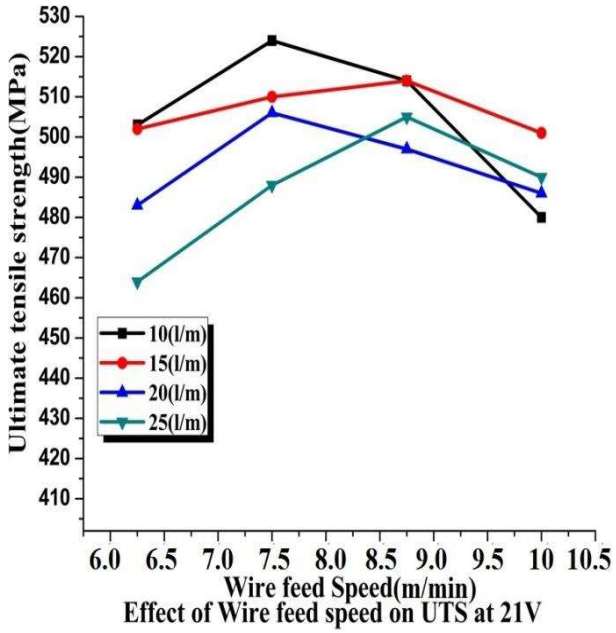

Figure 4.43 Effect of wire feed speed on the ultimate tensile strength of AISI 304 steel at 21V at a different shielding gas flow rate at 2.17 kJ/mm heat input

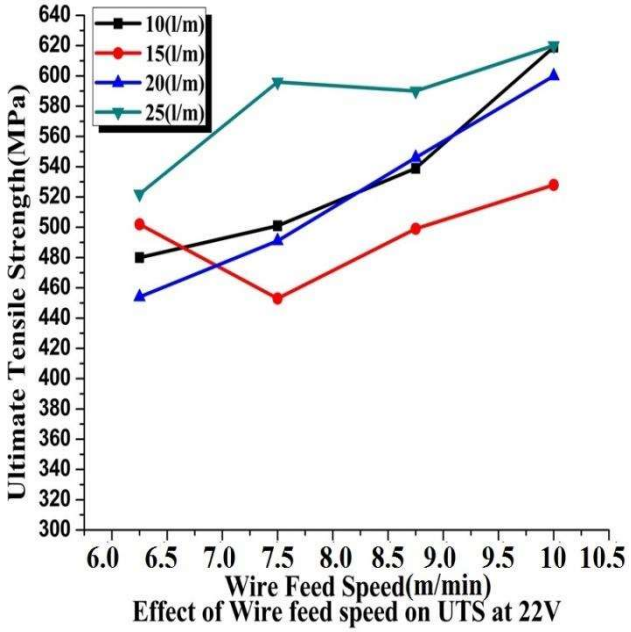

Figure 4.44 Effect of wire feed speed on the ultimate tensile strength of AISI 304 steel at 22V at a different shielding gas flow rate at 2.78 kJ/mm heat input

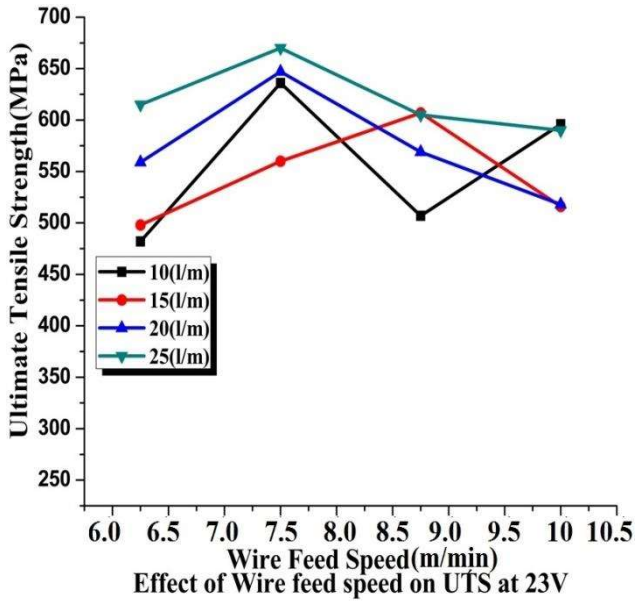

Figure 4.45 Effect of wire feed speed on the ultimate tensile strength of AISI 304 steel at 23V at a different shielding gas flow rate at 3.01 kJ/mm heat input

Figure 4.42 to 4.45 shows the effect of wire feed speed on the ultimate tensile strength of AISI 304 steel weldment test pieces. The voltage was varied from 20 to 23V and shielding gas flow rate varies from 10 to 25l/m at different heat input. Figure 4.42 is plotted for AISI 304 steel weldment at 20V, and at 10 to 25 l/m shielding gas flow rate at 1.89 kJ/mm heat input. From figure 4.42 & figure 4.43 it is clear that ultimate tensile strength of AISI 304 steel weldment having a decreasing trend but on again increasing the heat input ultimate tensile strength of AISI 304 steel weldment increases shown in figure 4.45, but further on increasing the heat input ultimate tensile strength decreases. The heat input and welding speed affect the solidification rate and mode of the weldment. The higher the heat input at a specified welding speed leads to a lowering temperature gradient [105]. The microstructure analysis discovered that the ferrite to austenite arrangement contributes in growing the weldment strength, whereby at weldment area (fusion zone) ferrite form occurred due to high temperature during welding. This makes the structure strength at weldment area weaker compared to HAZ and base metal [106].The ultimate tensile strength of ASS 304 weldment sample increase on increasing in core diameter of the electrode and best core diameter for welding of ASS 304 is 3.2mm [107].

Ravindra V. Taiwade et al (2013) [108] found that stainless steel 304 failed due to ductile fracture for all the passes of the weld. In Cr–Mn ASS, mixed types of fracture were found in single and double pass weld, whereas the intergranular fracture was found in triple pass welding and they also added that tensile strength of welded joint decreases on increases the number of passes.

4.10 Effect of voltage, wire feed speed, and shielding gas flow rate on toughness (Joule)

4 Effect of wire feed speed at on toughness (Joule) from 20 V to 23V at 10 to 25l/m respectively for AISI 304 weldment

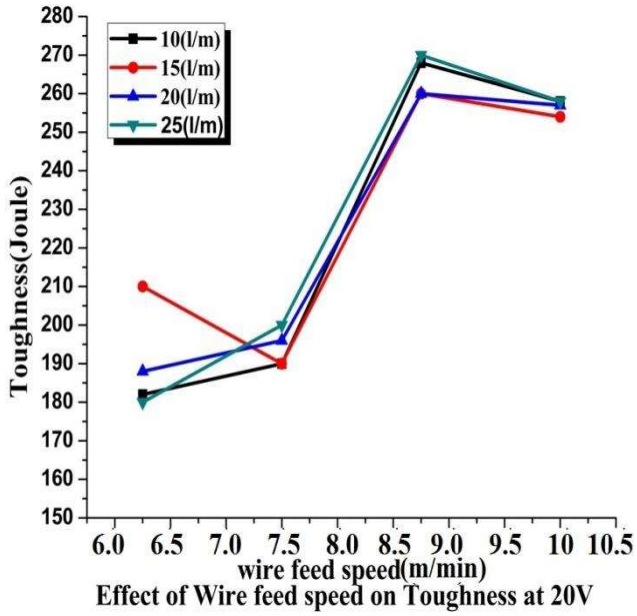

Figure 4.46 Effect of wire feed speed on toughness of AISI 304 steel at 20V at a different shielding gas flow rate at 1.89 kJ/mm heat input

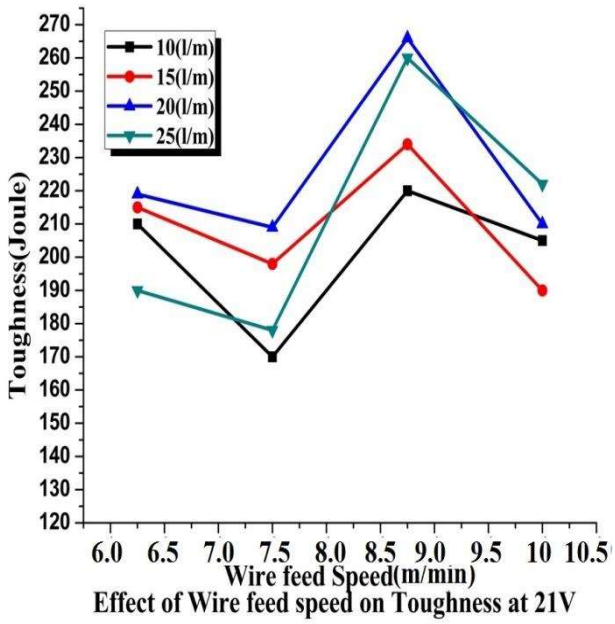

Figure 4.47 Effect of wire feed speed on toughness of AISI 304 steel at 21V at a different shielding gas flow rate at 2.17 kJ/mm heat input

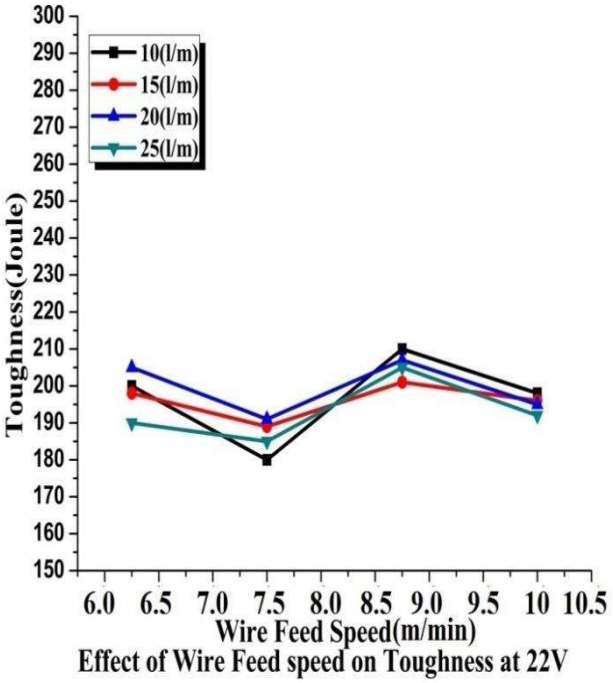

Figure 4.48 Effect of wire feed speed on toughness of AISI 304 steel at 22V at a different shielding gas flow rate at 2.78 kJ/mm heat input

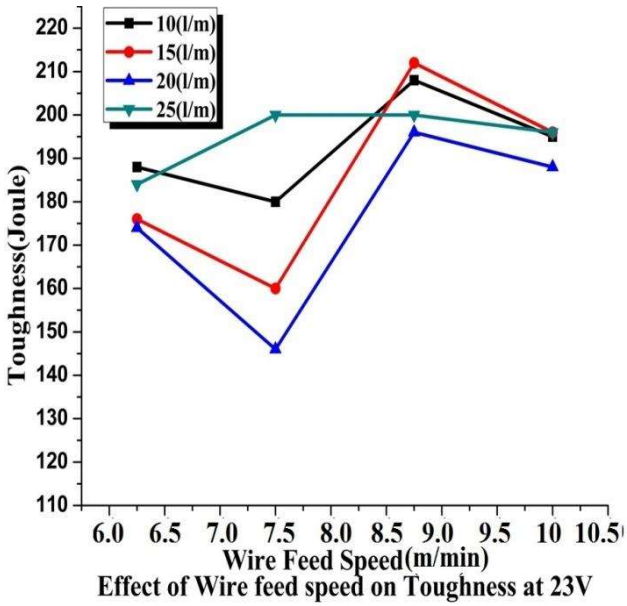

Figure 4.49 Effect of wire feed speed on toughness of AISI 304 steel at 23V at a different shielding gas flow rate at 3.01 kJ/mm heat input

Prabhu Paulraj and Rajnish Garg (2015) [109] declared that impact toughness of weldment decreases with increase in heat input as intermetallic phase formation, secondary austenite formation, and an increase in grain size of the microstructure of weldment at higher heat input value. The highest toughness values were 168 J for DSS and 140 J for SDSS at -46 °C and they also informed that Hardness values decreased at higher heat input for both DSS and SDSS steel weldment. At weld root area, high hardness values were observed due to the presence of hard and brittle intermetallic phases and varying weld thermal cycles.

4.11 Effect of voltage, wire feed speed, and shielding gas flow rate on microhardness (VHN)

Effect of wire feed speed at on microhardness (VHN) from 20 V to 23V at 10 to 25l/m

respectively for AISI 304 weldment

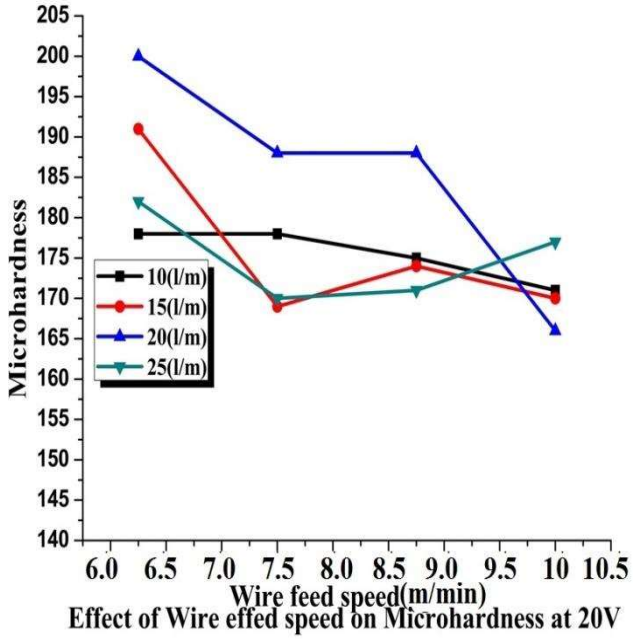

Figure 4.50 Effect of wire feed speed on microhardness (VHN) of AISI 304 steel at 20V at a different shielding gas flow rate at 1.89 kJ/mm heat input

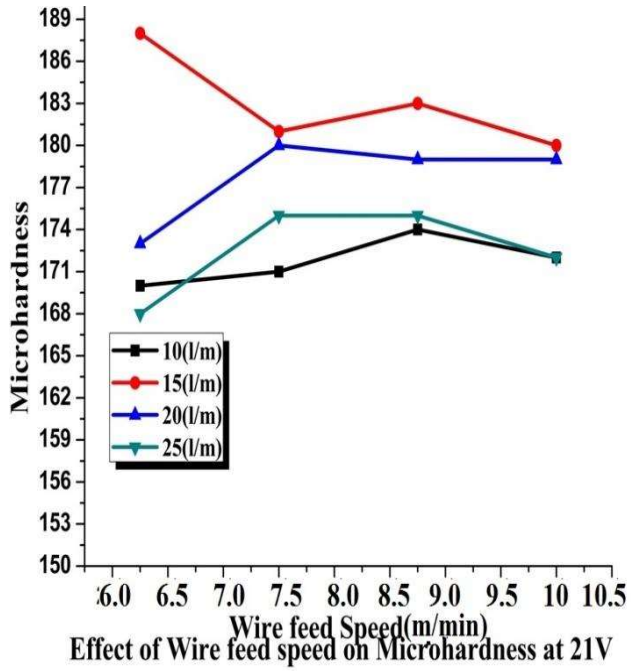

Figure 4.51 Effect of wire feed speed on microhardness (VHN) of AISI 304 steel at 21V at a different shielding gas flow rate at 2.17 kJ/mm heat input

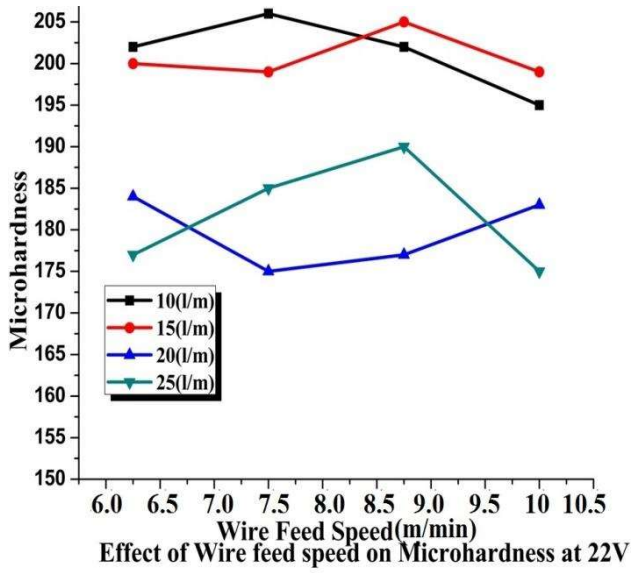

Figure 4.52 Effect of wire feed speed on microhardness (VHN) of AISI 304 steel at 22V at a different shielding gas flow rate at 2.78 kJ/mm heat input

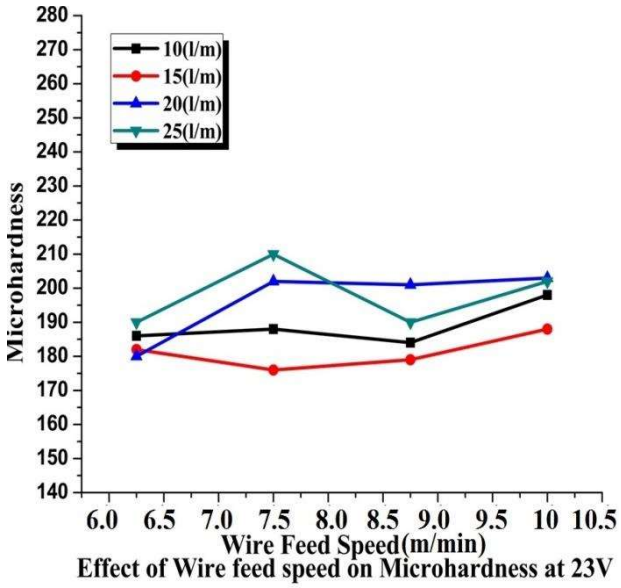

Figure 4.53 Effect of wire feed speed on microhardness (VHN) of AISI 304 steel at 23V at a different shielding gas flow rate at 3.01 kJ/mm heat input

The microstructure of 304L stainless steel parts fabricated by WAAM is filled with a huge number of dendrites, and the growth direction is along the temperature gradient [110].

Reihane Nafar Dehsorkhi (2016) [111] optimized the process parameters for 304 L steel welded by laser welding and they concluded that the microhardness of the optimized welded sample (315 HV0.5) was found to be close to the UFG base metal (350 HV). It was also found that the hardness of the heat affected zone (HAZ) was lower than that of the weld zone, which was related to the HAZ grain growth during laser welding. They also informed that microstructural of weldment consisting austenite and delta ferrite.

T. E. Abioye (2017) [112] concluded that the hardness value of the weld joints (ranging within 234-275 HV0.1) was noticed to decrease with increase in the heat energy per unit length of weld and the optimal ultimate tensile stress of 550 MPa was determined at a heat energy input of 9680 J/mm and they also told that microstructure of the weld joints comprises austenite and δ-ferrite phases.

Apurv Choubey, Vijaykumar S. Jatti (2014) [113] they found from their experimental work that hardness of material increases with increase in heat input in weld pool and decreases in HAZ zone. Optical microscopy reveals that smaller dendrite sizes and lesser inter-dendritic spacing were observed in the fusion zone at lower heat input and long dendrite sizes and large inter-dendritic spacing were formed in the fusion zone of the joint welded at high heat input they also added that tensile strength of test piece decreases with increase in heat input.

S. M. Amer et al (2015) [114] they found that the usual hardness values of the weld metal of S 9 material using current 130 A, and travel speed 50 mm/ min, and 98 % argon, and 2% nitrogen was noticed the lowest value due to using high current and low travel speed and using nitrogen all of this increase heat input that decreases the cooling rate of weldment, consequently hardness values were decreased and they also added that the dendrite size and inter-dendritic spacing in weld zone was lesser when using low current by increasing the current the dendrite size and interspacing increase. Hardness of heat affected zone (HAZ) was slightly higher than that of weld metal regardless of gap. Parent metal (PM) hardness was always lower than that of HAZ and weld zone (WZ) [115].

4.12 Effect of voltage, wire feed speed, and shielding gas flow rate on % age elongation

Effect of wire feed speed at the %age elongation from 20 V to 23V at 10 to 25l/m respectively for AISI 304 steel weldment.

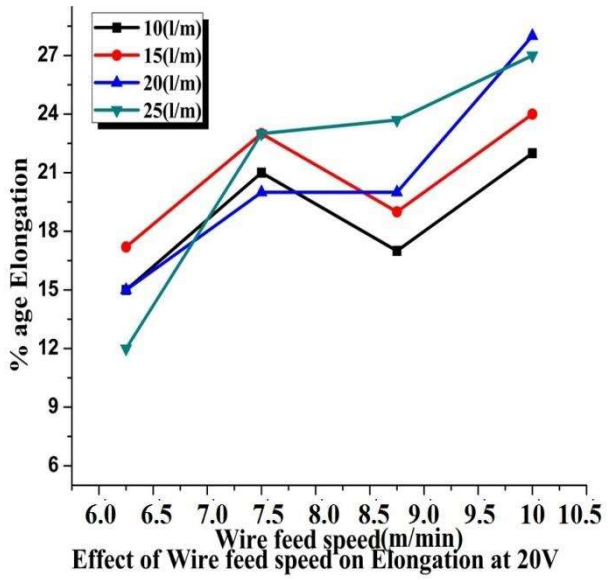

Figure 4.54 Effect of wire feed speed on the %age elongation of AISI 304 steel at 20V at a different shielding gas flow rate at 1.89 kJ/mm heat input

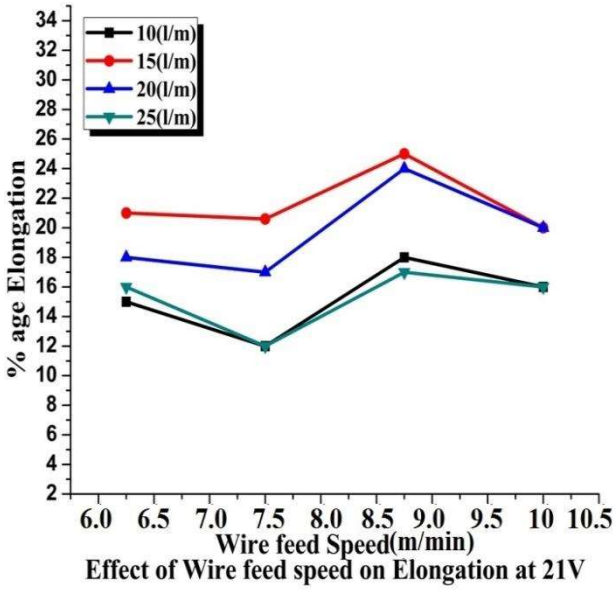

Figure 4.55 Effect of wire feed speed on the %age elongation of AISI 304 steel at 21V at a different shielding gas flow rate at 2.17 kJ/mm heat input

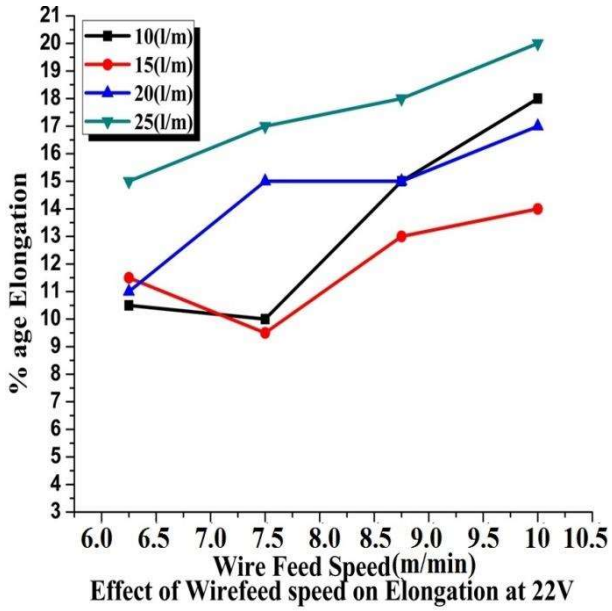

Figure 4.56 Effect of wire feed speed on the %age elongation of AISI 304 steel at 22V at a different shielding gas flow rate at 2.78 kJ/mm heat input

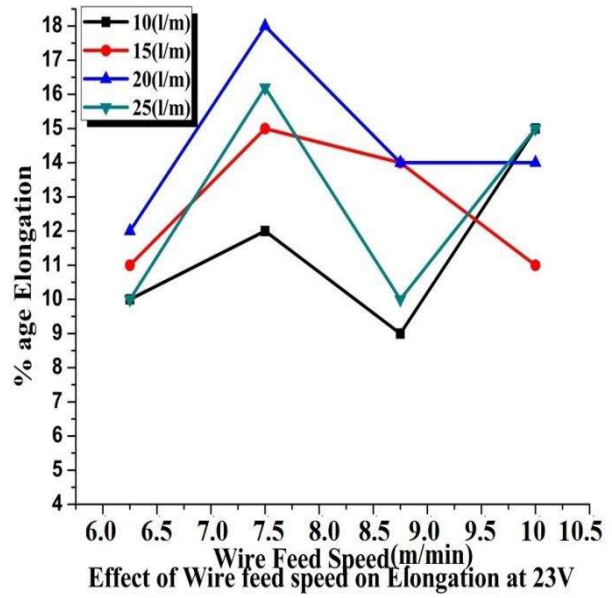

Figure 4.57 Effect of wire feed speed on the %age elongation of AISI 304 steel at 23V at a different shielding gas flow rate at 3.01 kJ/mm heat input

4.13 Microstructure photograph of AISI 304 steel weldments

The microstructural formation of stainless steel (AISI) is relatively complex and exposure to high operating temperature adds to the complexity of the diversity of phases can be observed.

Tae-Hoon Nam et al (2018) [116] examined the effect of post weld treatment on the microstructure and mechanical properties on 304 steel weldment and they mentioned in their result that after heat treatment the lathy δ-ferrite changed to vermicular type due to the heat treatment process and the size of the individual dendrite of δ- ferrite increased at 850 °C in comparison with 650 °C. The phase boundary between austenite and δ- ferrite is considered to migrate in favor of dropping the interfacial energy. At the start thin dendrites of δ- ferrite could thus be thicker during heat treatment without losing their total volume fraction.

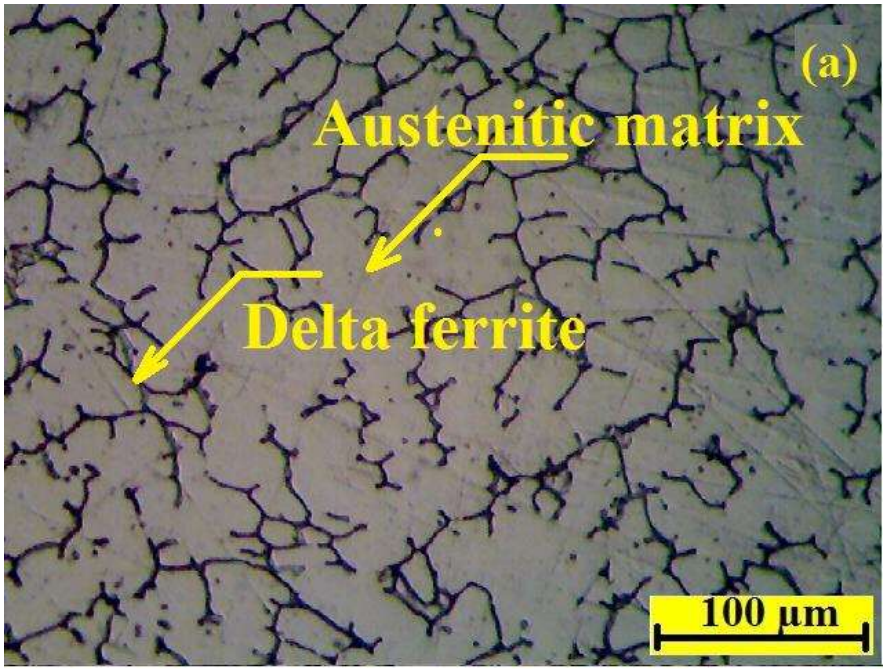

Grain size 26.8 µm

By using the GMA welding δ ferrite contents in the welded joint did not reduce and δ-ferrite contents increases as increasing in the magnitude of welding current [117] and same is achieved in the present research work.

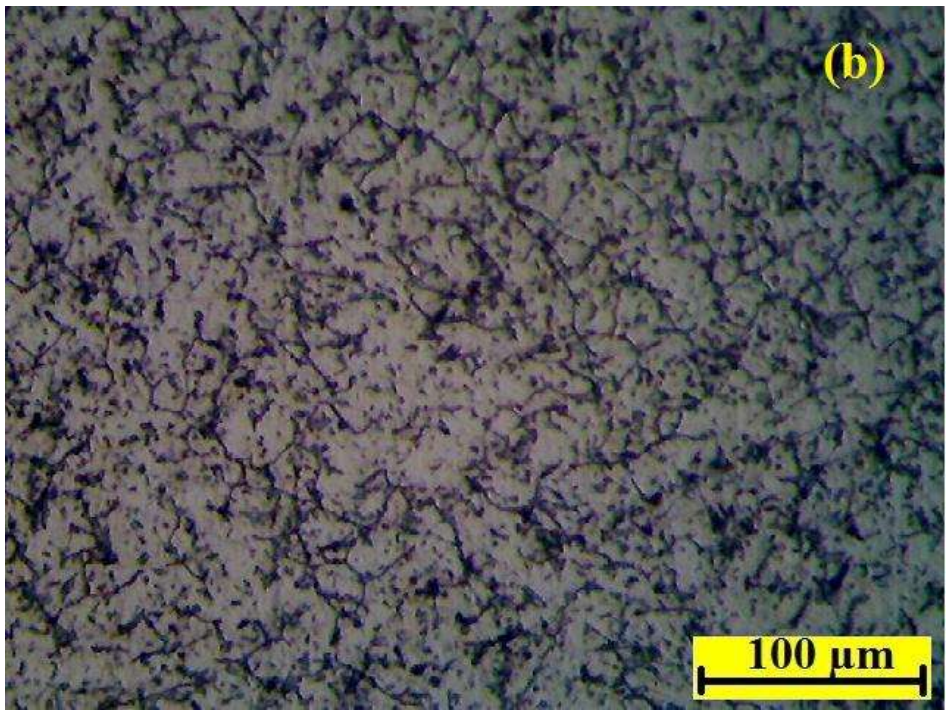

Grain size 30.2 µm

Carbide revealed in the weldment

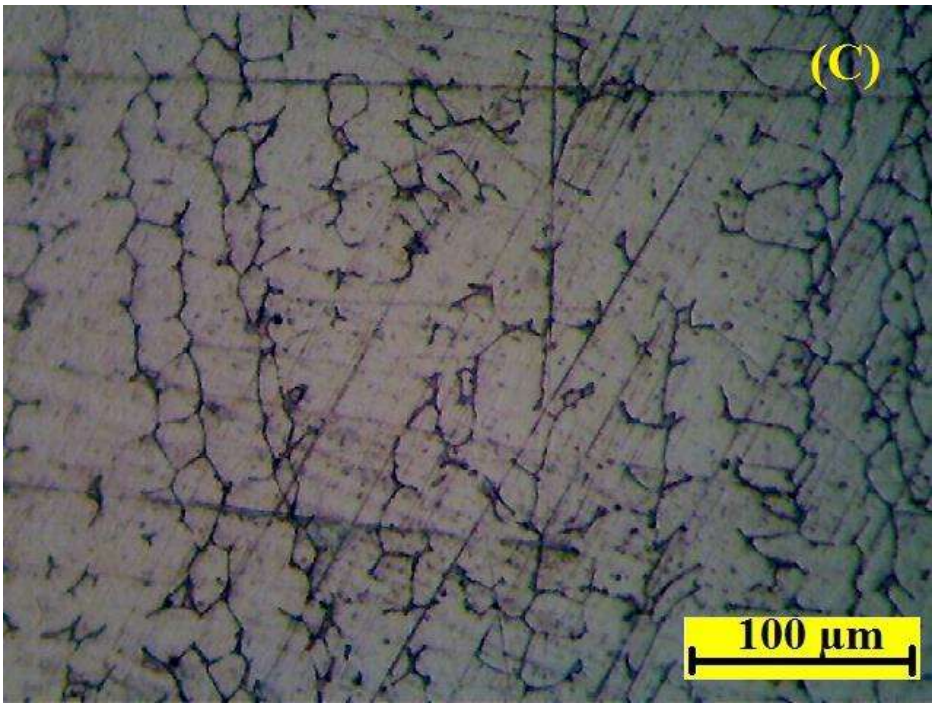

Grain size 38.1 µm

Fine microstructure

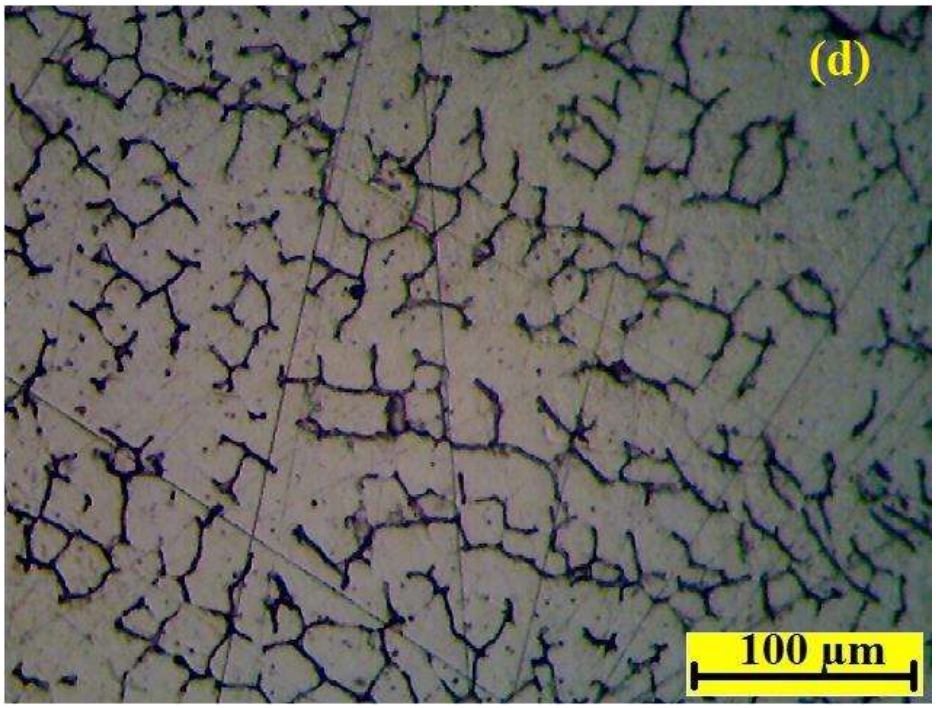

Grain size 25.8 µm

Figure 4.58(a-d) microstructure photograph of heat affected zone (HAZ) of AISI 304 steel weldment at 10-25 l/m shielding gas flow rate, at 6.35 m/min produced at 1.89 kJ/mm heat input

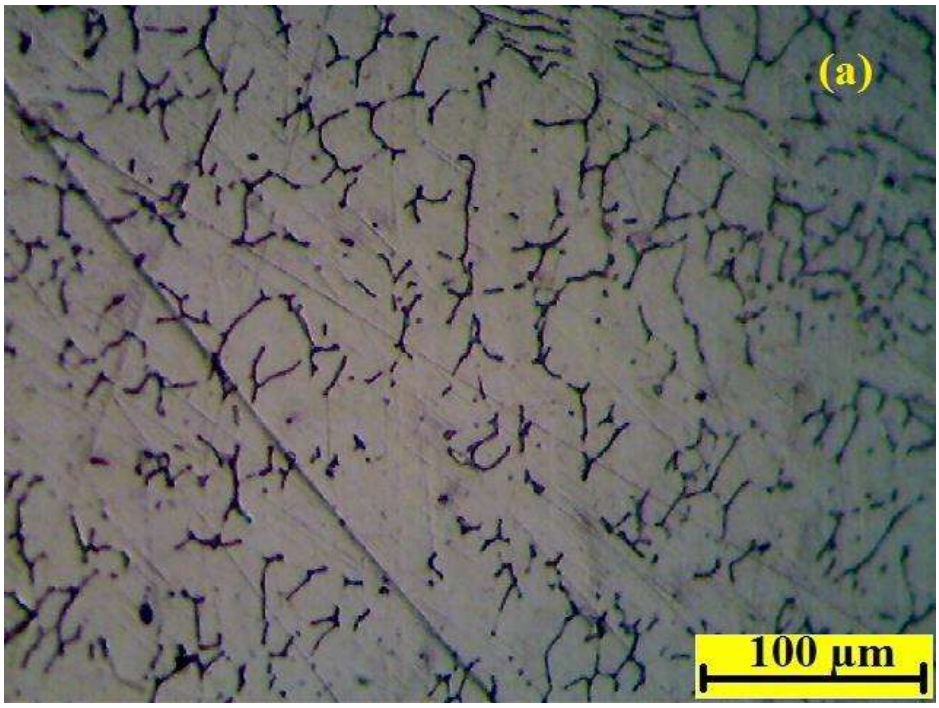

Grain size 26.7 µm

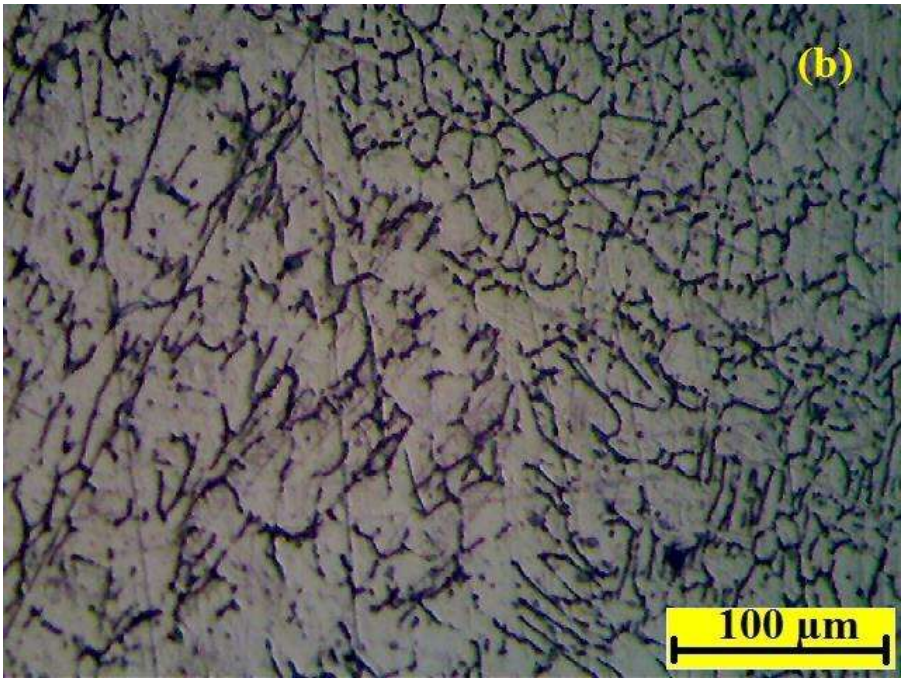

Grain size 28.9 µm

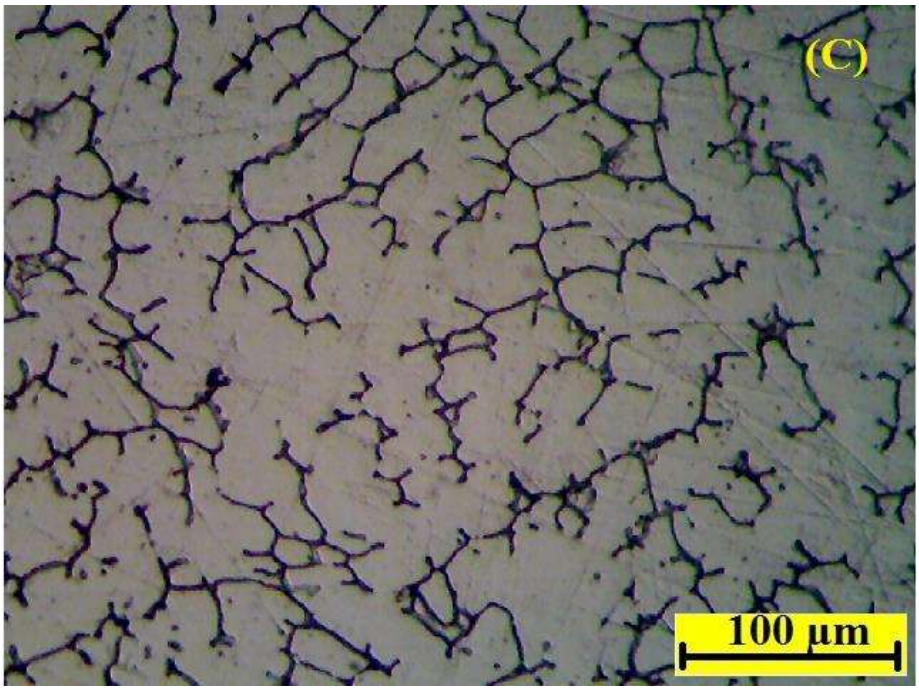

Grain size 27.7 µm

From result it is observed that the microstructures of 304 stainless steel weldments are totally different from that of the parent metal (fig 4.22). All weldments have dendrite structure (δ-ferrite + austenite) phases, but the parent metal is fully austenitic structure (fig.4.22).

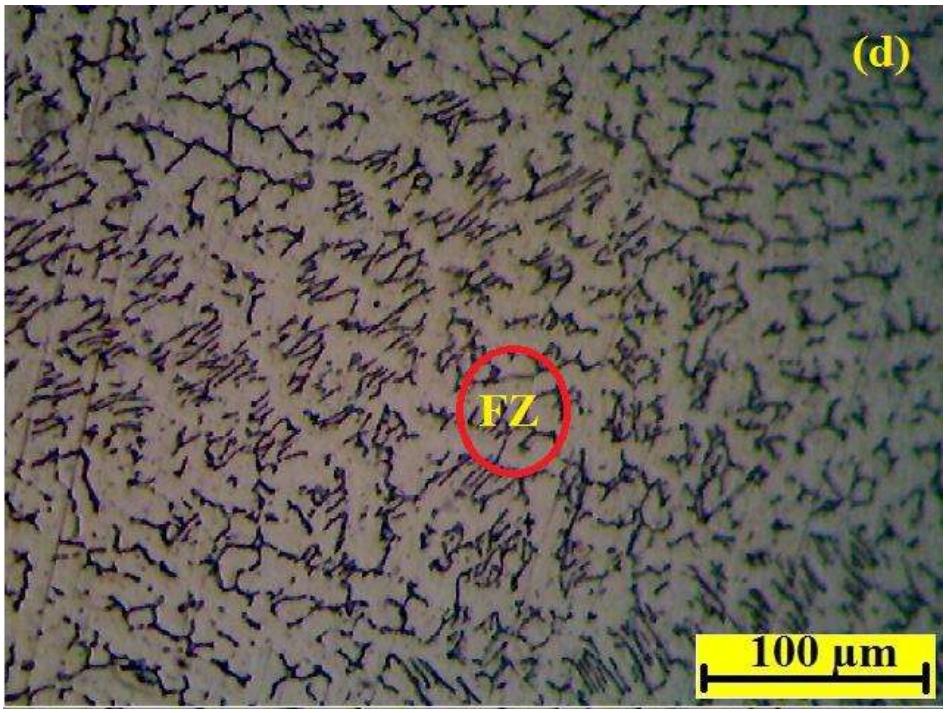

Grain size 20.7 µm

Figure 4.59(a-d) microstructure photograph of heat affected zone (HAZ) of AISI 304 steel weldment at 10-25 l/m shielding gas flow rate, at 7.62 m/min produced at 1.89 kJ/mm heat input

Jun Yan et al (2010) [118] studied the microstructure and mechanical properties of SS 304 welded joint by TIG, laser, and laser-TIG hybrid welding and they concluded that all joints consist the dark δ-ferrite dendrite structure in austenite matrix and The primary and secondary dendrite arm spacing of J_T joint are approximate 10–14 and 3– 7mm, respectively and they further added that e J_L joint shows the smallest dendrite size in all joints. The primary dendrite arm spacing of J_L and J_H joint are about 2–5 and 4–8 mm, respectively.

It is also observed from the result that dendrite size in the weld metal increase with increasing the heat input. With increasing the heat input resulted in decreasing the cooling rate of weld metal which allow more time for the dendrites to growth. Our results of microstructure match with the result of Jun Yan et al [118] and other researchers' work.

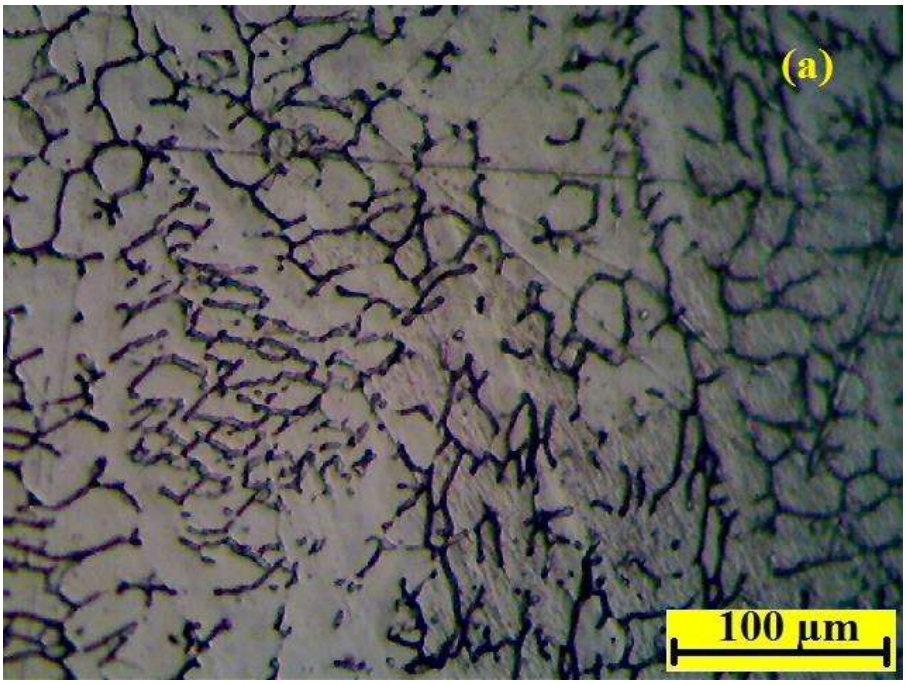

Grain size 26.7 µm

Dilution of the parent metal plate which ultimately guided to the variation in δ-ferrite morphologies in austenite matrix. In general, SS 304 welded joints reveal lathy and skeletal δ-ferrite morphologies [119].

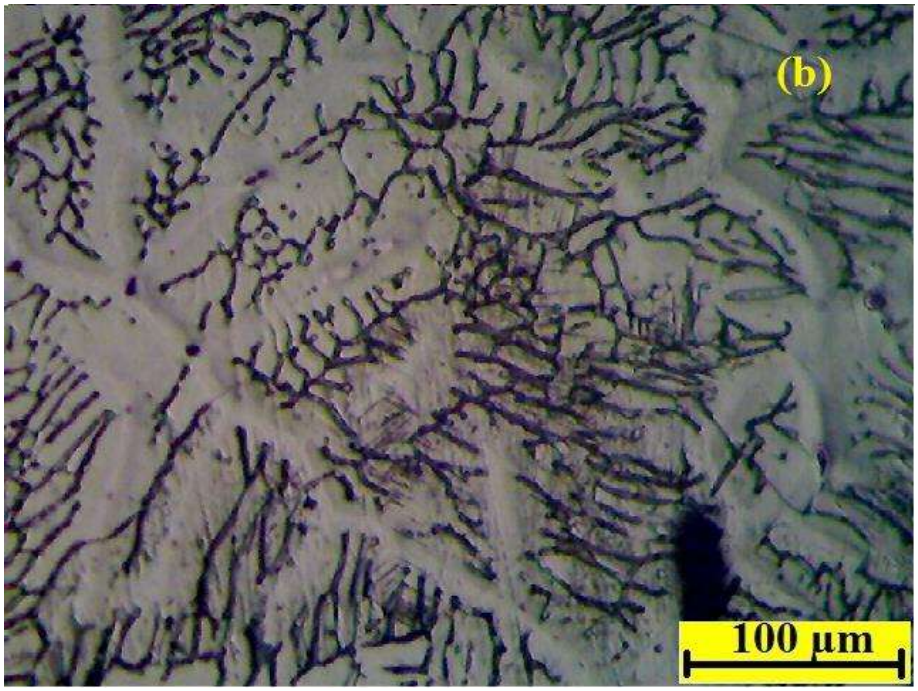

Grain size 18.3 µm

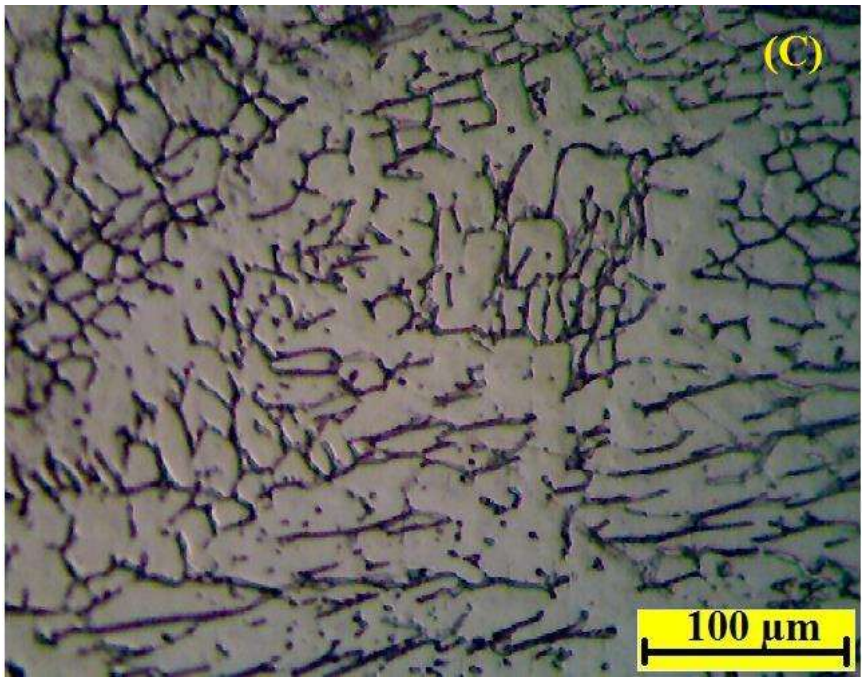

Grain size 20.2 µm

Skeletal δ-ferrite in austenite matrix of fusion zone of AISI 304 steel weldment

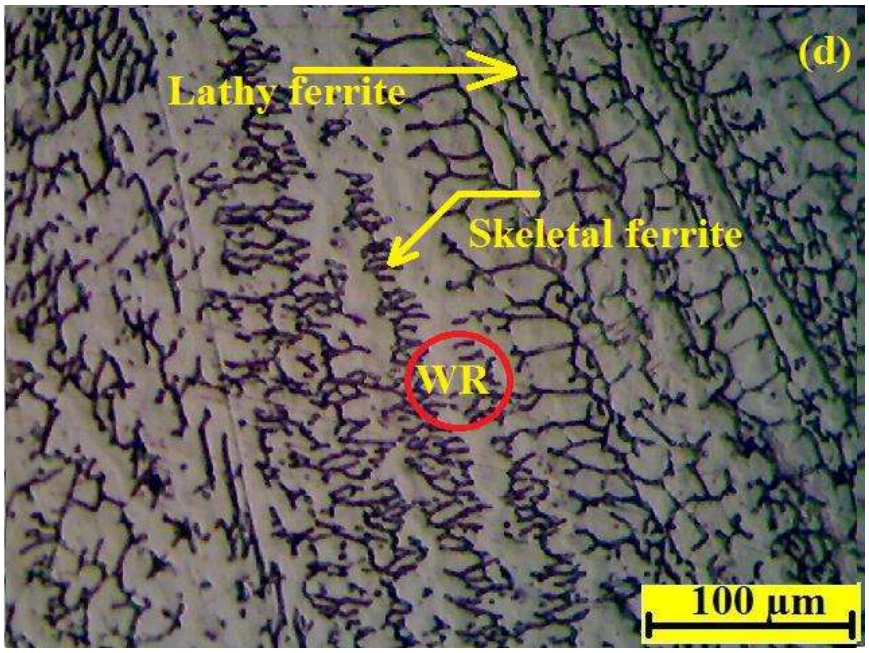

Grain size 19.7 µm

In fig (d) presence of two delta-ferrite (dark phases) morphologies-network morphology (right side) and vermicular (skeletal) morphology (left side).lathy type δ-ferrite changed into vermicular ferrite.

Figure 4.60 (a-d) microstructure photograph of heat affected zone (HAZ) of AISI 304 steel weldment at 10-25 l/m shielding gas flow rate, at 8.89 m/min produced at 1.89 kJ/mm heat input

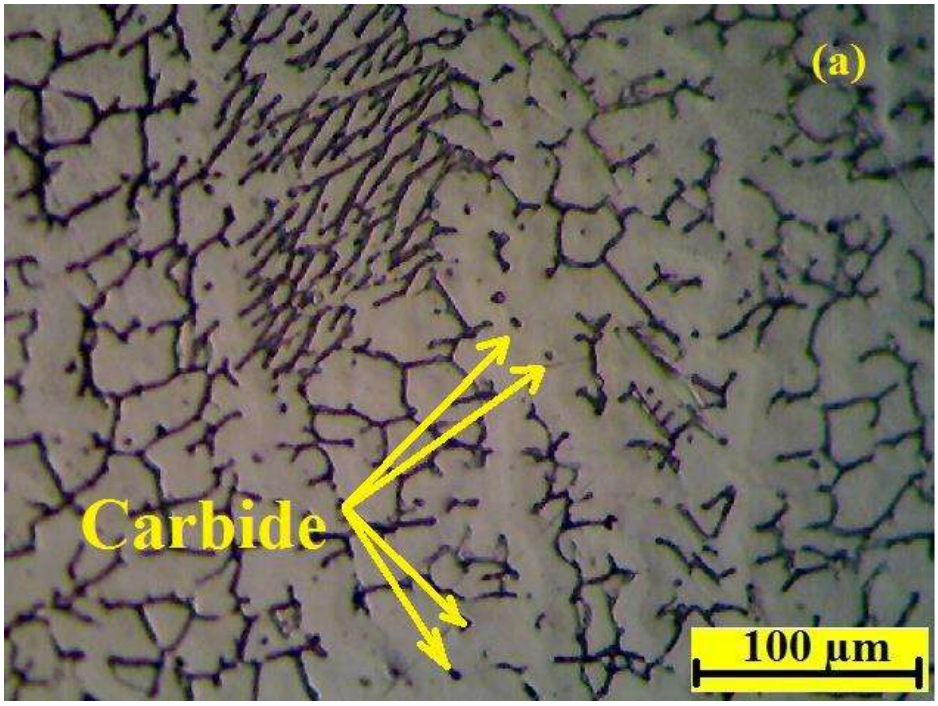

Grain size 39.4 µm

The ferrite had much wider separation as compared to high heat input test piece and small dark particles are carbide in austenite matrix.

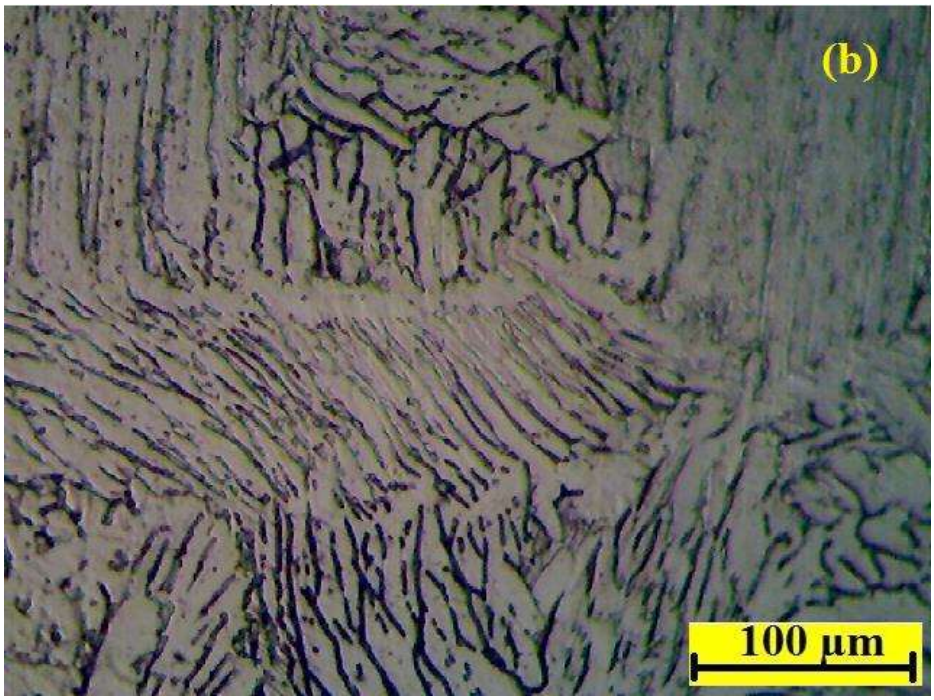

Grain size 19.9 µm

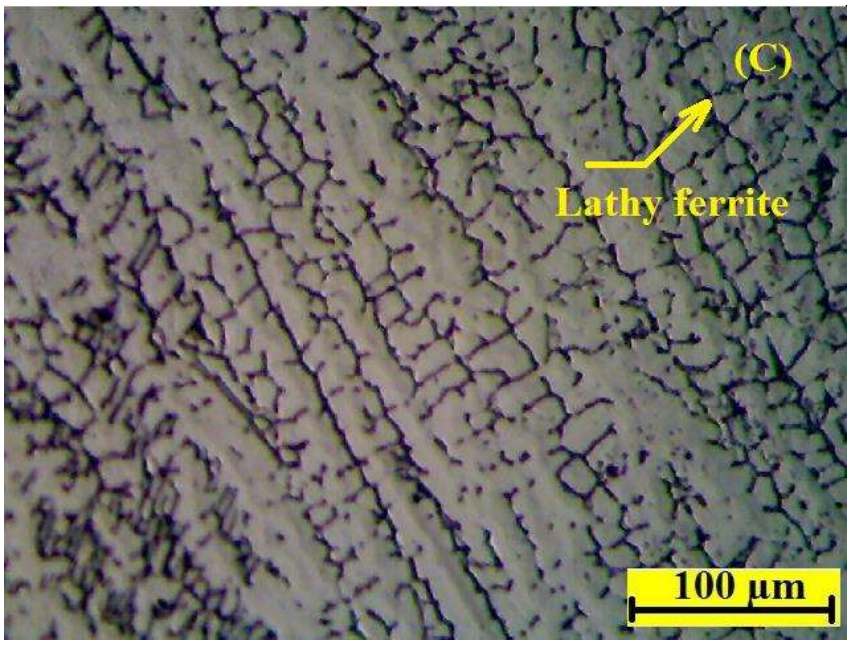

Grain size 22.4 µm

Fine microstructure for AISI 304 weldment.Fig (c) shows the transformation of δ-ferrite to lathy δ-ferrite. The δ-ferrite transformed from lathy ferrite to skeletal ferrite shape when welding pass number was increased from 1 to 2.

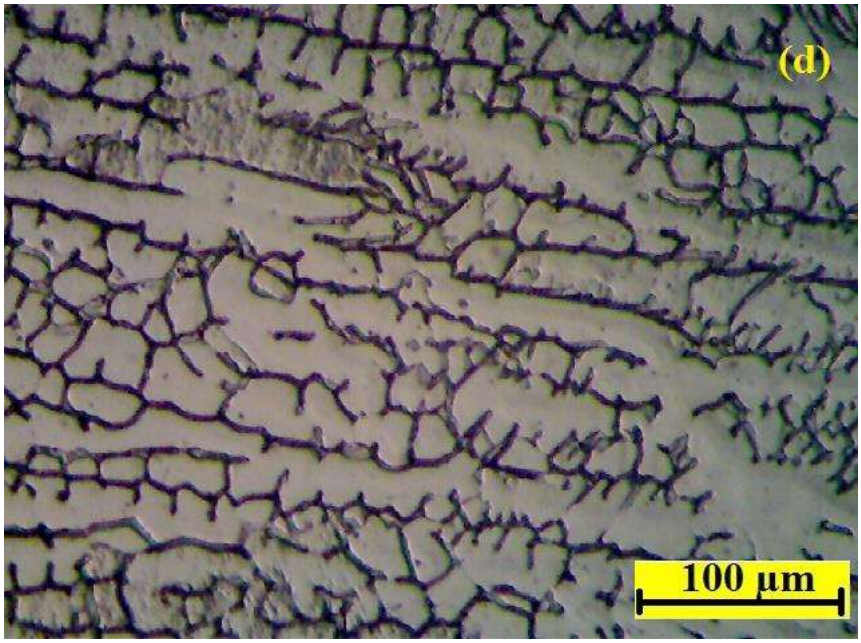

Grain size 27.2 µm

Figure 4.61(a-d) microstructure photograph of heat affected zone (HAZ) of AISI 304 steel weldment at 10-25 l/m shielding gas flow rate, at 10.16 m/min produced at 1.89 kJ/mm heat input

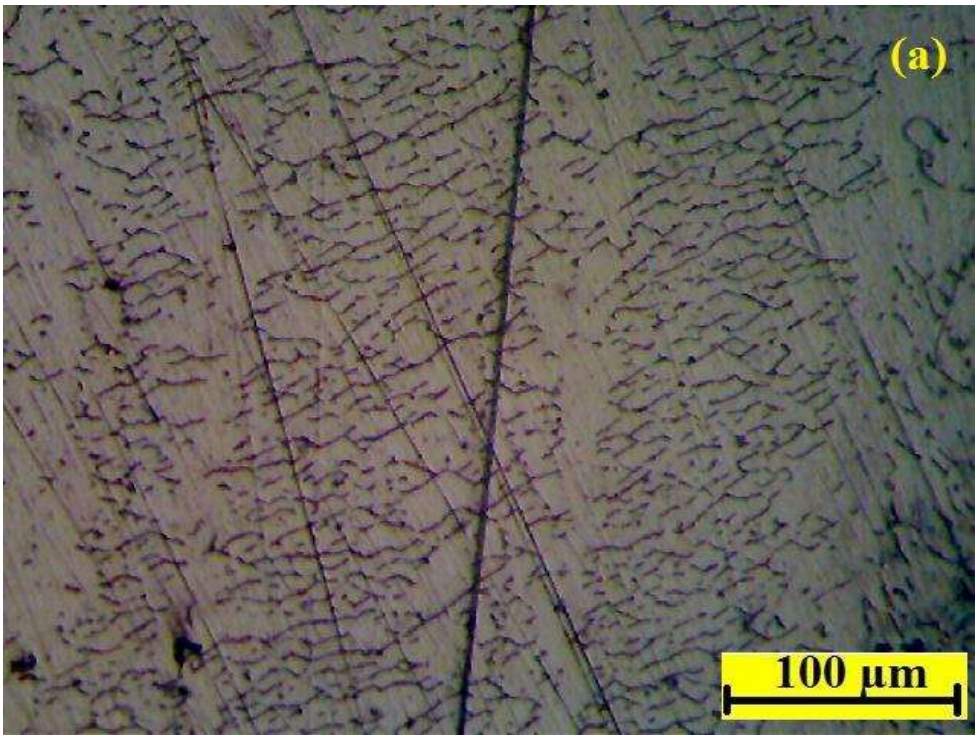

Grain size 27.6 µm

The ferrite had much narrow separation as compared to high heat input test piece. Larger the amount of δ-ferrite leads to increasing the tensile strength and hardness of weldment.

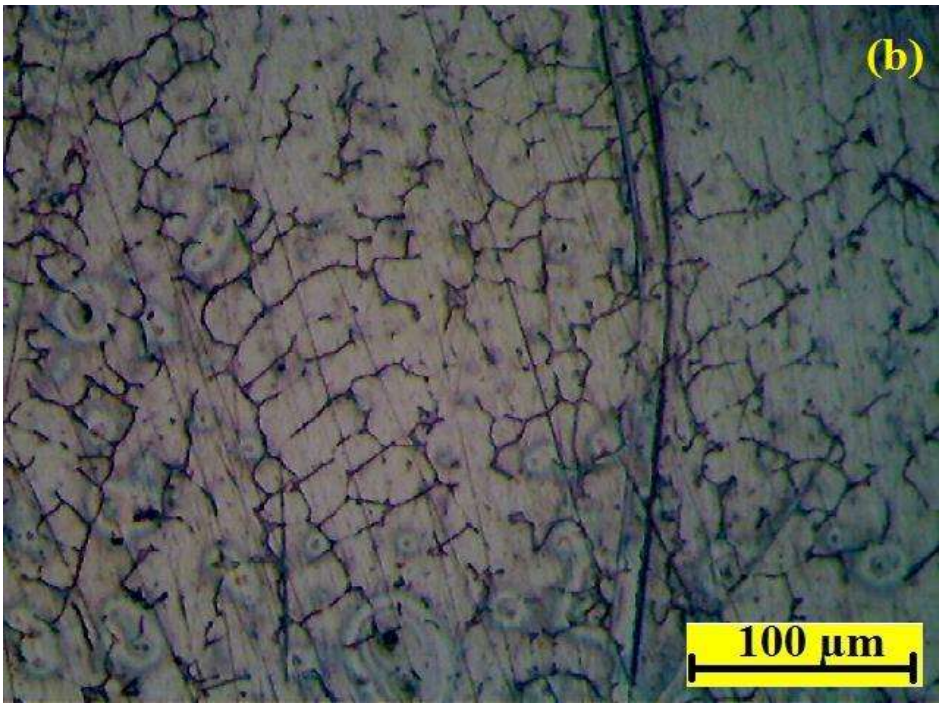

Grain size 39.4 µm

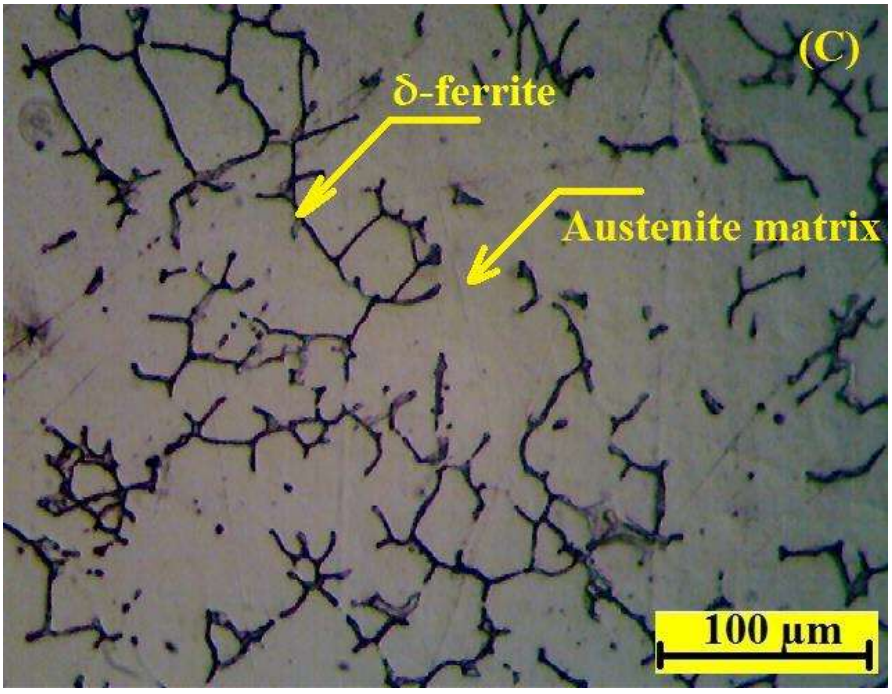

Grain size 28.9 µm

The microstructure of AISI 304 steel weldment with little δ-ferrite and more austenite

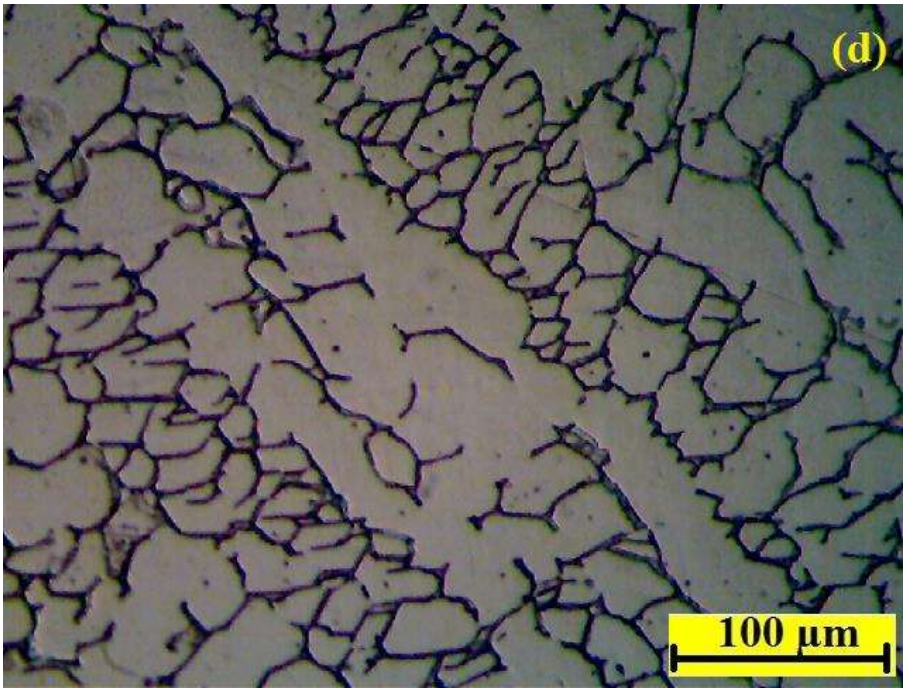

Grain size 21.8 µm

Figure 4.62(a-d) microstructure photograph of heat affected zone (HAZ) of AISI 304 steel weldment at 10-25 l/m shielding gas flow rate, at 6.35 m/min produced at 2.17 kJ/mm heat input

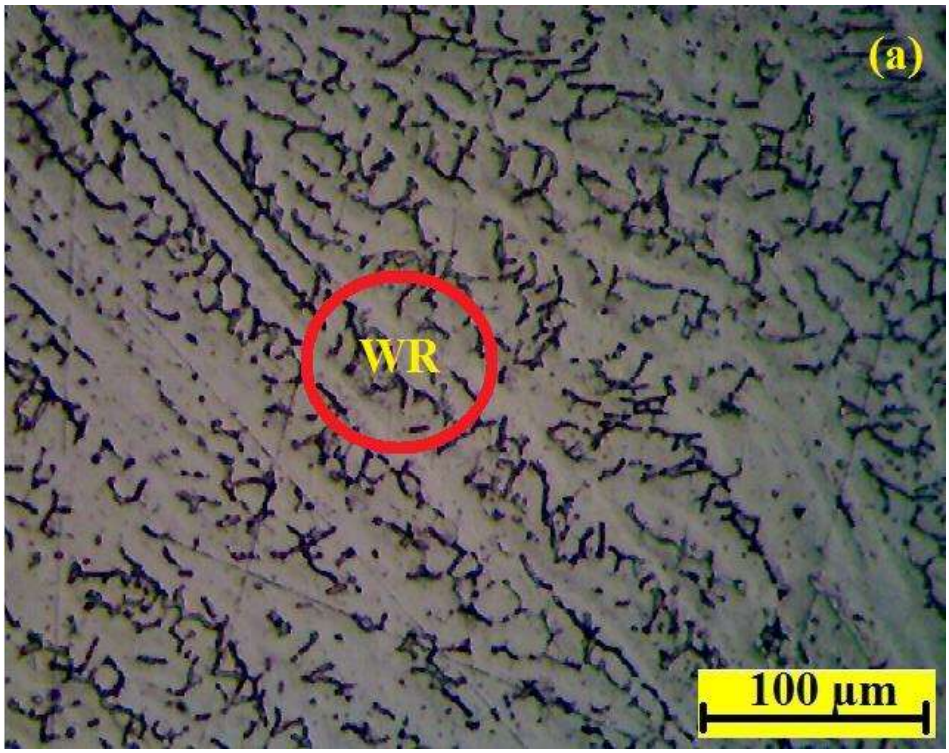

Grain size 20.3 µm

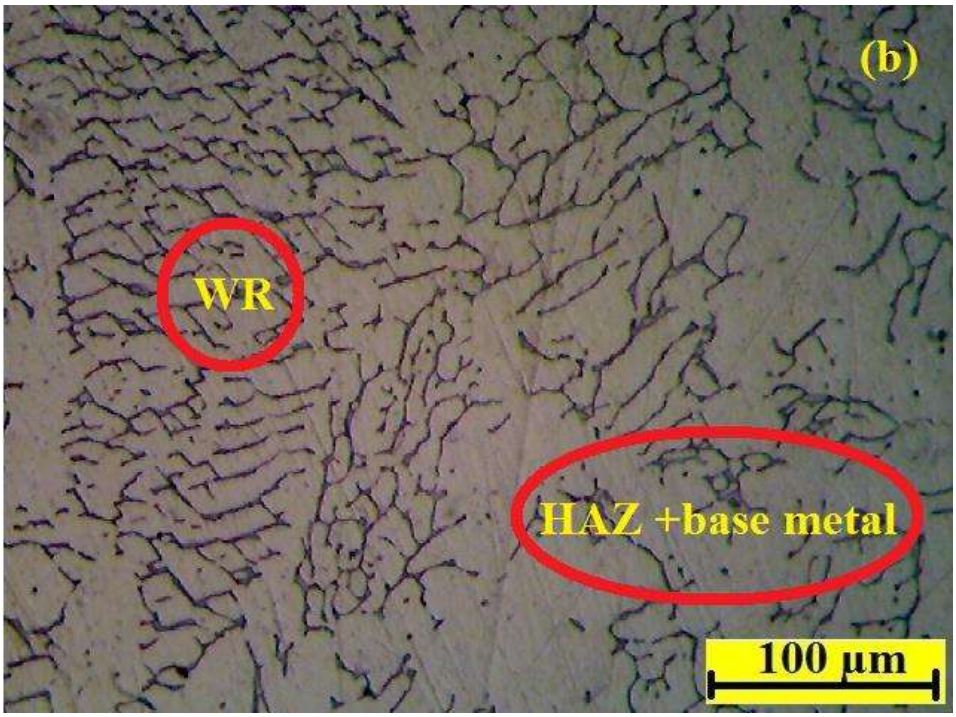

Grain size 23.7 µm

The microstructure of HAZ normally finer than the parent metal (PM) microstructure and this lead resulting in the higher mechanical properties.

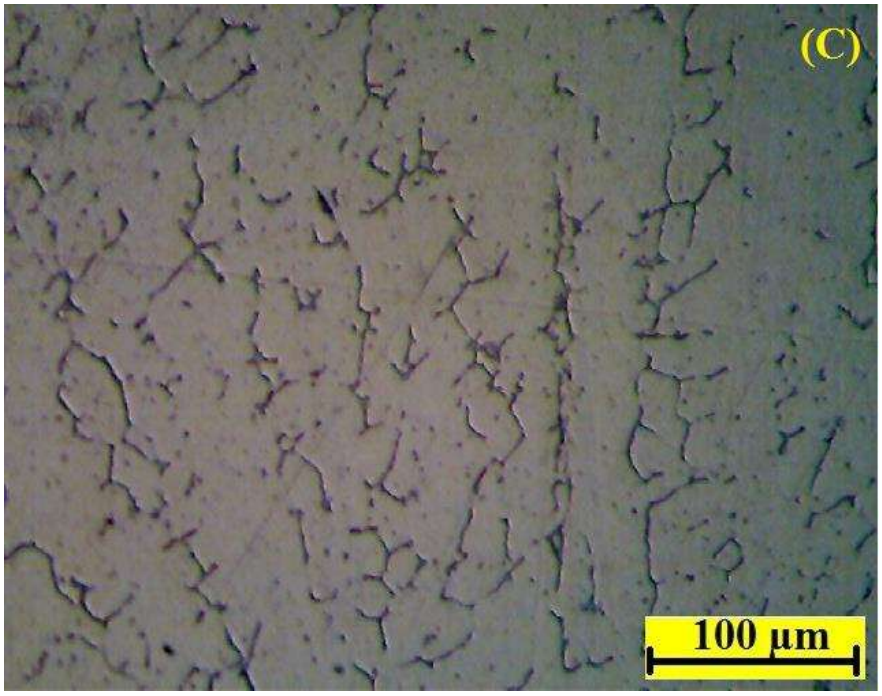

Grain size 30.1 µm

The fine microstructure of weldment. Microstructure is influenced by cooling rate of solidification

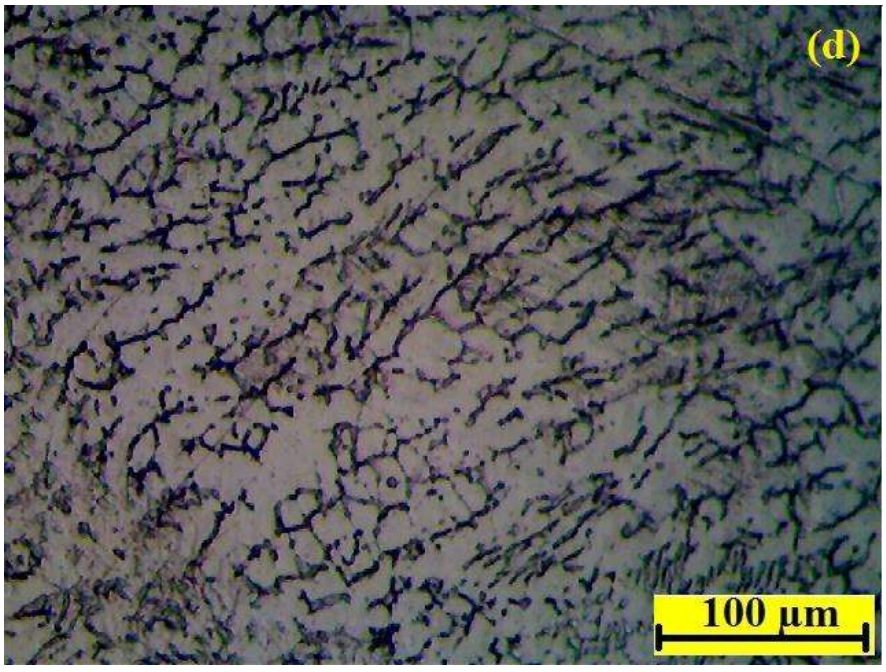

Grain size 19.9 µm

Figure 4.63(a-d) microstructure photograph of heat affected zone (HAZ) of AISI 304 steel weldment at 10-25 l/m shielding gas flow rate, at 7.62 m/min produced at 2.17 kJ/mm heat input

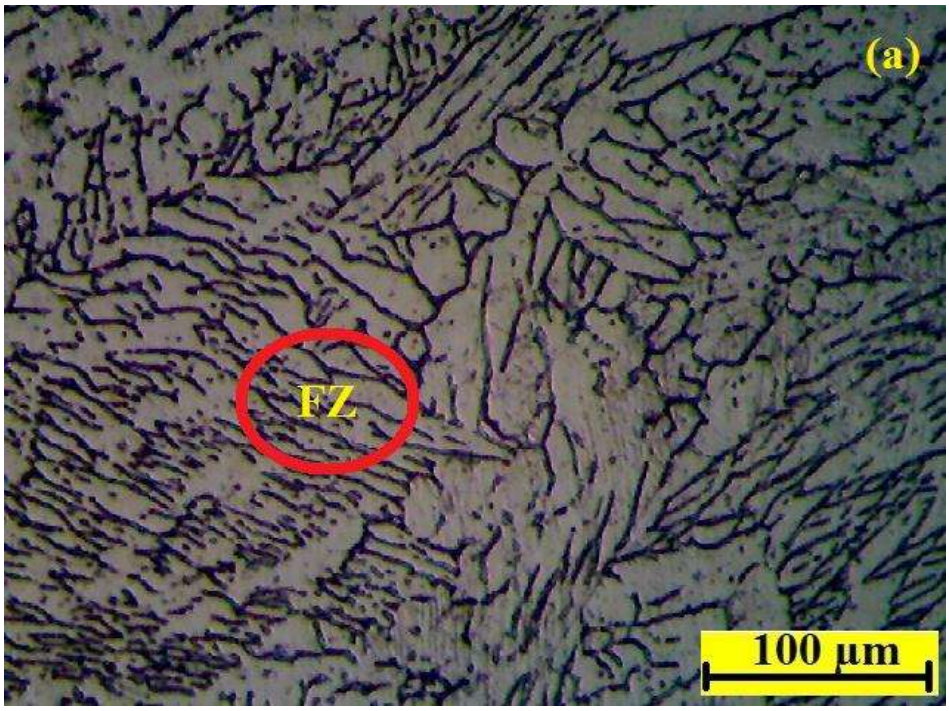

Grain size 18.8 µm

The microstructure analysis of AISI 304 shows some minor amount of carbide in fusion zone. Morphology of

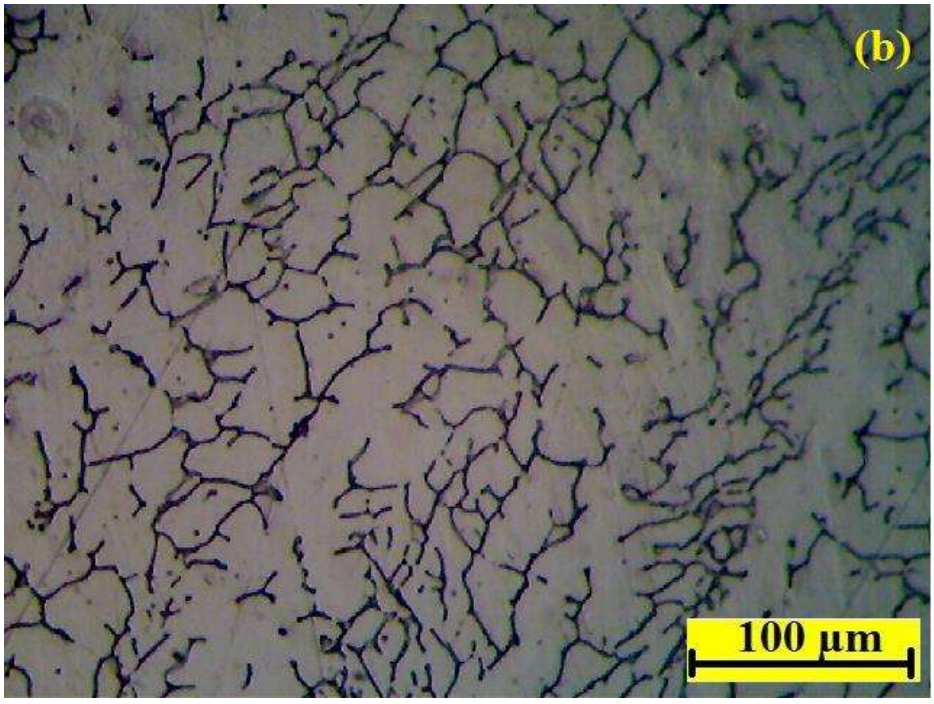

Grain size 24.4 µm

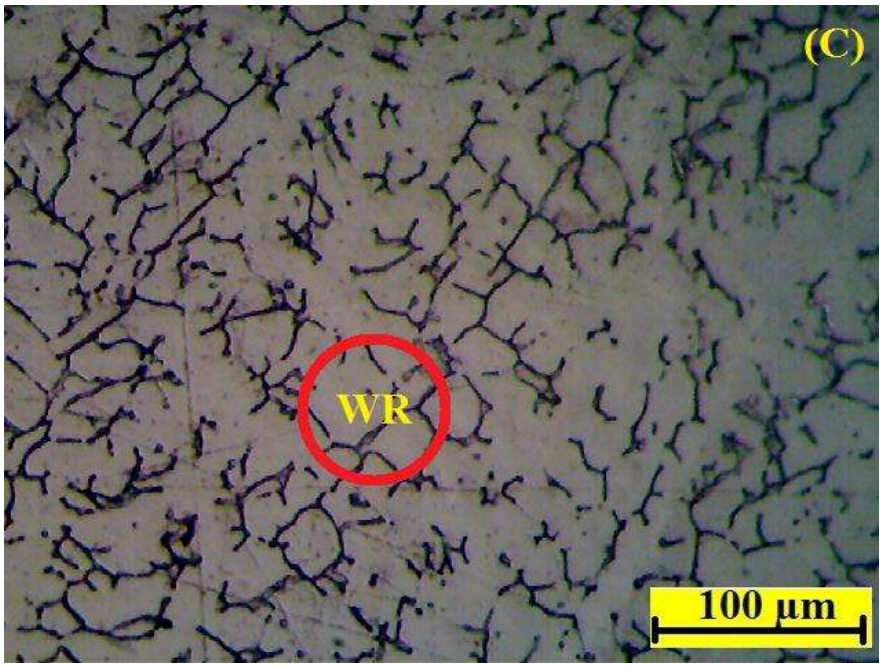

Grain size 23.2 µm

In the weld region, the ferrite contents increased, even hardness of test piece decreased with increase in heat input

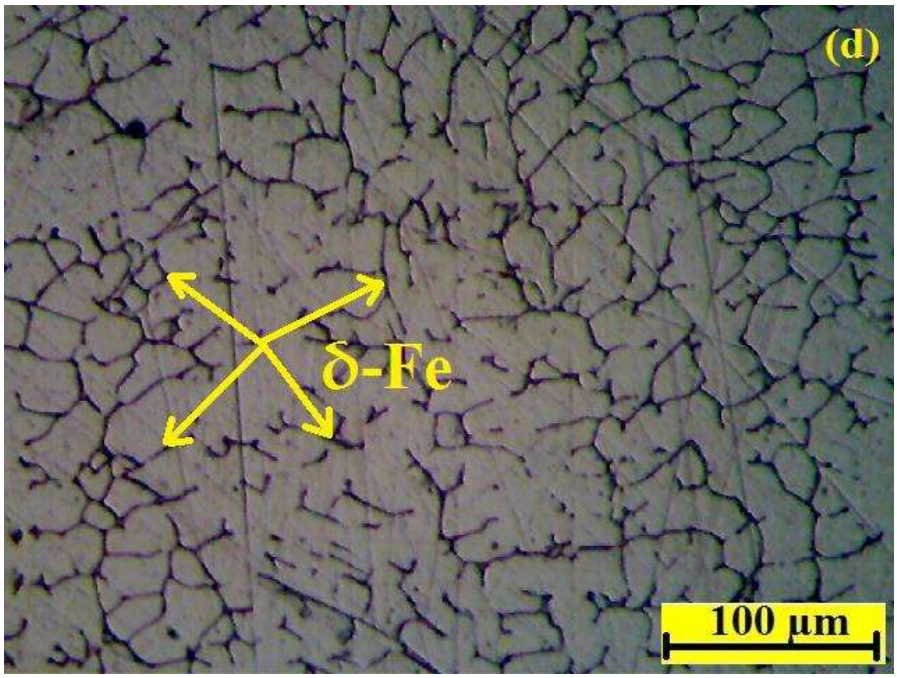

Grain size 25.5 µm

Figure 4.64(a-d) microstructure photograph of heat affected zone (HAZ) of AISI 304 steel weldment at 10-25 l/m shielding gas flow rate, at 8.89 m/min produced at 2.17 kJ/mm heat input

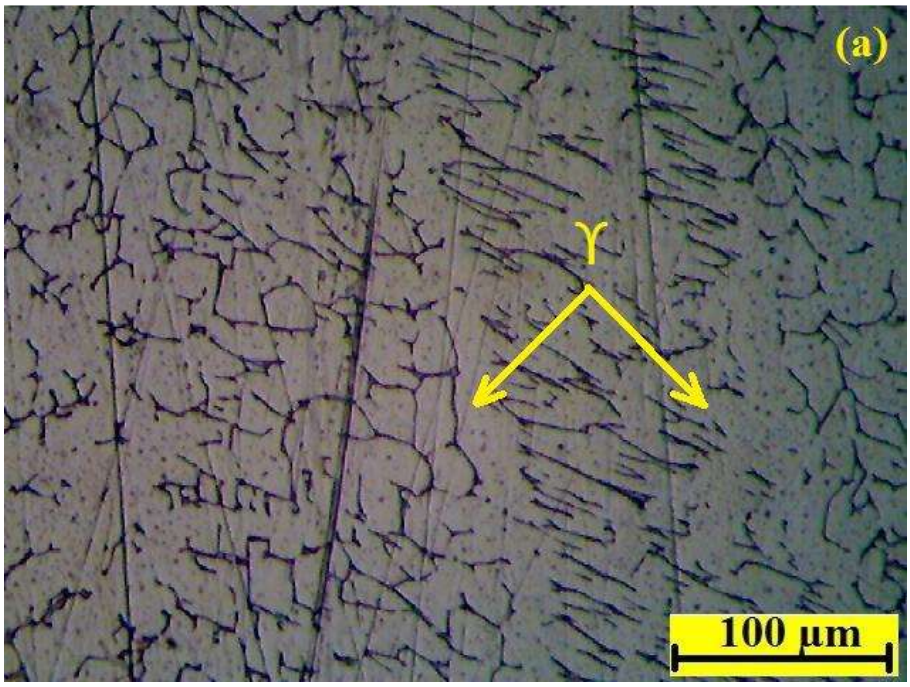

Grain size 32.5 µm

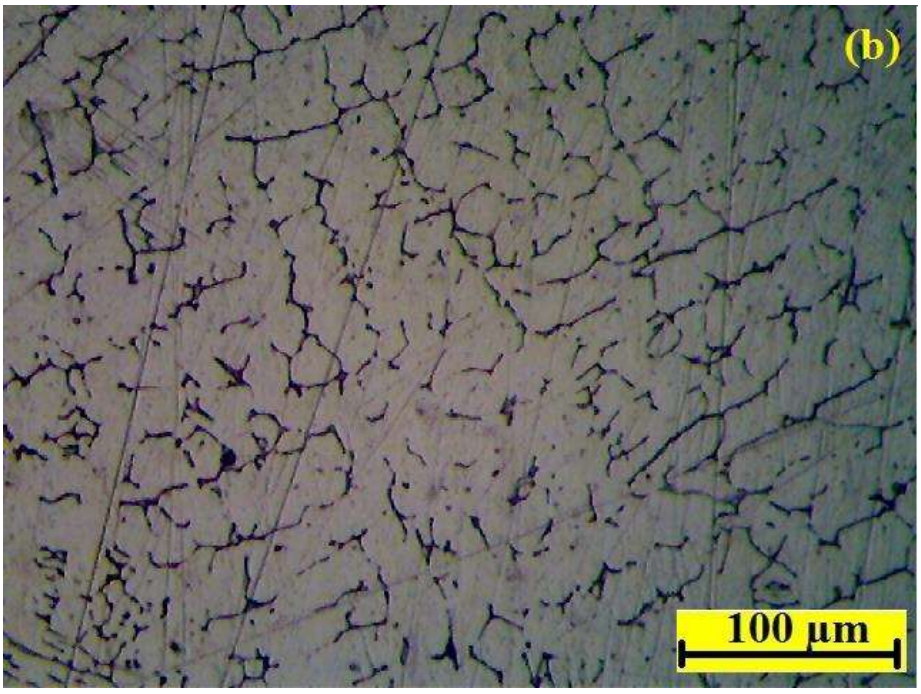

Grain size 34.7 µm

More portion of austenite matrix as compared to δ -ferrite.

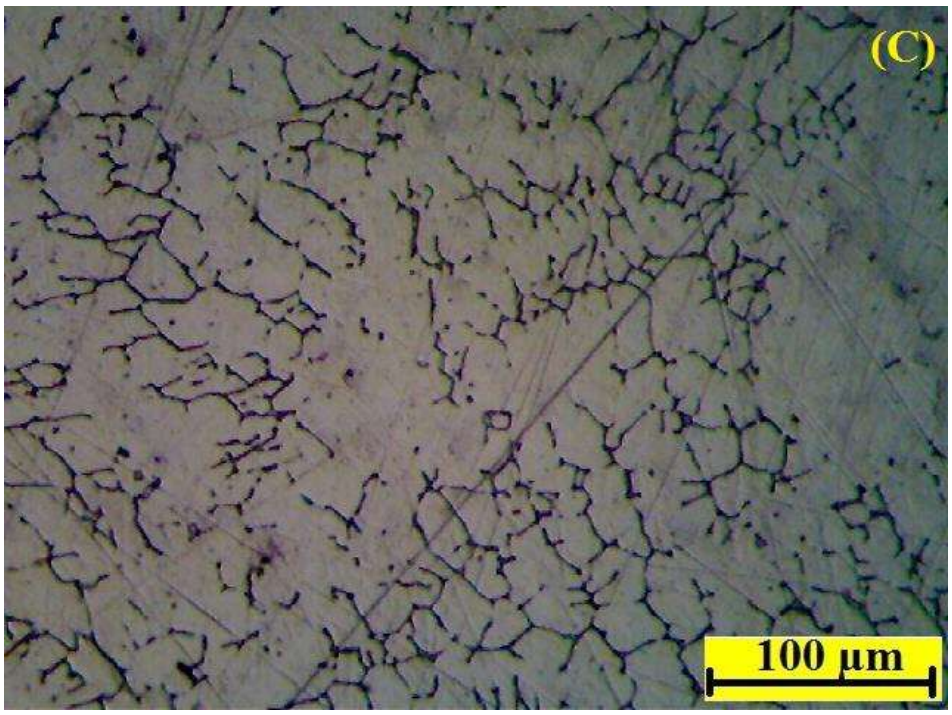

Grain size 37.1 µm

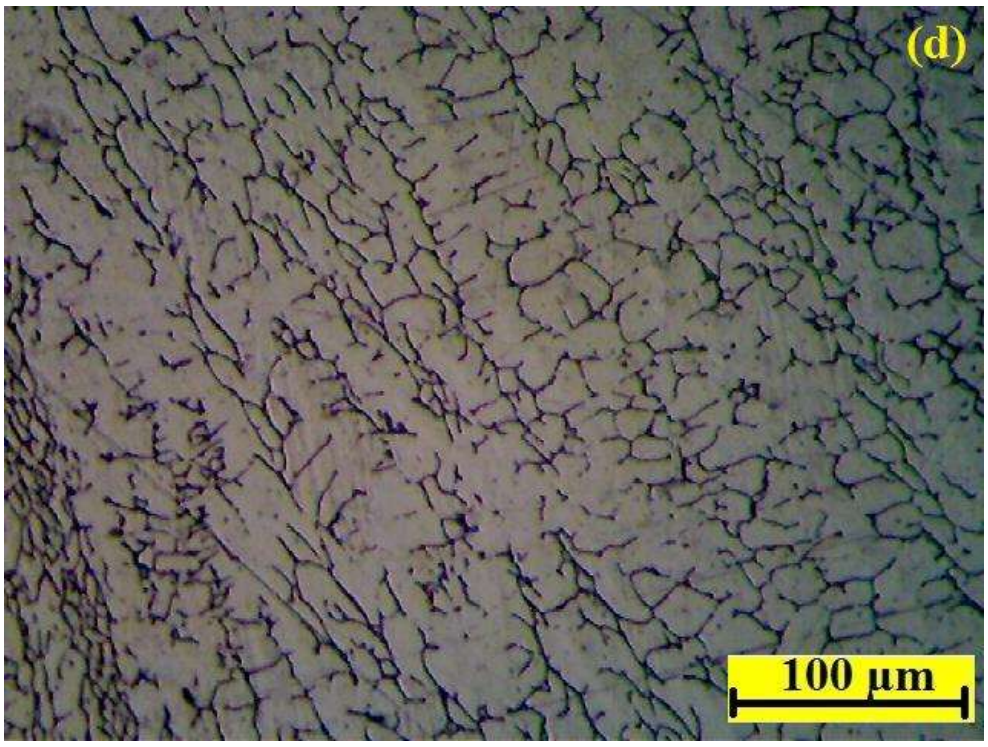

Grain size 23.8 µm

Figure 4.65(a-d) microstructure photograph of heat affected zone (HAZ) of AISI 304 steel weldment at 10-25 l/m shielding gas flow rate, at 10.16 m/min produced at 2.17 kJ/mm heat input

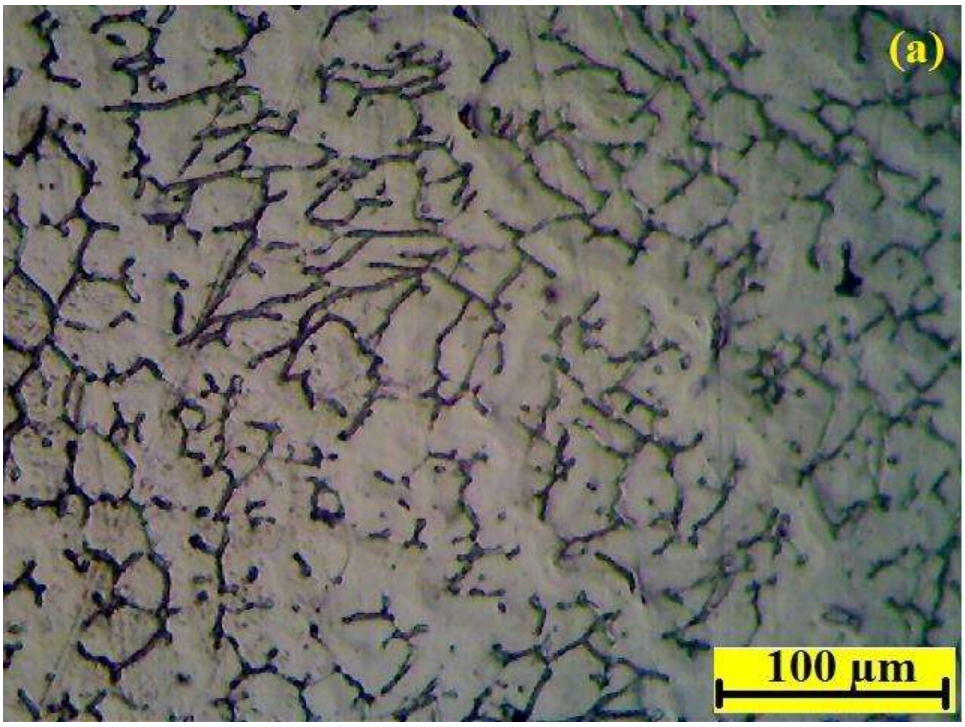

Grain size 30.7 µm

Coarse-grain structure of austenite in GMA welded test piece

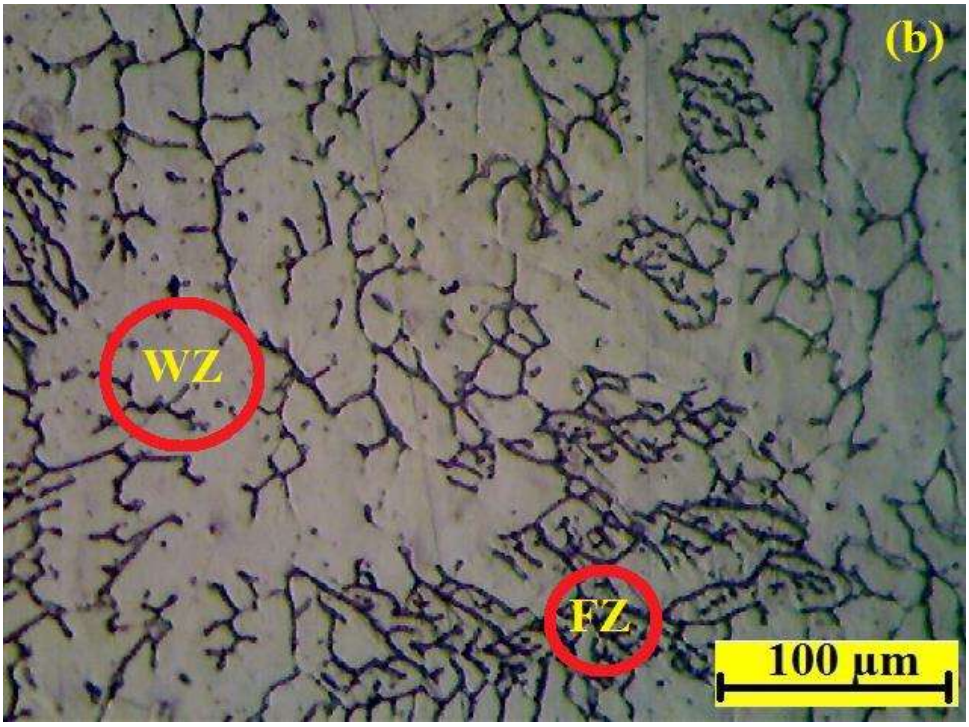

Grain size 29.9 µm

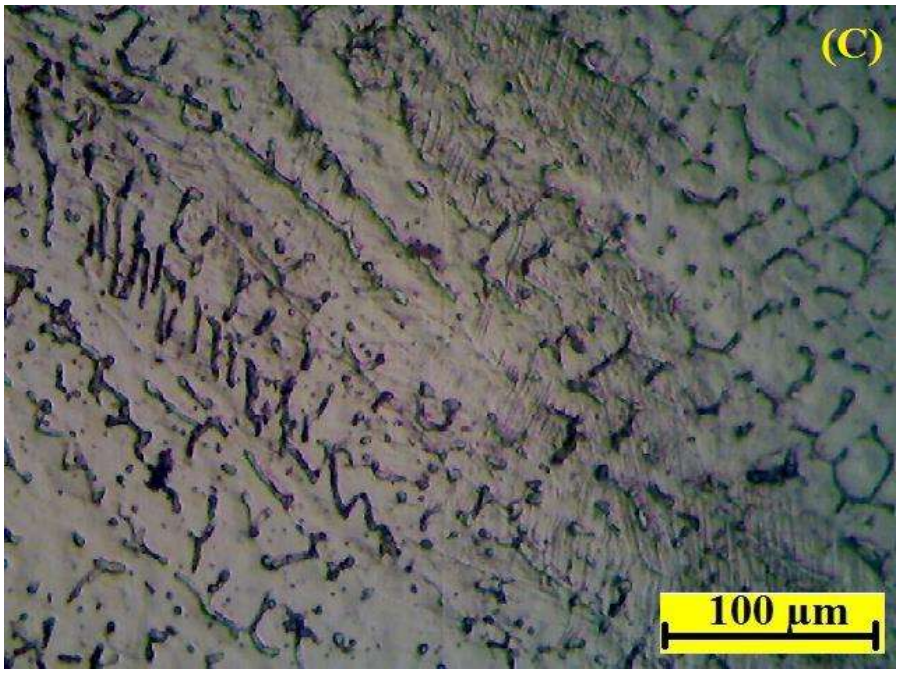

Grain size 22.9 µm

Dendrite is larger in size as compared to dendrite produced at high heat input.

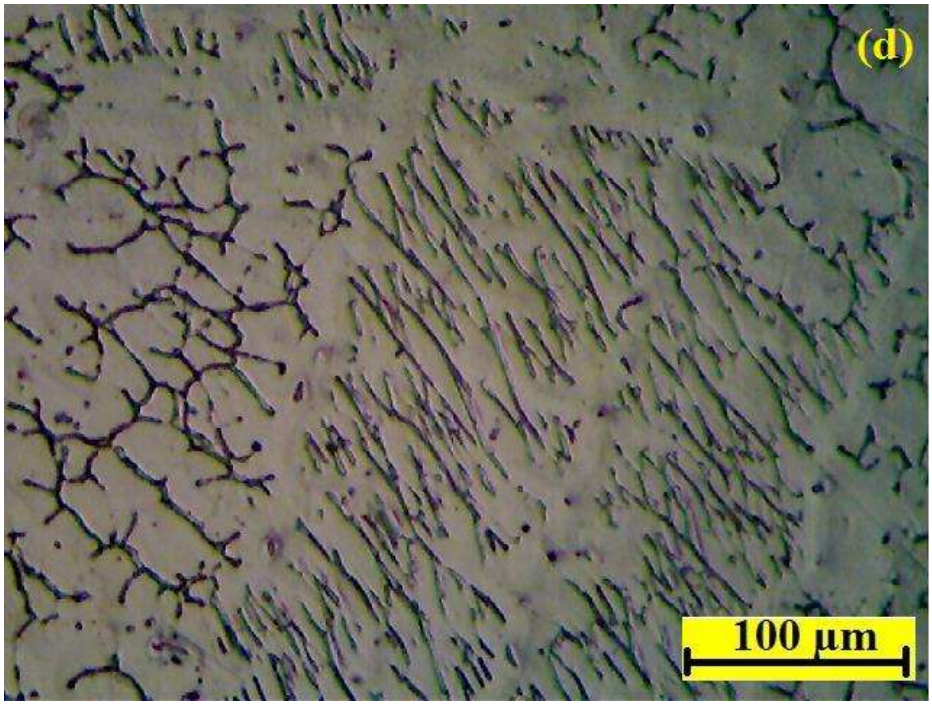

Grain size 35.5 µm

Figure 4.66(a-d) microstructure photograph of heat affected zone (HAZ) of AISI 304 steel weldment at 10-25 l/m shielding gas flow rate, and at 2.78 kJ/mm heat input

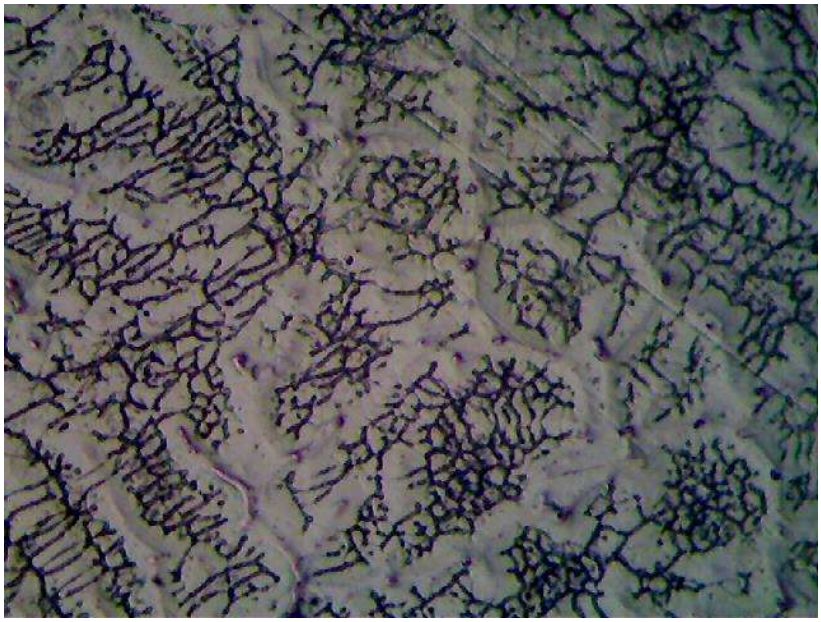

Grain size 20.6 μm. Fine dendrites in the weldment.

Figure 4.67 microstructure photograph of heat affected zone (HAZ) of AISI 304 steel weldment at 3.01 kJ/mm heat input

In fig 4.60 (d) the lathy nature of the ferrite is a result of a morphological instability of the interphase boundary during the diffusion controlled transformation of ferrite to austenite on cooling. The resultant laths often develop with a habit plane at an angle to the axis of the primary ferrite dendrite.

On microstructure examination of AISI 304 steel weldment, it is very clear from the literature review that thickness of fusion boundary increased with the increasing the heat input value. At high heat input, weldment shows a skeletal morphology of δ -ferrite as shown in above-mentioned figures [120]. On increasing the heat input dendrite thickness/width increased. Grain growth was observed near the fusion boundary, but no precipitation in HAZ or fusion zone was reported. Different dendrite sizes can be seen the AISI 304 steel weldments.

4.14 Grain size of IS 2062 and AISI 304 steel weldments

The grain size of the microstructure of IS 2062 steel weldments and AISI 304 steel weldments was determined by using a Pax-it image analysis software with micrographs at 100X magnification power. Image analysis provides average grain diameter in μm.

4.15 Microstructural analysis and nucleation of acicular ferrite

Scanning Electron Micrograph (SEM) analysis of fracture test pieces was carried out to establish the possible role of inclusion on the nucleation of acicular ferrite (AF) and to understand the fracture mode for IS 2062 structural steel weldment and AISI 304 steel weldment.SEM and EDS were conducted to determine the morphology and elemental composition of the inclusions in the welded joint.

4.16 Analysis of Inclusion by SEM

Few selected weld test pieces were polished and examined for inclusion by SEM apparatus. Figure 4.69 shows the typical SEM micrograph of the type of inclusion observed in the both IS 2062 structural steel and AISI 304 steel weldment. Only spherical type inclusion was observed in both types of steel weldments.

4.17 Analysis of weld metal inclusion chemical composition by SEM

The fracture surfaces were also evaluated by SEM, and the results are shown in Fig.4.68. As seen in the figure, inclusion of varying size and shape were observed in the fractured surfaces which show that fracture was ductile. Mode of fracture of weldment is usually affected by the various welding parameters as such strain rate, cooling rate of weldment and heat input.on fast cooling of

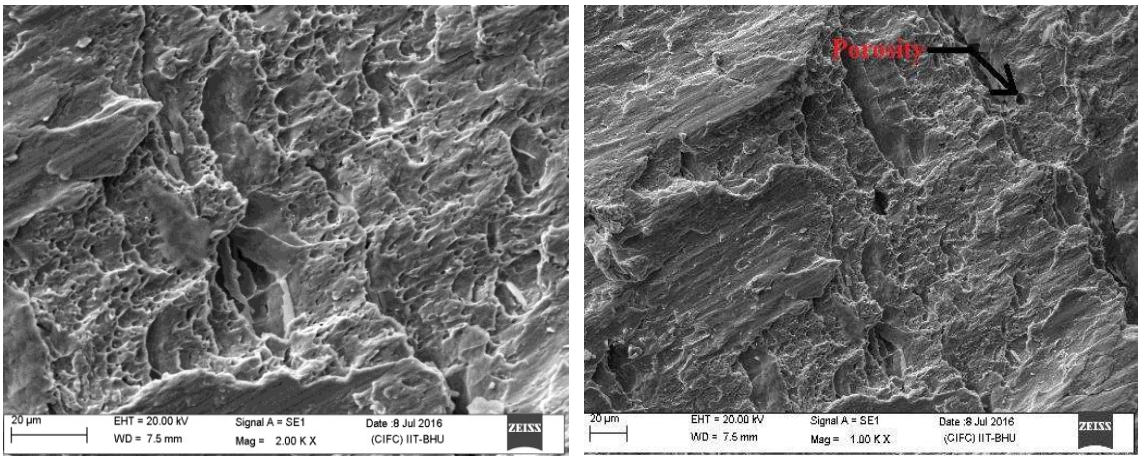

Figure 4.68 SEM image (Fracture morphology) of tensile specimen of IS 2062 steel weldment fractured at room temperature.

Weldment brittle fracture observed. The inclusion is indicated by the arrow. The EDAX spectrum of the inclusions of the weld joint of IS 2062 steel weldment is shown in Fig. 4.69

The EDS spectrum and chemical composition of the IS 2062 steel weldment samples is presented in fig.4.69. Elemental composition indicated the presence of (Fe and Mn). The Energy-dispersive X-ray spectroscopy (EDS) area analysis results that Fe is in major portion. The property of weldment is usually influenced by the element such as Fe. EDS analysis spectrum, taken at the weldment fractured position as shown in Fig. 4.69. From the analysis it is observed that substantial mixing of Iron (16.13%) and Manganese (1.64%) in weldment. presence of voids has been observed at the weld zone.

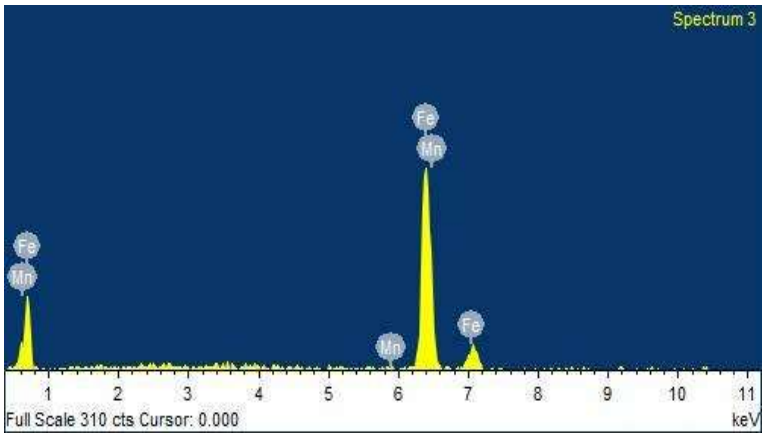

Figure 4.69 Typical EDAX spectrums: the distribution of alloying elements

4.18 SEM analysis of Charpy test for IS 2062 steel weldments

Scanning electron micrographs of fracture surfaces of Charpy impact toughness test specimens V-notched in welded metal and test is carried out at room temperature is shown in Fig.4.70 Accordingly, cleavage cracks propagate more easily in the GF than in AF. This examination confirms that Accicular Ferrite (AF) has a beneficial effect on the toughness of joint.

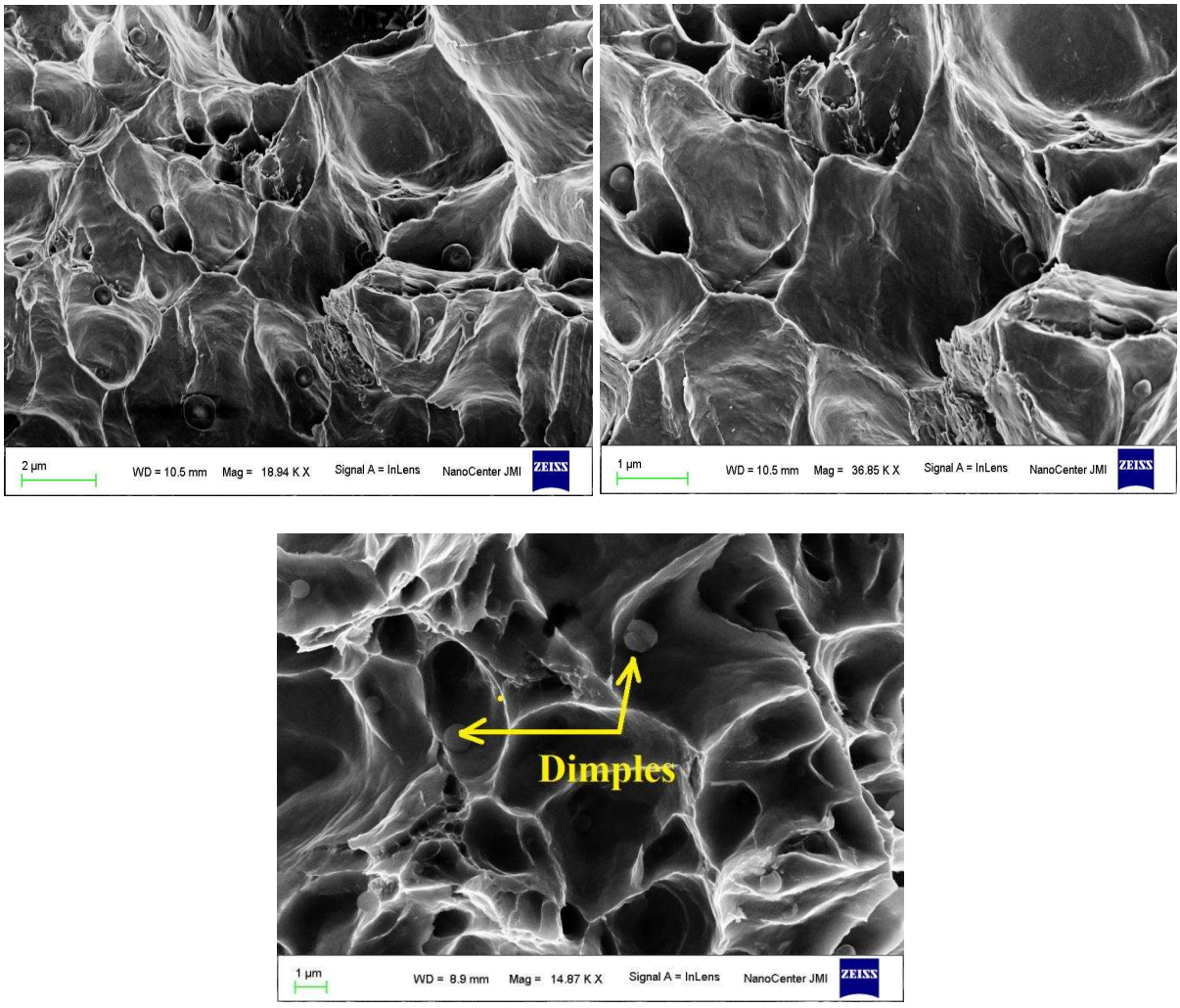

Figure 4.70 Fracture morphology (SEM image) of Charpy test specimen fractured at room temperature.

4.19 Fractography analysis

Impact test specimens of weldment were tested for the mode of fracture with scan electron microscope (SEM) to analyze the type of fracture has occurred. Fracture are usually two types, i.e. ductile fracture and brittle fracture. It is very important to when how ductile fracture occurred and when the brittle fracture occurred. When fracture surface was examined reticulated dimpled was obtained. Such fracture Figure 4.71 (a) and (b) depicts ductile fracture. The fracture surface of weldment at high heat input Figure 4.71 (c) exhibit brittle fracture. From figure 4.71(C) it was observed that transgranular fracture by quasi-cleavage due to high heat input.

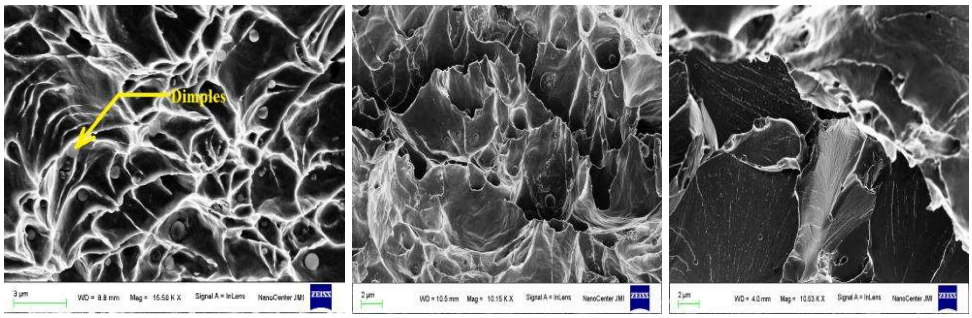

(a) (b) (c)

Figure 4.71 SEM images of the fracture surface of samples under low, medium and high heat input

SEM image of Toughness shows that on low heat input mode of fracture was ductile whereas on high heat input image shows a brittle fracture. Shielding gas mixture of 75%Ar+25%CO_2 produced acceptable of weld metal properties due to the balance of cooling rate and the formation of a high amount of AF which leads to the enhancement of strength and impact toughness

4.20 Fractography analysis of AISI 304 steel weldment

Figures 4.72 (a, b & c) shows SEM fractographic images of the tensile test specimen of AISI 304 steel weldment. The images clearly reveal numerous dimples indicating ductile fracture has occurred. It is also observed that there are some spherical particles with small and large dimensions near the bottom of the dimples.

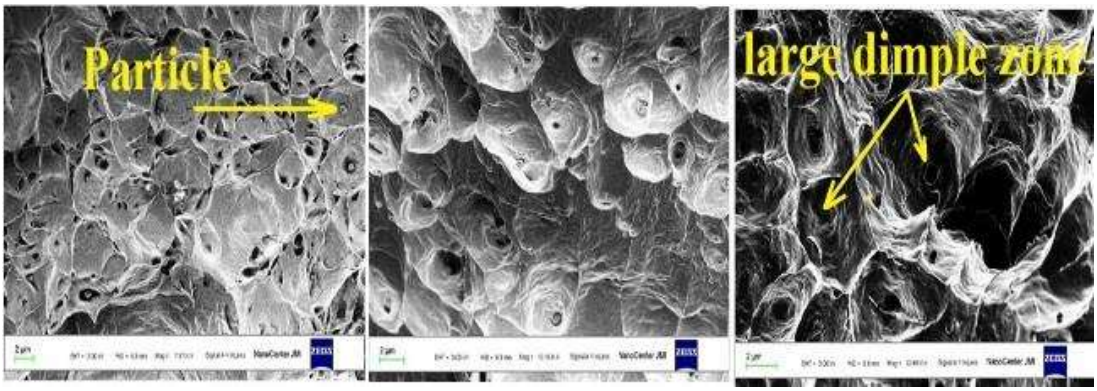

(a) (b) (c)

Figure 4.72 (a), (b) & (c).Fractography of AISI 304 welded joint after the tensile test at room temperature.

4.21 Energy dispersive spectrometer (EDS)

In order to determine microinclusions generated in the welded Joints during the welding process, EDS analysis was conducted on the fractured specimen. Fig. 4.73 shows the results of the analysis indicating that inclusion generated in the weld metal of AISI 304 contained Fe, C, Ti, Cr, and Mn elements in amounts of 6% or more whereas C, Al, Fe, Si are less than 2%. The EDS results of the AISI 304 steel weldment specimen imply that the inclusions are the oxides including MnO_2, NiO_2, CrO_2, SiO_2, and Al_2O_3. The size and amount of the oxides in the microstructures usually depend on the amount of CO_2 present in shielding gas. On the contrary, the amount of Al, S, and Si elements are comparatively low. For commercial steels, the typical non-metallic inclusions are oxides, nitrides, and sulfides. Manganese; Sulphur inclusions are effective in inducing Accicluar Ferrite formation.

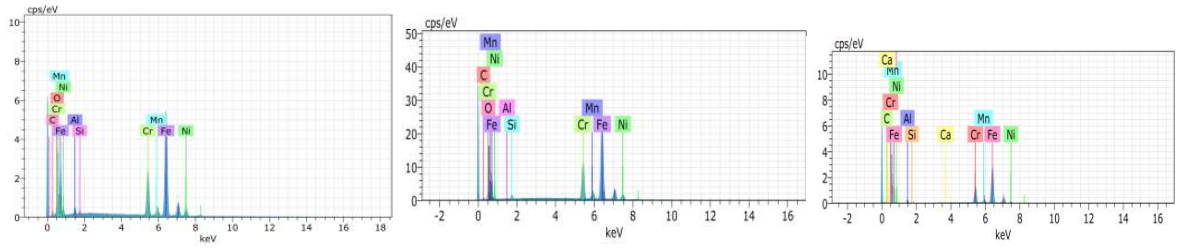

(a) (b) (c)

Figure 4.73. Energy-dispersive spectroscopy (EDS) analysis results of inclusions

4.22 fracture mode of toughness test specimen

To determine the toughness of AISI 304 steel weldment "V" notch Charpy samples were prepared as per ASTM A370-14. Specimens after fracture are shown in figure 4.74.Impact fractured specimens examined to determine the surface morphology. The morphology of the impact fracture surface of the different welded joints was observed. It was noticed that the failure path of cracking continued along the columnar crystal boundary of the deposited metal and the grain boundary was the weak link, which was associated to a large amount of the N_b phase on the grain boundary. The fracture morphologies of the all deposited metals were different [121].

Figure 4.74. Impact test samples after fracture

Figure 4.75 (a) and (b) shows the images of fractography of impact Charpy "V" notch test piece. Sample 1 in Figure 4.75 shows the ductile fracture with coarse dimples. Enough finer dimples are observed in sample 3 in figure 4.75. Combined ductile and brittle fracture mode formation is responsible for poorly absorbed energy. Sample 2 shows shallow dimples.

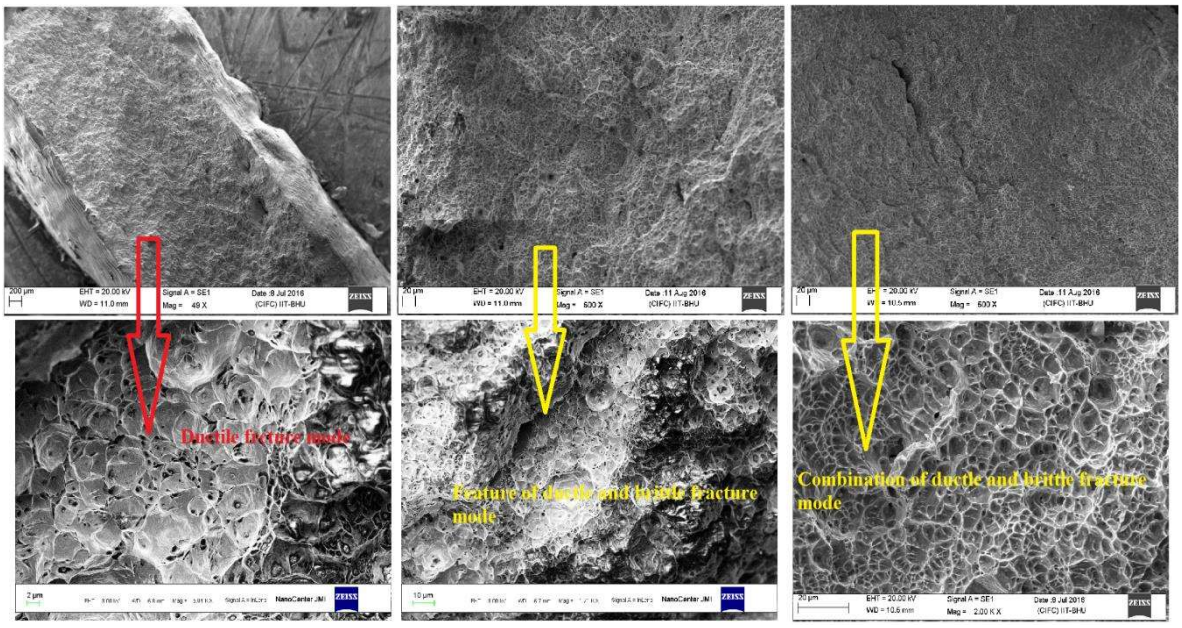

Figure 4.75 Macro images and SEM images of Impact fracture samples for morphology